

**TRANSFORMATIONS IN ARCHITECTURAL LIGHTING ANALYSIS:  
VIRTUAL LIGHTING LABORATORY**

**by**

**Mehlika N. Inanici**

A dissertation submitted in partial fulfillment  
of the requirements for the degree of  
Doctor of Philosophy  
(Architecture)  
in The University of Michigan  
2004

Doctoral Committee:

Associate Professor Mojtaba Navvab, Chair  
Assistant Professor Igor Guskov  
Associate Professor Jong-Jin Kim  
Professor James Turner

© Mehlika N. Inanici 2004  
All Rights Reserved

To Nebahat and Ahmet, my mother and father  
To Fateau and Mehmet, my sister and brother  
for their love, support, and encouragements

## ACKNOWLEDGMENTS

I would like to acknowledge the contributions of Prof. Mojtaba Navvab throughout my doctoral studies. Moji has shown enthusiasm and interest in my research from the start. He has been an exceptionally thorough critic of my work, and he has been a source of inspiration and challenges through our discussions. I thank him for his willingness to show me the different aspects of lighting design and research. Moji also provided the space and resources for my mini computer lab (Radiance-Zone), where I had the opportunity to render most of the images that I used in the dissertation.

Prof. Igor Guskov has provided help and guidance on the computer graphics issues. I would like to offer appreciation for his time and patience; he has helped me in many ways, probably more than he, himself realized. I would like to thank to my other committee members, Prof. Jong Jin Kim and Prof. James Turner, both of who provided timely feedback and support.

Emeritus Prof. Norman Barnett gave feedback on some of my studies and he was kind enough to provide the spreadsheet for the CIE chromaticity diagram and the iso-temperature lines, which I have used in Chapter IV and V.

Radiance Online Group has been an excellent source of information. I would like to acknowledge everyone who have contributed to the list by questions, answers, and discussions. I have benefited immensely.

During my doctoral studies, I have had the fortune to make many good friends. I have learnt something from all of them, mostly about life and diverse cultures. Of particular note, I would like to thank to Ruchi Choudhary, Ela Cil, Asligul Gocmen, and Elena Primikiri. Ruchi and I have worked in the ETLab on opposite corners and have

shared the unforeseen challenges and joys of the doctoral studies in parallel phases. Ela has been a source of good humor, even under adverse circumstances. Asli and Mark have been enthusiastic companies, especially for some of my hobbies. Elena has been a dependable friend through thick and thin.

Most of all, I would like to thank to my family for making everything possible. Behind all of my accomplishments, I have their enduring love, support, and encouragement. They have always been very compassionate about my education. They have provided tremendous comfort throughout the difficult times, despite the fact that I have been living so far away from them. I am indebted and extremely privileged to have them as my family.

## TABLE OF CONTENTS

<b>DEDICATION</b> .....	ii
<b>ACKNOWLEDGEMENTS</b> .....	iii
<b>LIST OF FIGURES</b> .....	viii
<b>LIST OF TABLES</b> .....	xiii
<b>Chapter I. INTRODUCTION</b> .....	1
Background.....	1
Objectives .....	3
Overview of the Dissertation .....	4
<b>Chapter II. PHYSICALLY BASED RENDERING AND IMAGE TECHNOLOGY</b> .....	5
Lighting in the Physical World versus Computer Graphics .....	7
Definition and Modeling of Light.....	7
Physically Based Modeling of Light Sources.....	14
Physically Based Modeling of Material Appearance and Light Absorption, Reflection, and Transformation.....	20
Physically Based Modeling of Light Transport .....	24
High Dynamic Range Images .....	25
Image Generation and Analysis Guidelines.....	27
Remarks .....	28

<b>Chapter III. THE VIRTUAL LIGHTING LABORATORY .....</b>	<b>30</b>
Physical and Virtual Photometry .....	34
Virtual Luminance Meter.....	35
Virtual Illuminance Meter.....	38
Virtual Contrast Meter .....	42
Virtual Integrating Sphere.....	44
Virtual Colorimeter.....	48
Virtual Scotopic Meter.....	50
Application Examples on Virtual Photometry .....	51
Remarks .....	60
<b>Chapter IV. DATA ANALYSIS TECHNIQUES IN THE VIRTUAL LIGHTING LABORATORY .....</b>	<b>62</b>
The Design Scenario .....	65
Data Analysis .....	69
Quantity.....	69
Distribution .....	72
Directionality .....	95
Glare.....	100
Spectral Content.....	101
Remarks .....	102
<b>Chapter V. DESIGN DECISION-MAKING PROCESS IN THE VIRTUAL LIGHTING LABORATORY .....</b>	<b>103</b>
Design Objectives .....	104
Design Alternatives.....	106
Analysis Results.....	106

Remarks .....	118
<b>Chapter VI. CONCLUSIONS</b> .....	119
Dissertation Summary.....	119
Contributions.....	120
Future Work.....	123
<b>BIBLIOGRAPHY</b> .....	125

## LIST OF FIGURES

### Figure

2.1. Technical features of physically based rendering within the domain of architectural lighting design and research .....	6
2.2 The calculation of the photopic light by weighting an example spectral power distribution curve with the CIE Standard Photopic Observer.....	8
2.3 RGB tristimulus space .....	9
2.4 CIE 1931 (2°) and 1964 (10°) Standard Colorimetric Observers ( $\bar{x}(\lambda)$ , $\bar{y}(\lambda)$ , $\bar{z}(\lambda)$ ), and an example on the calculation of the CIE XYZ tristimulus values .....	11
2.5 CIE 1931 Chromaticity coordinates.....	12
2.6 Comparison of the CIE 1924 (photopic - $V(\lambda)$ ) and 1951 (scotopic - $V'(\lambda)$ ) Observers .....	12
2.7 RGB discrepancy in comparison to full spectral data, as demonstrated through the interaction of incoming light with the reflective properties of materials .....	14
2.8 Definition of the sun as a light source in computer graphics.....	15
2.9 CIE standard sky models for Ann Arbor on Dec. 21, at 12:00 solar time .....	17
2.10 Luminance intensity distribution and a partial IES luminaire file.....	20
2.11 Spectral change in the reflected (transmitted) light at each wavelength with respect to the spectral properties of the incident light and the material .....	21
2.12 CIE standard illuminating and viewing (measurement) geometries.....	22
3.1 Conceptual pipeline for the VLL .....	31
3.2 HDR image analysis pipeline in the VLL.....	32

3.3	Lighting matrix, as parallel processed in the VLL .....	33
3.4	Masking, as parallel processed with lighting matrix in the VLL.....	33
3.5	Data Analysis techniques in the VLL .....	34
3.6	Mathematical model for the virtual luminance meter.....	37
3.7	Mathematical and geometric model for the virtual illuminance meter and the Nusselt Analog: illuminance is calculated from hemispherical fisheye images.....	40
3.8	Hemispherical fisheye images used to calculate the illuminance at the eye, vertical and horizontal illuminance values on the task .....	41
3.9	Mathematical, geometric, and material model for the virtual contrast meter .....	43
3.10	Mathematical, geometric, and material model for the virtual integrating sphere.....	46
3.11	Mathematical model and CIE chromaticity diagram for the virtual CCT.....	49
3.12	Mathematical model suggested for the virtual scotopic luminance meter .....	51
3.13	Virtual laboratory for CRF measurements.....	53
3.14	Ceiling views as seen by the illuminance meter while measuring the horizontal illuminance on the table.....	54
3.15	Viewer's sight as the luminance contrast variability is determined for the different source positions.....	55
3.16	CRF and CP variation with respect to the source position in physical and virtual environments .....	56
3.17	Left wall material as varied from a scotopically poor color (yellow) to a neutral (grey), and a scotopically rich color (blue).....	56
3.18	Photopic and scotopic luminance variations in relation to the yellow, grey, and blue wall materials under the same light source .....	58
3.19	CCT variations in relation to the yellow, grey, and blue wall materials under the same light source .....	58
3.20	Chromaticity values of pixel data from scenes with the yellow, grey, and blue wall materials .....	59

4.1	Data analysis techniques in the VLL .....	64
4.2	The office space during the daytime and nighttime.....	66
4.3	Set of analyzed images in VLL a) viewer looking at the computer screen, b) viewer looking at the paper task, c) viewer looking through the window, d) computer view e) paper view, f) paper: east view, g) paper: south view, h) paper: north view, and i) paper: west view .....	68
4.4	Illuminance reaching the eye throughout Dec. 21 when the viewer is looking at the computer screen, paper, and window.....	70
4.5	Horizontal illuminance on the paper and vertical illuminance on the computer screen; the IESNA recommendations for common visual tasks .....	71
4.6	Minimum, maximum, and mean luminance values in logarithmic scale throughout Dec. 21, when the viewer is looking at the computer screen .....	74
4.7	‘Maximum to minimum’, ‘maximum to average’, and ‘average to minimum’ luminance ratios throughout Dec. 21, when the viewer is looking at the computer screen .....	74
4.8	The scene is decomposed into architectural elements to study the luminance ratios .....	76
4.9	The decomposition of different scenes into architectural elements.....	77
4.10	Contrast variation on the paper and computer screen throughout Dec. 21 .....	78
4.11	The decomposition of a scene into human field of view .....	80
4.12	Luminance variations in different parts of the visual field throughout Dec. 21 .....	81
4.13	Luminance ratios (eye2pc:eye2pc, eye2pc:eye2pap, eye2pc:eye2win) in different regions of the visual field as the viewer switches between the visual tasks.....	82
4.14	Per-pixel illuminance values on the paper for Dec. 21 on selected hours.....	85
4.15	The VCR for illuminance on the paper throughout Dec. 21 .....	86
4.16	Mesh plots for the luminance distribution at nighttime when the viewer is looking at the computer screen.....	87

4.17	Luminance distribution histograms for the nighttime when the viewer is looking at the computer screen .....	88
4.18	Mesh plots for the luminance distribution on Dec. 21, at 12:00, when the viewer is looking at the computer screen.....	89
4.19	Luminance distribution histograms for Dec. 21, at 12:00, when the viewer is looking at the computer screen.....	89
4.20	Viewer's sight of the computer screen a) Clear sky with the sun b) Clear sky without the sun: the 'skylight' c) Difference of a and b: the effect of the 'sun' .....	93
4.21	Luminance distribution histograms analyzing the viewer's sight of the computer screen a) Clear sky with the sun b) Clear sky without the sun: the 'skylight' c) Difference of a and b .....	93
4.22	Rate of change in the luminance values between hourly images on Dec. 21, when the viewer is looking at the computer screen.....	94
4.23	V/H ratio for Dec. 21 on the paper in four cardinal directions .....	96
4.24	Dissection of light into the directional and diffuse components.....	97
4.25	Image subtraction method for determining the directional-to-diffuse ratio .....	98
4.26	Directional-to-diffuse luminance ratios for Dec. 21 when the viewer is looking at the paper task .....	99
4.27	Identification of the glare sources and DGI index for Dec 21, at 13:00.....	101
5.1	The base case and the design alternatives analyzed in comparison to the base case, when the viewer is looking at the computer screen on Dec. 21, at 12:00.....	107
5.2	The base case and the design alternatives analyzed in comparison to the base case, when the viewer is looking at the paper task on Dec. 21, at 12:00 .....	108
5.3	The illuminance at the eye when the viewer is looking at the computer screen and paper on Dec. 21 .....	109
5.4	Illuminance on the computer screen and paper on Dec. 21 .....	110
5.5	Comparison of the illuminance values between the horizontal and 30° tilted venetian blinds for the double skin façade alternative .....	110
5.6	The contrast on the computer screen and paper on Dec. 21 .....	111

5.7	Luminance ratios between the task and the surrounding on Dec. 21, at 12:00 .....	112
5.8	Luminance distribution patterns between the design alternatives .....	113
5.9	Luminance distribution histograms of the design alternatives on Dec.21, at 12:00, when the viewer is looking at the computer screen.....	114
5.10	Viewer's sight of the computer screen and the paper for the 'double skin façade with tilted blinds (30°)' alternative on Dec. 21, at 12:00 .....	115
5.11	The base case and the design alternatives at night.....	116
5.12	Comparison of the illuminance at the eye when the viewer is looking through the window at night .....	117
5.13	The window view with and without outside obstructions .....	118

## LIST OF TABLES

### Table

4.1. Illuminance ratios between the tasks when the viewer is looking at the computer screen, paper, and window.....	70
5.1 The maximum, minimum, and mean luminance values when the viewer is looking at the computer screen.....	113

## **ABSTRACT**

### **TRANSFORMATIONS IN ARCHITECTURAL LIGHTING ANALYSIS: VIRTUAL LIGHTING LABORATORY**

By

Mehlika N. Inanici

Chair: Mojtaba Navvab

Lighting can be better analyzed and integrated in the architectural design process through computational tools. The dissertation presents a framework for a computer generated luminous environment that supports the knowledge acquisition between the theory and the practice of architectural lighting. Most of the current lighting analyses provide tenuous links to real world applications: their theory and the methodologies are based on predominantly simplified assumptions; their applications are limited; and the indicators are based on instantaneous lighting values that ignore temporal and spatial variations.

Virtual Lighting Laboratory (VLL) proposes transformations in the utilization of physically based digital images in lighting analysis and the design decision-making process. Digital images are transformed into lighting laboratory or design settings where the user possesses manipulative and predictive power over a variety of lighting parameters and indicators. Per-pixel lighting information is extracted from the high dynamic range images through virtual meters and photometry systems. Formation and utilization of these virtual meters (luminance meter, illuminance meter, contrast meter, integrating sphere, colorimeter, and scotopic meter) are demonstrated.

In the VLL, various analysis methods come together to support and complement each other. The total, regional, and per-pixel lighting data are processed through built-in functions to study the quantity, distribution, directionality, and spectral content of lighting. The current analysis techniques are thus utilized with additional advantages. The VLL also offers unique analysis options and metrics that are pertinent to the computational approach. The high resolution measuring capabilities and novel data analysis techniques lead to the exploration and generation of new lighting indices. The transformation of psychophysical experiments from laboratory environments to real world environments is supported. On the whole, the dissertation demonstrates the flexibility of capabilities within a virtual laboratory environment to handle various lighting design and analysis problems as opposed to imposing limited number of predetermined lighting tools and metrics.

# **CHAPTER I**

## **INTRODUCTION**

### **Background**

Lighting design and research are dominated by four broad goals: to achieve visual comfort, to maximize visual performance, to create an aesthetically pleasing environment and to improve energy efficiency. Recently, a fifth goal has been introduced: to enhance the physiological health and well being through positive effects of light exposure on the human circadian system [1]. Architects and lighting designers need analytic tools to envision the performance of their designs, make sound decisions, and reduce the uncertainty of the outcome.

Lighting analyses are categorized here as quantities and indicators. The analysis with the quantities usually refers to checking the quantities and ratios with the recommendations suggested by the national and international committees. The analyses with the indicators usually refer to visual comfort and visual performance studies. Visual comfort studies address the quantitative relation between the stimulus and the sensation. Visual performance studies address the quantitative relation between the stimulus and the speed and accuracy of processing the visual information [2].

Some of these current lighting analyses provide a tenuous link to real world applications. There are three significant problems: First, the theory and the methodology of these studies are based on predominantly simplified assumptions. Second, the mathematical models cannot be easily applied to lighting design evaluations because the necessary lighting information cannot be easily determined with the mainstream

measuring equipments. Additionally, feasible methods of measuring some of the parameters have never been fully developed outside of laboratory conditions. Therefore, some of these metrics are inaccessible to most of the lighting professionals. The common tendency in practice is to make more simplified assumptions. Third, analyses are based on instantaneous lighting values, which ignore temporal and spatial variations. These deficiencies point to the need for better analytical tools for architectural lighting design and research.

Full-scale and scale model measurements and hand calculations provide limited information about the metrics of the luminous environment. Further information is attainable through computer simulation and visualization by analyzing numeric and visual data. Over the past years, significant progress has been made toward this goal, with the development of the physically based rendering tools. Light transport, reflection/refraction/transmission algorithms implemented in the physically based rendering tools simulate the properties of light in complex environments with reasonable accuracy. The computational power makes it possible to perform the lighting calculations which are too complex to be performed manually. The direct and recurrent interreflected light transport between various architectural surfaces can be modeled with different material properties and light sources.

Visual inspection of the renderings may provide useful information about the appearance of the space. There are many visual details in the luminous environment that cannot be expressed through numerical information. For instance, misaligned luminaries and disturbing light-shade patterns can be easily detected. However, due to the restricted capabilities of the display devices, it may be impossible to evaluate the quantity and quality of the architectural lighting only through the appearance of a displayed image. The current solution is to accompany the digital images with a number of analysis tools such as false-color images, daylight factor values and glare indices.

Predetermined analysis options ignores the idiosyncratic nature of each lighting design and research that might require special analysis techniques. The computationally expensive data remains embedded in digital images and is not fully utilized since the designer and the researcher does not have full control over the numerical data. This is the starting point of the research presented in this dissertation.

Recognizing the need for better lighting analysis capabilities, Virtual Lighting Laboratory (VLL)<sup>1</sup> has been developed. The VLL is an image based lighting analysis methodology, which operates with High Dynamic Range (HDR) digital images. Through appropriate modeling, rendering, and image technology, digital images are transformed into laboratory settings. The user is provided with per-pixel lighting information. The virtual laboratory is equipped with virtual lighting meters that supply the lighting data. The data is processed with several different data analysis techniques. The built-in analysis techniques can be employed or new analysis options can be developed, based on the project requirements.

### **Objectives:**

The VLL aims to provide transformations for the utilization of physically based imagery, from a representation medium where visualization and basic lighting analysis are performed, to a laboratory environment where advanced lighting analysis and experimentation can be performed. The specific objectives of the study are:

---

<sup>1</sup> Parts of the research have been presented and published in modified forms as [3-6]:

- Inanici, M.N. "Transformation of High Dynamic Images into Virtual Lighting Laboratories", *Proceedings of Eight IBPSA Conference*, Eindhoven, Netherlands, Aug. 11-14, 2003.
- Inanici, M.N. "Utilization of Image Technology in Virtual Lighting Laboratory", *Proceedings of the CIE 2003 Conference*, San Diego, June 26-28, 2003.
- Inanici, M.N. "Post-processing of Radiance Images: Virtual Lighting Laboratory", *First International Workshop on Radiance*, University of Applied Sciences of Western Switzerland, Sep. 30–Oct. 1, 2002.
- Inanici, M.N. "Application of the state-of-the-art Computer Simulation and Visualization in Architectural Lighting Research". *Proceedings of Seventh IBPSA Conference*, Rio de Janeiro, Brazil, Aug. 13-15, 2001.

- Development of the VLL framework that is flexible enough to handle various lighting design and research problems and needs;
- Endorsement of lighting analysis by making indices accessible beyond physical laboratory settings;
- Exploration of rigorous and systematic architectural lighting analysis techniques.

The goal is to enhance the integration of the lighting analysis into the architectural design process through computational tools that make the analysis more convenient, more accessible, more accurate, and more rigorous.

### **Overview of the Dissertation**

In Chapter II, physically based rendering algorithms are discussed within the domain of architectural lighting analysis. Image generation and analysis guidelines have been established to achieve meaningful lighting information from digital images.

The VLL pipeline and Virtual Photometry are described in Chapter III. The virtual meters developed in this chapter are the luminance meter, illuminance meter, contrast meter, integrating sphere, colorimeter and scotopic meter. They are used to provide the lighting data for analysis.

The analysis techniques developed in Chapter IV provide a comprehensive approach for analyzing the lighting data. Total, regional, and per-pixel data analysis techniques are employed to study the quantity, distribution, directionality, glare, and spectral content properties of light within an environment.

The design alternatives presented in Chapter V exemplify the utilization of the VLL for a design decision-making process.

Finally, Chapter VI summarizes the advances presented in the dissertation and discusses the directions for future work.

## **CHAPTER II**

### **PHYSICALLY BASED RENDERING AND IMAGE TECHNOLOGY**

Computer visualization is a powerful tool for architects. Visualization has always been the permanent part of the discipline, though it fluctuates in the wide range of 2D drawings, 3D modeling, rendering, animation, walkthrough, and full-scale immersive environments. Most of the visualization tools are used for presentation, where the sole aim is to produce visually appealing imagery. Such applications are inadequate for analysis and research. With physically based rendering techniques, it is possible to use computer generated images as performance evaluation and design decision-making tools for architectural lighting.

Lighting algorithms constitute a fundamental part in computer graphics. Physically based rendering tools use mathematical models to simulate the complex physical processes that occur during the light transport and reflection/refraction/transmission to generate digital images that mimic the physical world [7]. On one hand, computer approach facilitates the advanced lighting calculations. On the other hand, every model is a simplification and approximation of physical phenomena. The objective is to achieve meaningful and reasonably accurate photometric information that is consistent with the objectives of the analysis and research.

This chapter is not intended for software review. The Illuminating Engineering Society of North America (IESNA) software survey [8] offers a detailed list of the features of currently available lighting software packages. The scope of the chapter is to discuss the technical features of physically based rendering algorithms within the domain of the architectural lighting design and research (Fig. 2.1). The discussions are limited to

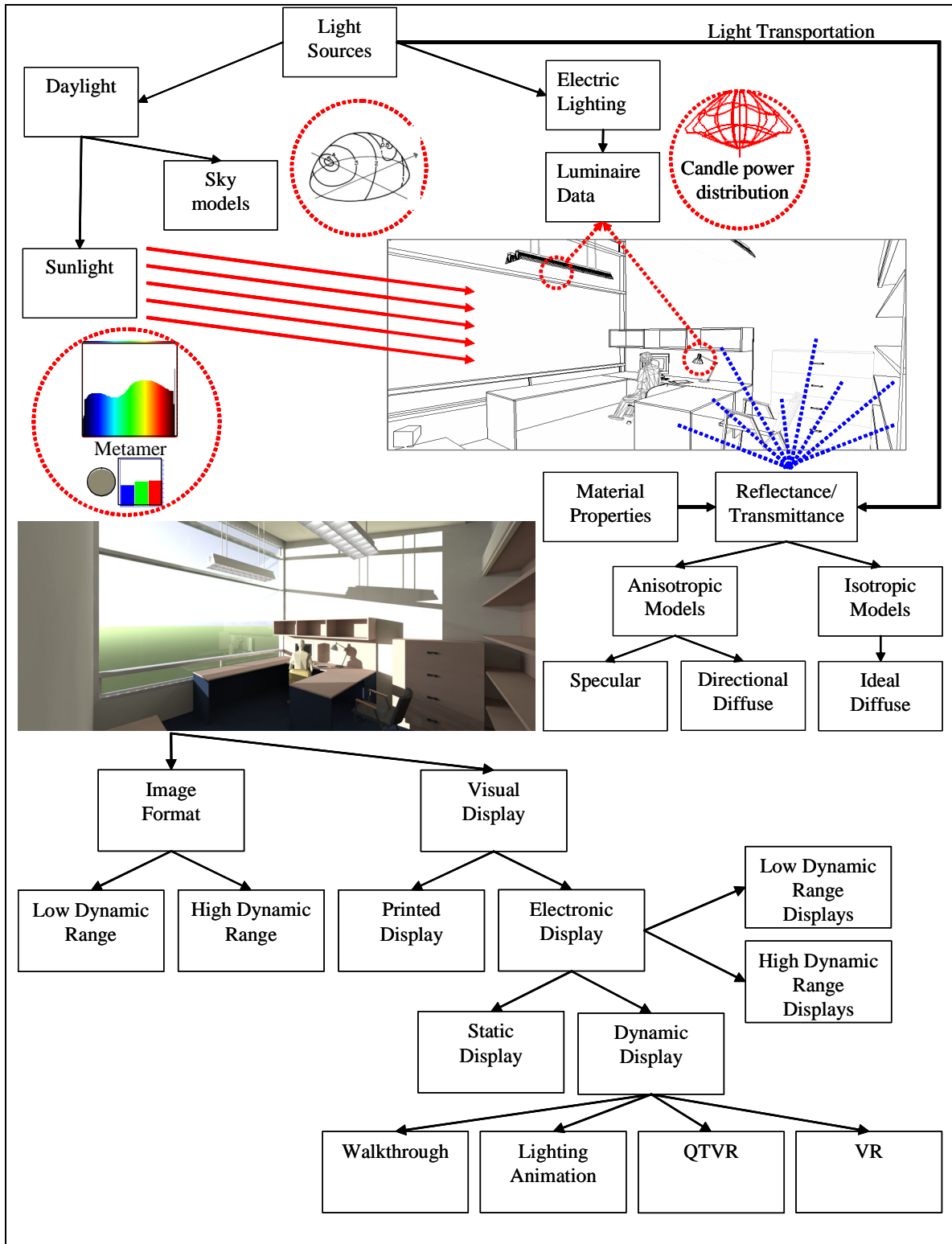


Fig. 2.1 Technical features of physically based rendering within the domain of architectural lighting design and research

algorithms where accuracy precedes computational efficiency. Simplistic light transport and reflection models that generate images without numerical accuracy are excluded.

## **Lighting in the Physical World versus Computer Graphics**

### **Definition and Modeling of Light**

As a physical quantity, light is defined as the visible portion of the radiant energy, which is capable of stimulating the retina of the human eye and producing visual sensation. Radiometry is the science of measuring radiant energy in the electromagnetic spectrum. Although light is part of the electromagnetic spectrum (extending from 380 to 780 nm), the radiometric measures cannot be used to measure light because the effect of radiation on the human visual system varies distinctly with the wavelength [2].

Photometry is a special branch of radiometry for measuring the human visual response to the visible portion of the electromagnetic spectrum. In photometry, spectral power distribution of light is weighted by the spectral luminous efficiency functions of the human eye. There are two classes of photoreceptors in the human retina, known as rods and cones. There is not a single function that represents all individuals in all conditions. Therefore, spectral luminous efficiency functions are defined based on a number of assumptions and average statistics from large groups of subjects with reference to their adaptive state of rod and cone photoreceptors [2, 9].

In 1924, CIE (Commission Internationale de L'éclairage - International Commission on Illumination) adopted the Standard Observer response curve,  $V(\lambda)$ , (a.k.a. the spectral luminous efficiency function for photopic vision). It is pertinent to cone vision and luminance levels higher than  $3\text{cd/m}^2$ . It is based on heterochromic brightness matching function obtained using  $2^\circ$  visual fields (Fig. 2.2). The basic principle is to match the brightness of any uniform light stimulus to a second stimulus by

suitably adjusting the radiant power.  $V(\lambda)$  provides the function to integrate the light at all visible wavelengths and thus, it is the basis for all current photopic lighting units, photometers, measurement techniques, and metrics [2, 9, 10].

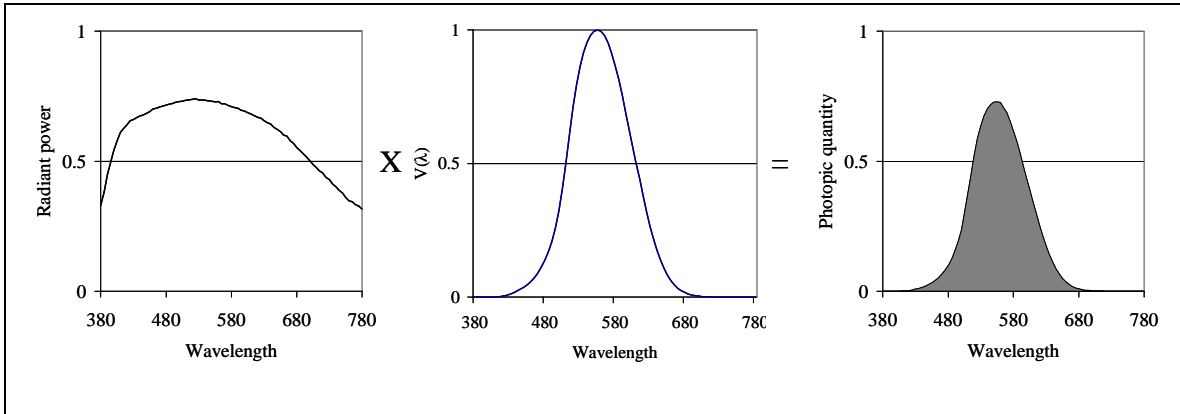


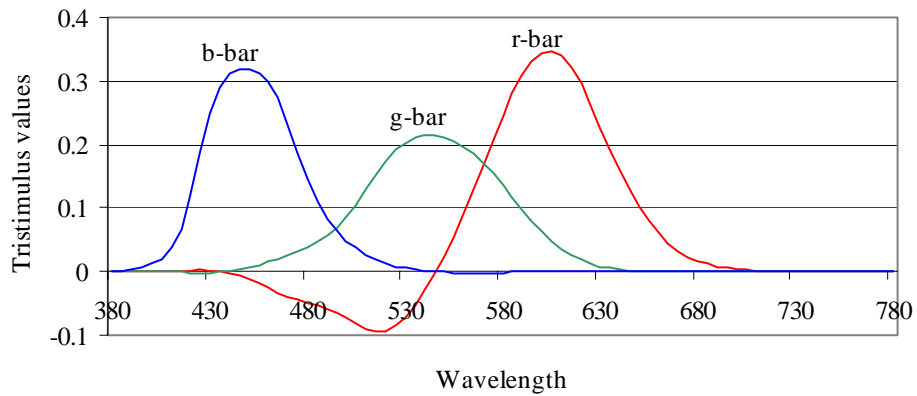
Fig. 2.2 The calculation of the photopic light by weighting an example spectral power distribution curve with the CIE Standard Photopic Observer<sup>2</sup>

The CIE has also adopted two sets of standard color matching functions: CIE 1931 and 1964 Standard Colorimetric Observers. The basic principle in color matching functions is to match the color of any light stimulus with the additive mixtures of three primary stimuli by suitably adjusting the respective radiant powers. Humans are trichromat, i.e. they perceive color through three types of cones in the retina. That is, the entire spectrum of incident stimulus is reduced to three signals at the retina. Therefore, it is possible and practical to present color stimuli in a three-dimensional space. The significance of trichromacy lies in metamerism, i.e. stimuli with different spectral properties can be perceived as color matched by the human photoreceptors if they trigger the same cone signals [10, 11].

---

<sup>2</sup> The spectral power distribution curve used in Fig.2.1 is based on data for clear glass which is measured by a spectrophotometer. The equations and the data of various CIE Standard Observer functions that are used in Figures 2.2-2.6 are taken from [10].

Red, green, and blue (RGB) are chosen as the fixed primary stimuli. In principle, any primary stimuli set can be chosen provided that any one of the stimuli cannot be matched by the other two stimuli. The specific combination has been chosen so that the set of spectral tristimulus values  $\bar{r}(\lambda)$ ,  $\bar{g}(\lambda)$ ,  $\bar{b}(\lambda)$  would yield to equal energy stimulus with unit radiant power [10, 11].



Stimulus defined by a spectral power distribution  $\{P_\lambda d\lambda\}$ :

$$(P_\lambda d\lambda)E_\lambda = (P_\lambda d\lambda)\bar{r}(\lambda)R + (P_\lambda d\lambda)\bar{g}(\lambda)G + (P_\lambda d\lambda)\bar{b}(\lambda)B$$

$$R = \int_{380}^{780} P_\lambda \bar{r}(\lambda) d\lambda$$

$$G = \int_{380}^{780} P_\lambda \bar{g}(\lambda) d\lambda$$

$$B = \int_{380}^{780} P_\lambda \bar{b}(\lambda) d\lambda$$

$\bar{r}(\lambda)$ ,  $\bar{g}(\lambda)$ ,  $\bar{b}(\lambda)$  are the spectral tristimulus values

$E(\lambda)$  is the equal-energy stimulus

$$\lambda_R = 700$$

$$\lambda_G = 546.1$$

$$\lambda_B = 435.8 \text{ nm}$$

Fig. 2.3 RGB tristimulus space

As seen in Fig. 2.3, spectral tristimulus values  $\bar{r}(\lambda)$ ,  $\bar{g}(\lambda)$ ,  $\bar{b}(\lambda)$  include negative values. A negative value denotes that the ‘negative’ amount of the primary stimulus should be added to un-saturate the original stimulus. Having negative values is inconvenient in terms of computation and instrumentation. Therefore, CIE created another colorimetric system to eliminate the negative values. It requires a linear transformation of the RGB system to an imaginary XYZ system [10].

CIE 1931 Standard Colorimetric Observer is based on the XYZ system devised for 2° visual fields. The spectral power distribution of any stimuli is weighted by the color matching functions,  $\bar{x}(\lambda)$ ,  $\bar{y}(\lambda)$ ,  $\bar{z}(\lambda)$  to compute the CIE XYZ values. It is important to note that  $\bar{y}(\lambda)$  has been appropriately chosen to match the CIE 1924 Standard Observer ( $V(\lambda)$ ). Therefore, the 1931 Standard Colorimetric Observer combines the color matching and heterochromatic brightness matching properties in a single system (Fig. 2.4) [10, 11].

In 1964, CIE adopted another standard photopic function, which is devised for a 10° visual field, denoted by  $\bar{x}_{10}(\lambda)$ ,  $\bar{y}_{10}(\lambda)$ ,  $\bar{z}_{10}(\lambda)$ . It is a supplement to the 1931 Standard Observer, and is suggested to be used with visual fields that have an angular subtense larger than 4° [2, 10].

CIE Chromaticity coordinates aims to represent color in a two dimensional space. The fractions of CIE X, Y, and Z values to their summation are labeled as CIE chromaticity coordinates, x, y, and z, respectively. The summation of x, y, and z is equal to unity; therefore it is practical to obtain a two dimensional representation by eliminating the z value. By convention, chromaticity coordinates are defined through a CIE Chromaticity diagram, (x,y), which is plotted in a rectangular coordinate system (Fig. 2.5) [2, 10].

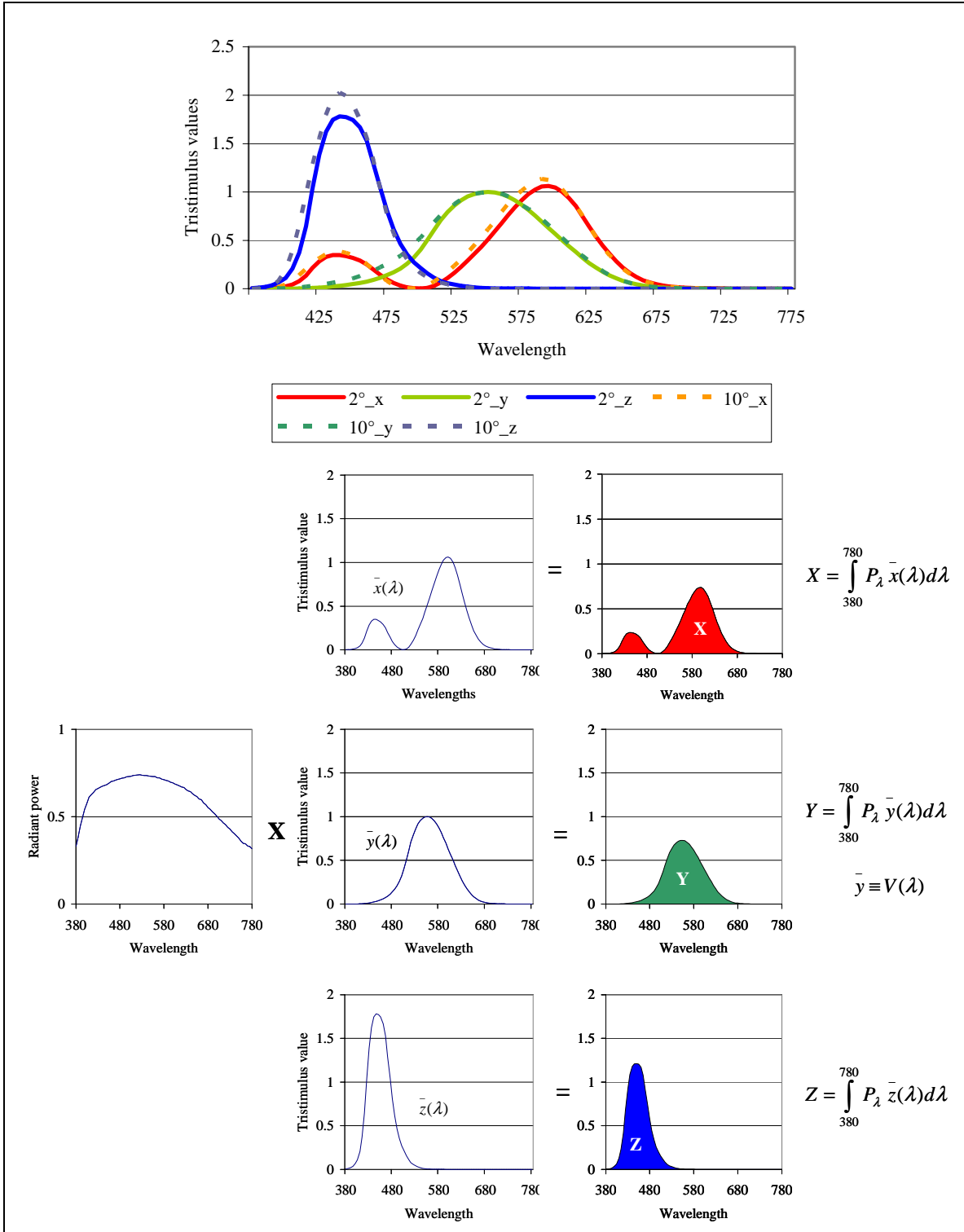


Fig. 2.4 CIE 1931 (2°) and 1964 (10°) Standard Colorimetric Observers ( $\bar{x}(\lambda)$ ,  $\bar{y}(\lambda)$ ,  $\bar{z}(\lambda)$ ), and an example on the calculation of the CIE XYZ tristimulus system

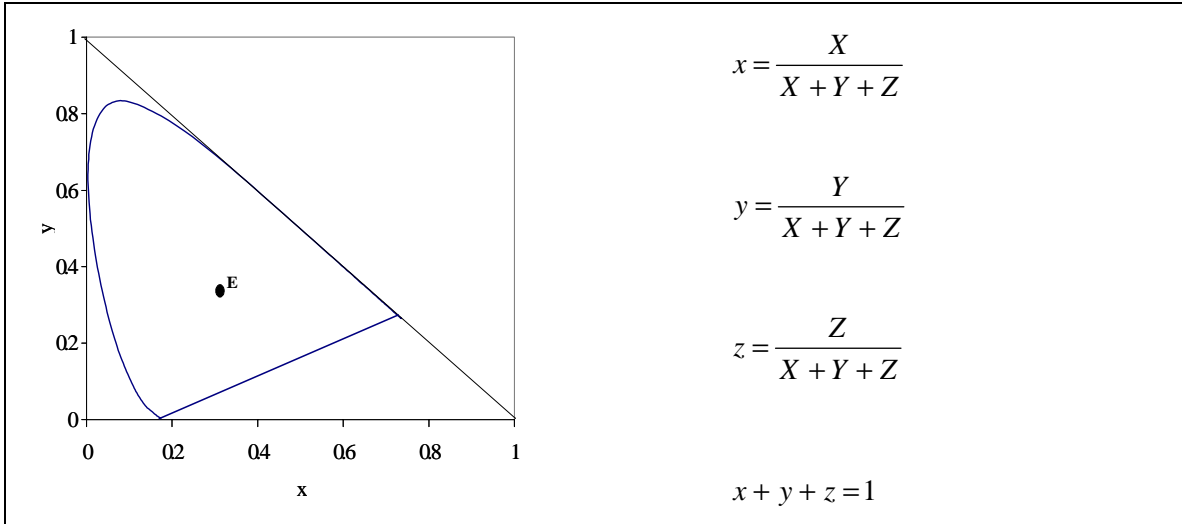


Fig. 2.5 CIE 1931 Chromaticity coordinates

In 1951, CIE adopted the Scotopic Observer,  $V'(\lambda)$ , which defines the spectral luminous efficiency function for the rod vision. The scotopic curve is based on approximately  $20^\circ$  field of view and applies to luminance levels between  $10^{-6}$  and  $10^{-3}$   $\text{cd/m}^2$  [10]. Fig. 2.6 demonstrates the comparison of the photopic and scotopic curves. In Fig. 2.5a, both curves are plotted in unity, where as in Fig. 2.5b, they are plotted in their absolute powers.

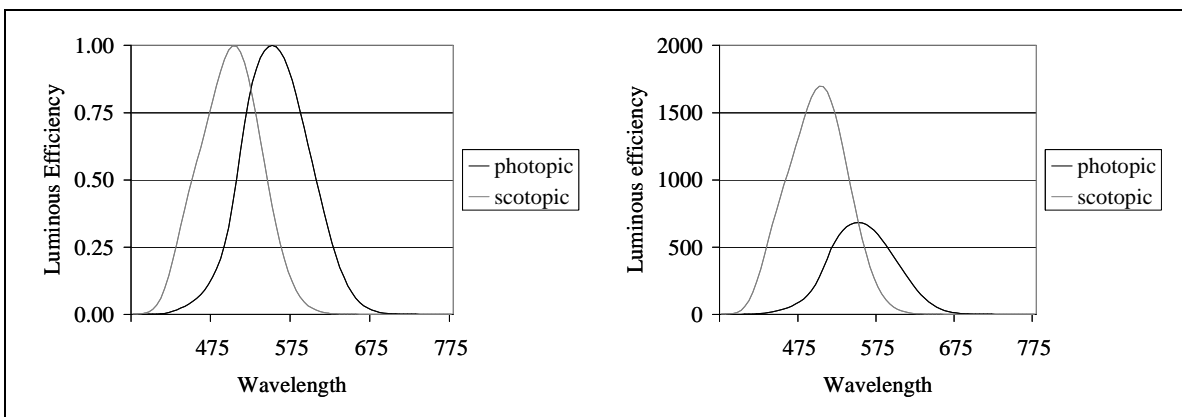


Fig. 2.6 Comparison of the CIE 1924 (photopic -  $V(\lambda)$ ) and 1951 (scotopic -  $V'(\lambda)$ ) Observers

In sum, from an architectural lighting perspective, light can be described with colorimetric and photometric quantities, in the form of 1) spectral power distribution, i.e. relative power emitted at each wavelength; 2) photopic quantities such as illuminance and luminance, as defined by the CIE (1924) Standard Photopic Observer; 3) tristimulus generalization, i.e. CIE XYZ (1931 or 1964) Tristimulus Matching Functions; 4) CIE chromaticity diagram; and 5) scotopic quantities defined by the CIE (1951) Standard Scotopic Observer. These quantities can be measured by a spectrophotometer, illuminance meter, photopic luminance meter, colorimeter, and scotopic luminance meter.

In computer graphics, computation of light at each wavelength through the visible spectrum is prohibitively time consuming. Therefore, physical properties of light are modeled through tristimulus color space such that spectral information for lights and materials are converted into, and then processed with the RGB data. RGB combinations are metamers in computer graphics for the spectral power curves of light in the physical world. The spectral distribution and the intensity of light are modeled simply by varying the RGB combinations [12, 13].

In principle, it is appropriate to use the tristimulus color space, since it is the way that the human eye perceives the light. However, there are certain discrepancies associated with the simulation of light in the RGB color space. Light and color computation involves the interaction of light source and material through three color samples. However, in the physical world, the interaction between the lights and materials occurs through the full spectrum [12-15]. Fig. 2.7 illustrates the consequences of simulating light and materials with the RGB values in comparison to the full spectral data. Additionally, as demonstrated in Fig. 2.3, the RGB color system requires negative weights for some of the spectrum colors. The colors with negative weights cannot be represented in computer environments [16]. Furthermore, computer modeling of light precludes phosphorescence, luminescence, polarization, and diffraction [17].

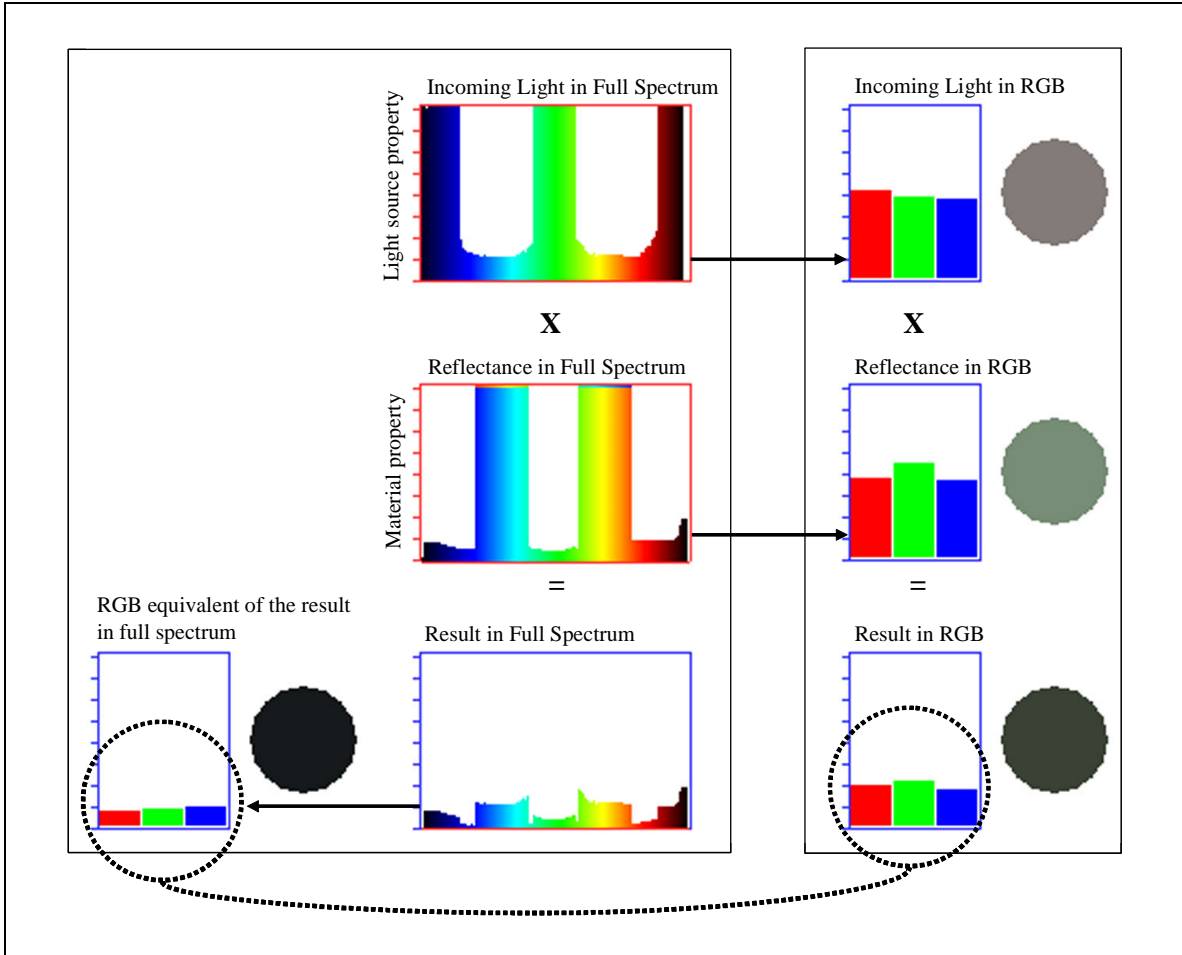


Fig. 2.7 RGB discrepancy in comparison to full spectral data, as demonstrated through the interaction of incoming light with the reflective properties of materials<sup>3</sup>

### Physically Based Modeling of Light sources

Light sources can be categorized into daylight and electric light. Each category is modeled by specific parameters and they are discussed in detail in the next subsections. The common parameters in modeling of all light sources are the spectral properties, intensity, and luminance distribution values.

<sup>3</sup> The images are generated with a Java applet from [18].

### Daylight:

The source of daylight is the sun. Yet, it is possible to categorize daylight as sunlight, which is the visible portion of the direct radiation; and skylight, which is the diffuse radiation from the sky [19].

Sunlight is a directional light source. Solar geometry calculations predict the daily and seasonal movement of the sun for a particular geographic location in terms of the intensity and direction. The input information includes the Julian day number, local clock time, longitude and latitude of the site, longitude of standard meridian, and daylight savings hour. The series of calculations include the solar declination angle, equation of time, true solar time, hour angle, solar altitude angle, and solar azimuth angle [2, 20].

In physically based rendering, the geometry of the sun is represented as a solid angle (0.5 steradian) rather than a surface or a solid so that it can be modeled as being infinitely distant from the rest of the scene [21]. The position is defined through solar geometry calculations and expressed with the solar altitude angle and the azimuth angle (Fig. 2.8). The intensity and the spectral content are expressed with the RGB values.

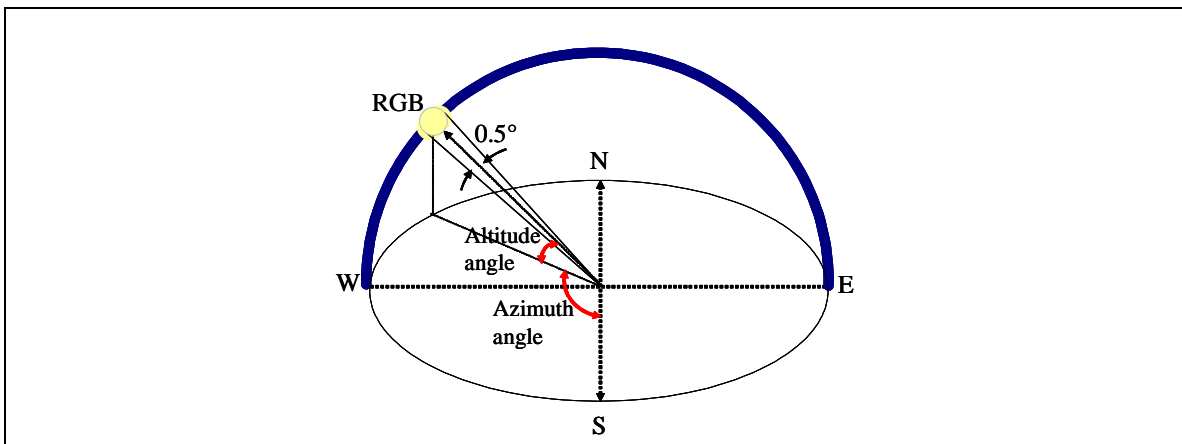


Fig. 2.8 Definition of the sun as a light source in computer graphics

Skylight is the diffuse radiation from the sun, which has been scattered in the atmosphere by dust, water vapor, and other suspended particles. The illumination produced by the sky depends on its luminance. The sky luminance depends on a series of meteorological and seasonal parameters, such as the atmospheric turbidity, water mass, temperature, and cloud cover. Theoretical sky models have been developed to represent the average sky brightness patterns as smooth continuous functions that provide the best fits to the long-term daylight measurements. The relative luminance of any point/patch in the sky is defined through two angles: the angle between the point/patch and the zenith; and the angle between the point/patch and the sun (in non-overcast skies). Obviously, the actual sky luminance distributions are far more complex than the theoretical sky models. The models do not represent the instantaneous illuminance and luminance values at any particular site. Still, they provide reference conditions and they are commonly used in daylighting simulation applications [2, 22-25].

The two extreme sky types are modeled as the CIE Standard Overcast Sky and CIE Standard Clear Sky. Fig. 2.9 illustrates the CIE sky models for Ann Arbor on December 21, at 12:00 solar time. The CIE Standard Overcast Sky [26], originally known as the “Moon and Spenser Sky” [27], has a luminance distribution that varies with the altitude of the point in the sky such that the maximum ratio is 1:3 from horizon to zenith.

The CIE Standard ClearSky [28], originally known as “Kittler Sky” [29], has a complex luminance distribution that varies with the solar position, the altitude and azimuth of the point in the sky, atmospheric moisture content, and turbidity. Complexity of the clear sky distribution is pertinent to the modeling of the circumsolar region, which significantly varies in size and intensity with turbidity and water mass values [30, 31].

The other commonly used sky types are CIE Intermediate Sky and Perez All-Weather Sky. The CIE Intermediate Sky [32] defines the luminance distribution in skies with thin or moderate cloud cover and hazy atmospheric conditions. The Perez All-Weather Sky [33] model defines the random aspects of luminance distribution based on

parameters that define the magnitude and spatial distribution of cloud patterns, such as the solar elevation, sky clearness, and sky brightness indices.

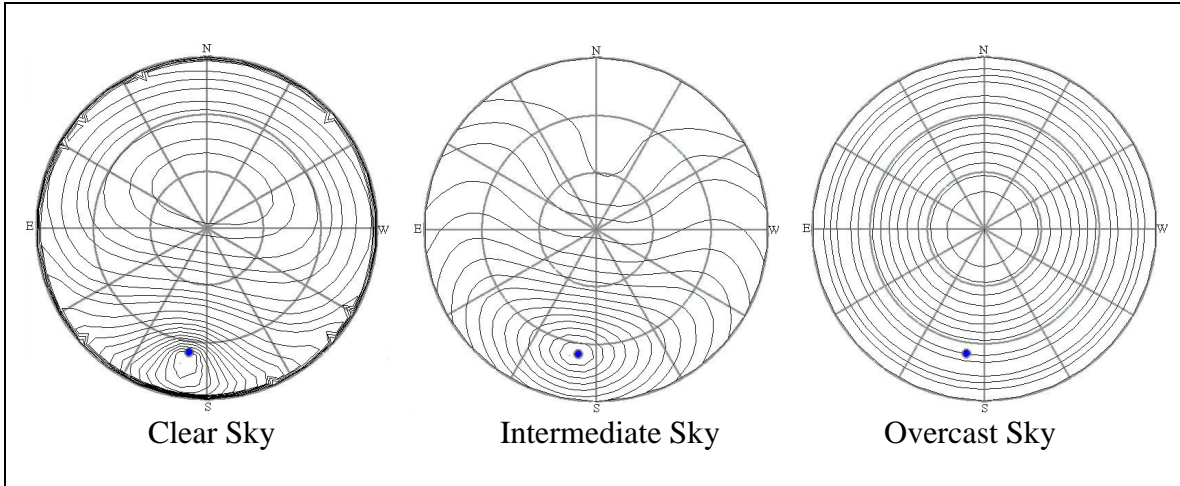


Fig. 2.9 CIE standard sky models for Ann Arbor on Dec. 21, at 12:00 solar time<sup>4</sup>

A new concept of CIE sky luminance distributions is being proposed as 15 sky models with 5 overcast, 5 clear, and 5 intermediate skies. This proposition aims to cover the whole occurrence spectrum from overcast to cloudless skies, including the different diffuse scattering and the direct sunlight effects by taking into account the local sunshine duration, turbidity and pollution situations. This proposition might enable the modeling of more dynamic daylighting models in simulation software [23, 25].

In physically based rendering, the geometry of the sky is defined through a fixed hemisphere, which is infinitely distant from the rest of the scene. The luminance distribution of the sky is defined by the theoretical sky models. The luminance distribution is seldom defined through measured luminance values that are applied as pattern modifiers to constant sky brightness [22]. The luminance intensity is either

---

<sup>4</sup> Plots are generated with a Java applet from [34], Parameters for Ann Arbor are defined as Latitude: 42°13'N; Longitude: 83°45'W, turbidity: 0.119 angstrom, moisture: 1.2 cm.

calculated from zenith luminance (or horizontal illuminance), or from the solar geometry and sky type as specified by the user.

It is known that the spectral content of daylight also changes depending on a series of meteorological, seasonal, and geographic parameters, such as the sky type, season, time of day, turbidity, and direction of observation [35]. Unfortunately, there are not any widely accepted mathematical models that describe the variability of the spectral content of daylight. In general, the simplified approach is to use a fixed sky color. Recently, two studies that aim to simulate the varying spectral content of daylight emerged. The first model [36] approximates the scattering effects of the atmosphere to model the color of daylight. The model is based on a parametric function that is fitted to daylight spectral computations, which are performed for multiple sun positions and turbidities. Perez All-Weather Sky model [33] is used to calculate the luminance distribution and Nishita et.al model [37] is used to calculate the atmospheric scattering effects. The second model [35] is based on spectral measurements of skylight. The model processes the global and diffuse horizontal irradiances, diffuse horizontal illuminance, and atmospheric precipitable water. Luminance distribution map is predicted through the Perez All-Weather Sky model [33]; color temperature is predicted based on the luminance values; and spectral content of the light is predicted based on the color temperature. Both models are developed to be used in physically based rendering tools.

### **Electrical Lighting**

A luminaire is a complete electric lighting unit that is composed of a lamp or lamps to generate light; optical devices to distribute light; housing and sockets to position and protect the lamps; connecting devices to supply electric power; and the mechanical components to support or attach the luminaire. The common types of lamps are incandescent filament, fluorescent, and high intensity discharge. Commonly used optical devices are reflectors, refractors, diffusers, and louvers [2].

The manufacturers document the luminaire photometric performance through photometric reports which include the physical description of the lamp and the luminaire and photometric measurements of the output. Luminous intensity values are specified in an angular coordinate system and they are determined from laboratory measurements that are done through far-field photometry. That is, the measurement distance is at least five times longer than the longest distance of the luminaire. It is assumed that the total luminous flux is emitted from the photometric center of the luminaire. The luminous intensity distributions can be plotted as polar graphs (Fig. 2.10). The intensity value at each horizontal angle is plotted in the spherical coordinate system as the vertical angle varies between  $0^\circ$  to  $90^\circ$  (or  $180^\circ$  for direct-indirect luminaires) [2].

In physically based rendering, electric lighting is simulated through luminaire geometry, luminous flux, color information, and candlepower distribution. Luminaire geometry can be constructed using any modeling software, similar to the modeling of the rest of scene. The luminance intensity distribution is supplied by one of the standard file formats for the electronic transfer of photometric data such as IESNA LM-63-2002 [38], CIE 102-1993 [39], and ELUMDAT [40].

It is common to model the luminance distribution with an invisible impostor to circumvent the actual complexities of the luminaires such as parabolic surfaces, louvers, diffracting lenses, convex or concave mirrors. These models provide a reasonable approximation because the candlepower distribution curves are generated from the measured data that already accounts for the geometric complexity of the luminaires [41]. Yet, it is important to realize that the luminous intensity distribution stored in standard file formats is a data of a single plane, which is an average of all horizontal planes [42]. The luminous flux and spectral content are expressed as RGB values. The total luminous flux can be either computed from the intensity distribution data or specified by the user.

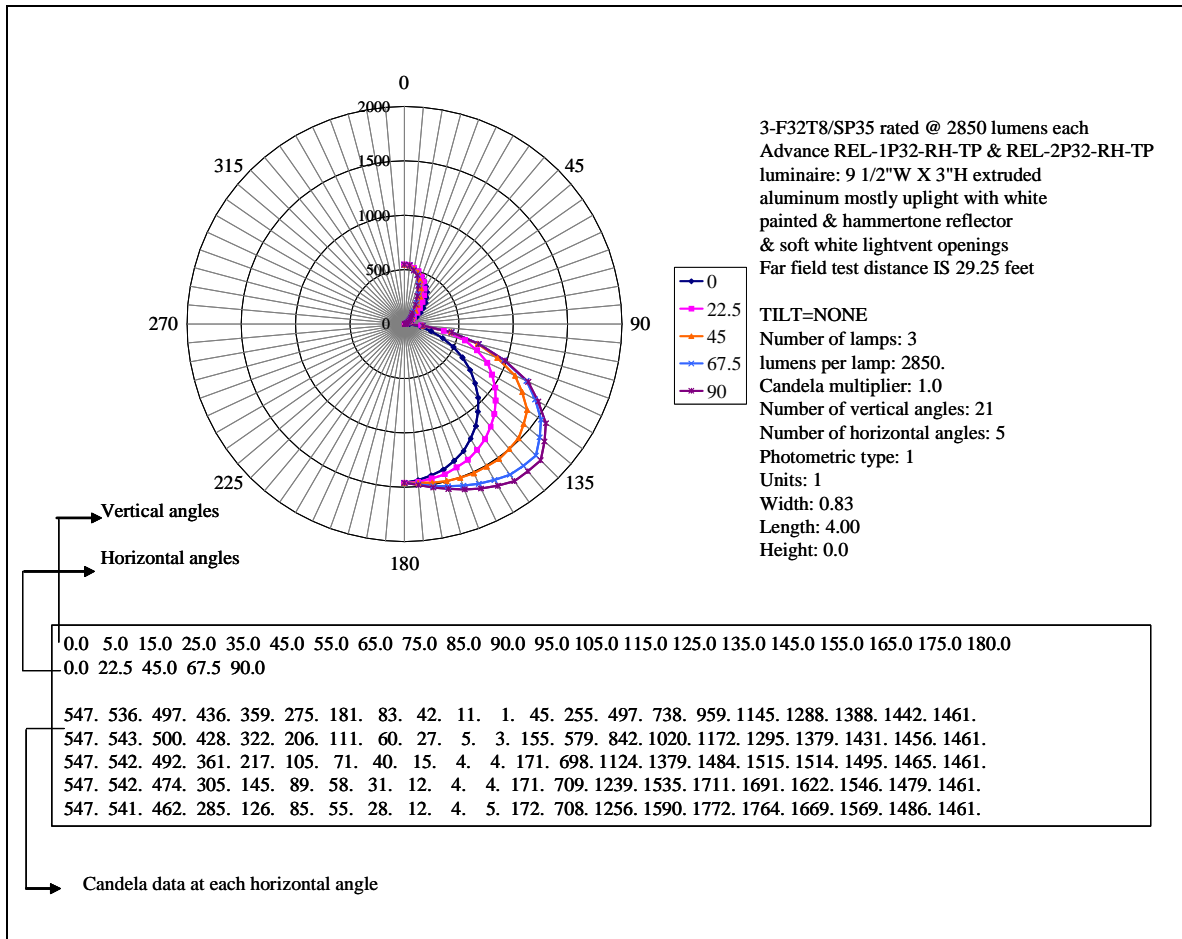


Fig. 2.10 Luminance intensity distribution and a partial IES luminaire file

### Physically Based Modeling of Material Appearance and Light Absorption, Reflection, and Transmission

In the physical world, light and material interaction results in various combinations of reflection, transmission, and absorption. The result of this interaction depends on the material properties, spectral properties of the light source and the material, and the goniometric properties of the light source and the viewing direction (i.e., the angle from which the incident light reaches the material, and the angle from which the material is viewed or measured) [11, 43].

Materials have series of effects on the reflected (transmitted) light. The intensity of the incident light is modified by the reflecting ability and surface properties of the material. The spectral content of the incident light is modified by the spectral properties of the material (Fig. 2.11) The goniometry of the incident light is modified by the surface roughness of the material: Smooth surfaces cause specular reflections whereas rough surfaces cause diffuse or directional diffuse reflections due to the subsurface reflection, diffraction and interference effects [11, 43, 44].

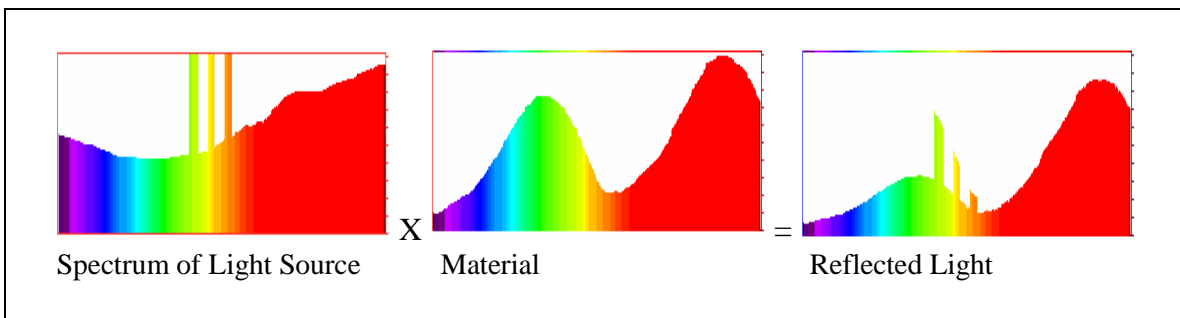


Fig. 2.11 Spectral change in the reflected (transmitted) light at each wavelength with respect to the spectral properties of the incident light and the material<sup>5</sup>

Measurement of light reflection (transmission) has been defined through standards. The CIE recommends using standard light sources with well defined spectral radiant power distributions [10]. The CIE also recommends four standard illuminating and viewing (measurement) geometries. In general, the illuminating and viewing geometries are defined as hemispherical, conical, and uni-direction (Fig. 2.12). The geometry of uni-direction/uni-direction (corresponding to illumination/viewing angles) is called bidirectional. Two of the CIE geometries are bidirectional, and they are labeled as 45°/normal (45/0) and normal/45° (0/45). The other geometries are diffuse/normal (d/0: a hemispherical incident light on the sample surface and uni-directional collection of the

<sup>5</sup> The images are generated with a Java applet from [18].

reflected light surrounding the sample) and normal/diffuse (0/d: a uni-directional incident light on the sample surface and hemispherical collection of the reflected light surrounding the sample) [9-11].

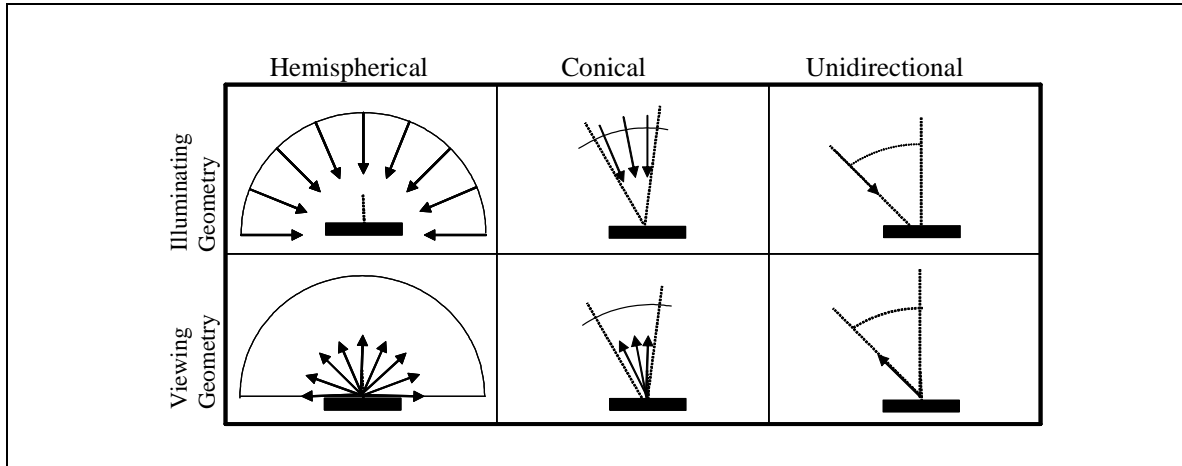


Fig. 2.12 CIE standard illuminating and viewing (measurement) geometries

The three primary instruments used for the physical measurements of reflected (transmitted) light are spectrophotometer, goniophotometer, and integrating sphere. The spectrophotometer measures the amount of light as a function of wavelength. A goniophotometer uses bidirectional geometries to measure the directional distribution characteristics of the reflected light. An integrating sphere measures the total luminous flux reflected from the material. The integrating sphere geometry facilitates a '0/d' geometry [2, 9-11].

Physically based modeling of material properties is somewhat different than the physical properties of real materials. Many mathematical models have been developed to describe the material appearance and physical behavior of reflection/transmission/refraction through the color and spatial distribution. It has not been possible to develop a unified model that would define all materials through a single practical equation, or set of equations [17]. Therefore, taxonomy of material models

(such as plastic, metal, dielectric, and etc.) has been built to describe the different material groups. Mixed models are usually handled in a modular format, such that each module forms the node of a tree and each node produces one or more of the appearance parameters [44].

Instead of reviewing the numerous appearance and reflection models developed over the years by the computer graphics professionals, common features of physically based modeling are listed here. The isotropic reflection is the ideal (Lambertian) diffuse reflectance/transmittance. The anisotropic reflection includes the specular and directional diffuse reflectance/transmittance. Most surfaces are neither ideal diffuse or specular. Therefore, a general reflecting model has been defined to predict the continuum of the diffuse, directional diffuse, and specular components of the reflected light. Bidirectional reflectance distribution function (BRDF), is a function that captures these components. It defines the fraction of the total reflected light in a specified uni-direction to the incident light onto the surface from another specified uni-direction. In general, goniometric properties are captured through two key components: microfacet distribution and Fresnel reflection. Surface roughness is modeled by using microfacets. Specular reflection is the result of first reflections from one or few microfacets. Diffuse reflection is the result of interreflection from several facets. Fresnel reflection models the increased reflectivity at grazing angles [16].

For transparent surfaces, the bidirectional transmission distribution function (BTDF) is employed. The total reflected (transmitted) light can be calculated by integrating the function over the surrounding hemisphere (sphere) [17, 45]. BRDF/BTDF data is seldom acquired through goniometric measurements.

## Physically Based Modeling of Light Transport

Light leaving a surface originates either by direct emission or by reflections or transmissions within the environment. Light reaching a surface comes either directly from a light source or from reflections and transmissions [7]. These complex interactions can be computed with the Kajiya rendering equation [46], which is the summation of the intensity of the emitted light and the scattered light toward a specified direction from all other surface points. Radiosity (finite element method) [47] and ray tracing [48] are the two generic global illumination algorithms that are employed to solve the rendering equation.

The principle idea in radiosity is the luminous equilibrium, which suggests that the direct and interreflected light reach a stable state within an enclosed space. In the stable state, all surfaces can be treated as light sources. The classic radiosity algorithm is based on the assumption that the interreflected light comes only from the diffuse surfaces. Each surface is subdivided into a number of patches. The lighting distribution is solved through a set of linear equations that computes the light exchange between all patches [2, 16, 49].

Studies have been done either to simplify the solution of the radiosity matrix or to model the non-diffuse reflection components. Overall, the radiosity approach poses theoretical and practical problems for non-diffuse surfaces and complex geometries [16, 49].

Ray tracing is a point-sampling technique that uses a tree of rays to trace the beams of light within a scene. In classic ray tracing, rays are traced backward from the eye into the environment through the pixel grid. When a ray intersects with a surface, new rays are spawned toward the light source direction and toward the reflection and/or refraction direction. The process is recursively repeated until the maximum number of reflections has been reached [16, 17, 49].

Basic ray tracing is limited to specular reflections and direct illumination. Subsequent ray tracing algorithms include Monte Carlo methods to integrate other effects such as diffuse and directional diffuse reflections, depth of field, motion blur, and caustics. Overall, ray tracing is a powerful approach for modeling the light transport. It may produce noise in rendered images, which can be eliminated with sufficiently large number of rays [17, 49].

### **High Dynamic Range Images**

The dynamic range of luminance values encountered in architectural spaces can be vast. The luminance variation from the starlight to sunlight is 14 logarithmic units ( $10^{-8}$  to  $10^6$  cd/m<sup>2</sup>) [50]. Physically based rendering tools and HDR photography techniques<sup>6</sup> produce images with pixel values that cover the total luminance span. However, both the display and storage of this data is troublesome.

#### **Digital Displays**

Computational accuracy does not necessarily produce a visual match of the real-world scene. Limited dynamic range, spatial resolution, and the color gamut of the display or printing devices are technical limitations that hinder the usability of a displayed image for the evaluation of the lighting analysis [50].

In a scene, the eye can adapt to the dynamic luminance ranges of 4 logarithmic units at once [2]. The conventional display devices limit the luminance range to a dynamic range of only 2 logarithmic units [52]. Regardless of source of origin, any displayed image faces this limitation. Therefore it is not possible to perceive large

---

<sup>6</sup> HDR photography, as coined by Debevec [51] is based on a method of capturing the complete dynamic range of radiances through multiple photographs taken with different amounts of exposure. The response function of the imaging process is recovered from these multiple photographs in order to be used as a scaling factor to fuse the multiple photographs into HDR imagery where the pixel values are proportional to the radiance values in the scene.

luminance differences, spectral characteristics or glare from a displayed image. However, it is important to emphasize that this is the limitation of the display<sup>7</sup>, rather than computation.

### **File Format**

The numerical data embedded in digital images can be invaluable for advanced lighting analysis. Image formats describe the means of storing images in electronic files. In physically based rendering, floating-point color representations are used internally, but the display and storage of this data is not feasible. For storage, the data is usually clipped into 24 bit/pixel integer values, which allows a dynamic range of about 2 logarithmic units. This solution is efficient in terms of disk space, but the lost information is irrecoverable in terms of extracting absolute photometric information, performing operations outside the dynamic range of the stored values, and readjusting the exposure.

For lighting analysis purposes, it is necessary to keep the original quantities with an adequate image format. There are image formats that enable the storage of HDR lighting data with lossless algorithms. RGBE (Red-Green-Blue-Exponent) format [57] maintains floating point data with a 32 bit encoding with an 8 bit mantissa allocated for each primary (RGB) that share a common 8 bit exponent. It can store a dynamic range of 76 logarithmic units. The 32-bit Logluv TIFF format [58] covers a range of 38 logarithmic units. The OpenEXR format [59] covers a range of 9.6 logarithmic units.

---

<sup>7</sup> The low dynamic range display problem is handled in two channels, as a software and hardware problem: As a software solution, tone mapping algorithms are developed. Tone mapping is a process to compress the luminance data from the absolute values to the display luminances. There are many different tone mapping operators. The algorithms usually utilize the threshold contrast sensitivity functions and/or spatial vision models to match the perceptual responses of a scene observer to the responses of the display observer by simulating the changes in threshold visibility, color appearance, visual acuity, and sensitivity over time that are caused by visual adaptation [52-54].

The hardware solution is an emerging new technology which is the HDR display systems. Two of them are briefly mentioned here: The system introduced in SIGGRAPH 2003 Emerging Technologies Program [55] is a HDR display device that has a luminance range of 10000cd/m<sup>2</sup> to 0.01cd/m<sup>2</sup>. The second display system [56] combines a 120° field of view stereo optics with an intense backlighting system (20,000 cd/m<sup>2</sup>) and layered transparencies to produce the full dynamic range of the human visual system.

## **Image Generation and Analysis Guidelines**

From an architectural lighting analysis perspective, it is crucial to generate digital images with reasonably accurate photometric data. There are essential criteria in order to achieve meaningful photometric information in absolute values and physical units. The image generation and analysis guidelines have been recapitulated here:

### **Image Generation:**

- The space should be reproduced in a computer-generated environment with reasonably accurate geometry, material properties, and photometry.
- The computer modeling should allow defining various sky conditions, at least the CIE standard sky models. Likewise, the wide range of luminaire libraries is highly desirable, with the capability of creating new luminaires. The luminaire descriptions should include geometry, lumen output, color information, and candle power distribution data.
- The algorithms should be capable of accurately describing the diffuse, directional diffuse, and specular characteristics of reflection and transmission. The computer modeling should allow measurable information as the material properties input.
- The software should employ global illumination algorithms that are capable of simulating the light transport within complex geometric environments with reasonable certainty.
- Computations are valid only if they are not extrapolated beyond the limited range of assumptions and restrictions of the algorithms. It is important to note that validation studies are needed to assess the accuracy of the results. These studies should range to cover complex geometries, various material properties, and daylighting and electric lighting.

- The absolute and physical units of photometric data should be stored in a file format that enables the storage of absolute HDR quantities.

#### Image Analysis:

- The rendering software internally defines the CIE chromaticity coordinates of the RGB values. CIE trichromaticity values for each pixel can be quantified from the RGB values.
- HDR images have dynamic lighting variation that is much wider than the display media. The data may be clipped or compressed through tone mapping operators. If these operations alter the pixel values, the alteration should be reversed before the CIE XYZ conversion. Another approach is to adjust the exposure to optimize the visibility of different areas of the scene over the wide range. Exposure value is a linear scaling factor applied to pixel values to map the computed luminance to the appropriate display range [60]. Exposure value is needed to compute the absolute CIE XYZ values.
- Color computation is based on linear intensity values. However, display devices like CRT's cannot produce a light intensity that is linearly proportional to the input voltage. Gamma correction is the process of balancing the nonlinearity of the display device, and is either stored in the image file, or executed at the time of display. The first technique assumes a certain gamma value and alters the pixel values accordingly [61]. Again, this operation has to be reversed before the CIE XYZ conversion.

#### Remarks

The digital images that are generated with these guidelines can be used for architectural lighting analysis. A common analysis tool is false color images (or contour lines), where a range of colors (or colored lines) is assigned to luminance or illuminance

values. Such analysis helps to visualize the luminance and illuminance distributions within a space. Still, the computationally expensive data remains embedded in the image and it is not fully utilized since it is not numerically studied for further lighting analysis.

A number of studies have been done to utilize physically based imagery for numerical lighting analysis. Daylight factor analysis and the tabulation of luminance and illuminance values in a specified grid on a specified surface or plane are some of the commonly used approaches. On a more advanced level, visual comfort computation [62] has been implemented to locate and quantify the glare sources with a selected discomfort glare index. Ashdown [63] has coined the term “virtual photometer”, which refers to calculation and display of 3D illuminance metrics (mean spherical illuminance, mean hemispherical illuminance, mean cylindrical illuminance, and mean semicylindrical illuminance). Another approach employs a spreadsheet-like lighting analysis tool [64] for manipulating the two dimensional spatial and temporal data for illuminance values on a workplane.

Predetermined analysis options ignore the idiosyncratic nature of each lighting design and research that might require special analysis techniques. The framework presented in Chapter III, proposes new transformations for the utilization of the physically based imagery from simple and rigid analysis tools to an advanced and flexible environment for the architectural lighting design and research.

## CHAPTER III

### THE VIRTUAL LIGHTING LABORATORY

“Virtual Environment’ is “*a computer system that generates a three-dimensional graphical ambient known as virtual world*” [65].

‘Laboratory’, is “*a place equipped for experimental study in a science or for testing and analysis; a place providing opportunity for experimentation, observation, or practice in a field of study*” [66].

The VLL is a computer generated environment where the user is provided with per-pixel lighting information extracted from high dynamic range digital images to perform lighting analyses and experiments. Digital images are transformed into lighting laboratory settings where the user possesses manipulative power over a variety of design decisions including geometric, photometric, and material properties; and predictive power over a variety of indicators including lighting quantity, visual comfort and performance indices. The idea is to provide the ‘laboratory environment’ to the designer and researcher to experiment and explore various lighting analysis techniques instead of imposing limited number of predetermined lighting metrics and tools.

From a programming perspective, the VLL is a collection of functions<sup>8</sup> developed in a toolbox style. A conceptual division of the VLL pipeline is given in Fig. 3.1. The main function of the pipeline is to facilitate the advanced lighting analyses. The pipeline starts with HDR imagery; progresses through a computer environment, which is equipped with lighting metrics, meters, and data analysis techniques; and ends with lighting

---

<sup>8</sup> Matlab<sup>®</sup> (Matrix Laboratory) [67] is used as the programming and data analysis environment. Matlab Language is a matrix/array programming language, which is very convenient for handling digital images that are composed of matrices.

analysis results. Each of these steps is a pipeline or parallel process in itself, which consist of several sub-steps. A pipeline process refers to steps that are executed sequentially, such that the output of a former step is an input for the latter one. A parallel process refers to steps that are executed independently on different portions of data by different functions [68, 69]. Each step or sub-step is written as a function, and completes a part of instruction.

Pipeline and parallel processes are commonly used in assembly lines and computer architectures. The idea is to speedup a well defined, fixed process. Instructions can be executed through the stages to yield a fixed product, such as the production of a car in an assembly line. In VLL, this approach has been adopted to provide flexibility. It is an efficient implementation technique where multiple functions can overlap in execution and can be linked in a command pipeline for a combined purpose. The toolbox style is used to form different pipeline and parallel processes through different combinations of functions. This is important for customizing the laboratory for specific problems. It is always possible to script new functions, reconfigure the analysis techniques, and expand the functionality of the laboratory for different experiment and research needs.

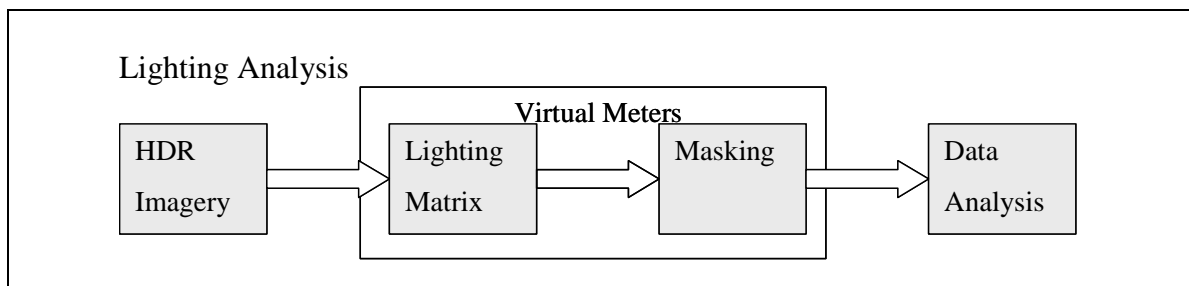


Fig. 3.1 Conceptual pipeline for the VLL

The different stages of the pipeline are briefly explained here, where the focus is on conception rather than implementation. The first stage, HDR imagery, is a pipeline process, where absolute values of CIE XYZ are extracted from images through a series of mathematical operations (Fig. 3.2). VLL can operate with any digital image that satisfies the guidelines listed in Chapter II. The key idea is to process the images that contain meaningful and reasonably accurate photometric information<sup>9</sup>. Strictly speaking, the user should be aware of the restrictions and assumptions of the image generation process to be able to interpret the results.

The HDR imagery (for instance, an RGBE image) is converted into floating point RGB numbers. CIE XYZ data for each pixel is quantified from the RGB values through conversions using the CIE 1931 Standard Colorimetric Observer Functions (as explained in detail in Fig. 3.6) [10]. These functions are suitable for pixel calculations because they are based on a 2° field of view and recommended for fields subtending 1-4°.

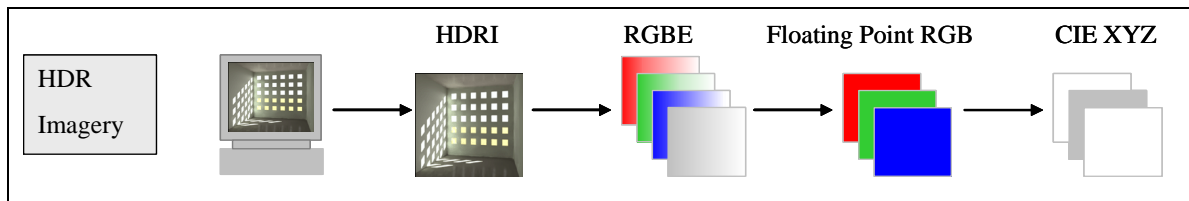


Fig. 3.2 HDR image analysis pipeline in the VLL

<sup>9</sup> In this dissertation, HDR images are generated with the Radiance Lighting Simulation and Rendering System [70]. Radiance is a physically based rendering software that is custom-made for architecture and lighting design. Radiance uses a backward ray-tracing method that efficiently blends the deterministic and stochastic (Monte Carlo) techniques in local and global illumination methods. Specular, diffuse, and directional diffuse reflections and transmissions are successfully modeled.

Radiance images are composed of HDR pixel values that correspond to the physical quantity of radiance. The radiance value is computed in three channels as floating point numbers and stored in RGBE format as integer values. Based on the chromaticity coordinates that represent the set of computer display phosphors and white point chromaticities, images can be post processed to retrieve the original radiance and luminance values [57, 60, 71].

The lighting matrices are calculated from the CIE XYZ values as parallel processes. The matrices consist of per-pixel values of photopic luminance, scotopic luminance, correlated color temperature, and CIE chromaticity coordinates (Fig. 3.3).

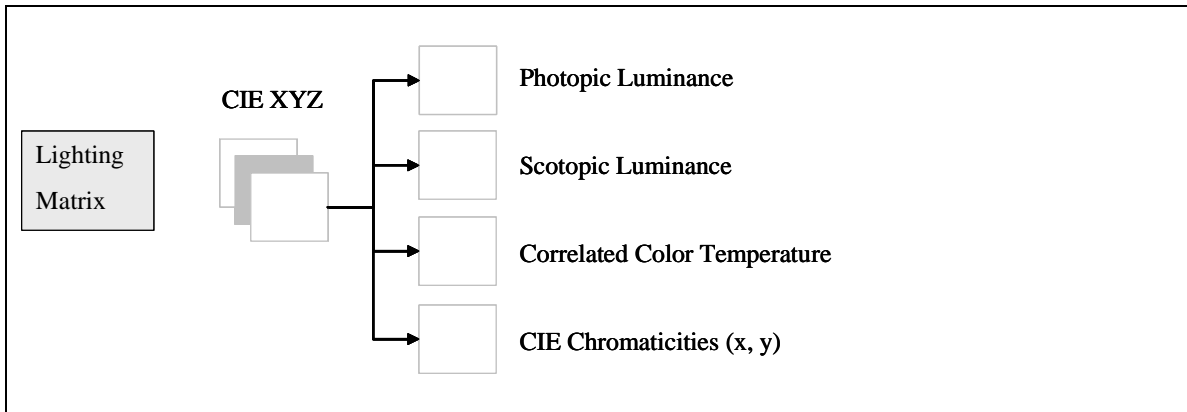


Fig. 3.3 Lighting matrices, as parallel processed in the VLL

The lighting matrices are then decomposed into regions through a masking process. The decomposition is done for the data analysis purposes. The masking process is categorized into three as fisheye mask (circular mask), element masks (such as the task and background), and vision masks (such as foveal mask, binocular mask, and peripheral mask) (Fig. 3.4). These categories are linked with the data analysis techniques.

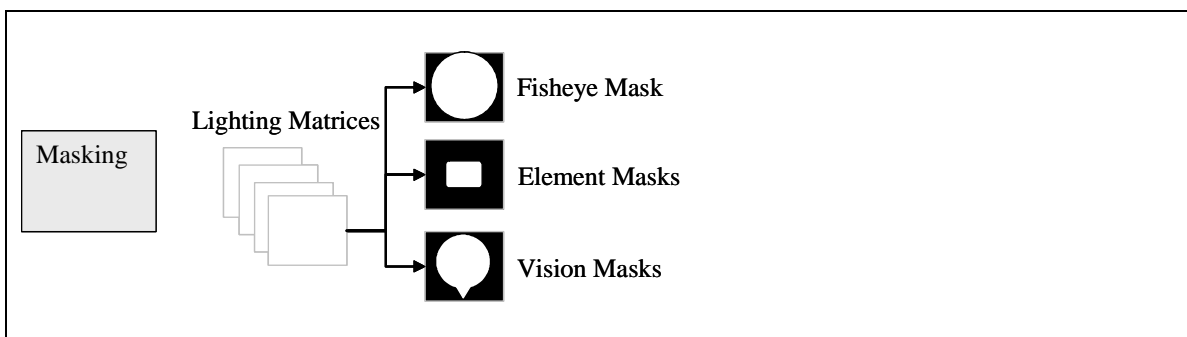


Fig. 3.4 Masking, as parallel processed with lighting matrix in the VLL

The data analysis techniques are broadly categorized as total data analysis, regional analysis, and per-pixel analysis (Fig. 3.5). The categorization refers to the parts of the lighting matrix being analyzed.

Virtual meters in the virtual laboratory correspond to the physical measuring equipments that are used in physical laboratories, field measurements, and full-scale and scale models measurements. In this chapter, physical and virtual photometries are discussed and compared. The theory, implementation, and application of various virtual meters are presented.

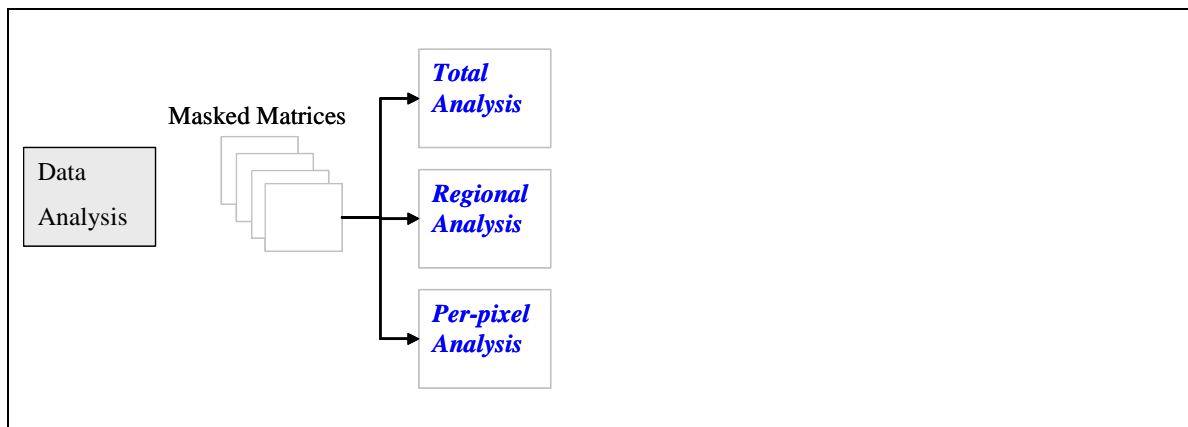


Fig. 3.5 Data Analysis techniques in the VLL

### Physical and Virtual Photometry

Various photometers can be built by filtering the electromagnetic radiation by the CIE Standard Observer and Colorimetric Observer Functions. Photometric measurements are done through a variety of instruments that are either used as discrete photometers or in combination with other instruments as photometer systems. These measurements are referred to as “*Physical Photometry*”. The common instruments are [2, 72]:

- Illuminance meters (illuminance)
- Luminance meters (luminance)

- Integrating sphere photometers (total luminous flux)
- Goniometers (luminous intensity)
- Spectroradiometers (spectral power distribution)
- Colorimeters (color temperature)

Virtual meters and photometer systems are developed by applying CIE Standard Observers and Colorimetric Observer Functions to per-pixel data extracted from HDR images. The fundamental equipments in the VLL are the virtual luminance meter, illuminance meter, contrast meter, integrating sphere, colorimeter, and scotopic meter.

### **Virtual Luminance Meter**

Luminance is defined as the luminous intensity leaving, passing through, or arriving at a surface per unit area in a given direction. It is the metric that thoroughly describes the scene as perceived by the human visual system [2]. In Physical Photometry, luminance can be measured one at a time by a luminance meter. Alternatively, cameras equipped with a charge-coupled devices capture and digitize electronic images of visual scenes. These digital images may be used to determine the luminance at a pixel scale with adequate precautions. However, capturing the complete dynamic range of luminances is challenging: lens distortion has to be adjusted; and multiple images have to be captured at different exposure settings to obtain the HDR luminance values [2, 51].

Luminance is the fundamental photometric quantity in Virtual Photometry. It is the value stored in a pixel. In physically based rendering, RGB values are calculated through radiance values in three channels, which represent the intensity reflected from a surface towards each pixel. The mathematical model for quantifying the CIE XYZ values from RGB data is shown in Fig. 3.6.

The image generation process refers to a particular set of RGB values, which are defined by their CIE chromaticity coordinates. First, floating point RGB values are

calculated from RGBE integer values<sup>10</sup>. The conversion from RGB to CIE XYZ is done through a matrix, which takes a three element vector representing an RGB color and transforms it to an equivalent XYZ vector<sup>11</sup> [17]. The CIE Y curve is the CIE Standard Observer Function,  $V(\lambda)$ , that is used to convert radiance to luminance<sup>12</sup>.

It is necessary to compare the physical and virtual photometry for measurement uncertainties. In physical photometry, calibration of the equipments is an important factor for the measurement uncertainty. The expected errors in physical luminance meters are listed as follows:  $V(\lambda)$  match (3%), UV response (0.2%), IR response (0.2%), directional response (2%), effect from the surrounding field (1%), linearity error (0.2%), fatigue (0.1%), polarization (0.1%), and errors of focus (0.4%). The percentage values are published by the CIE [73] and they correspond to representative errors that are collected from the best available commercial instruments. The error total is 7.2%.

---

<sup>10</sup> RGBE images are composed of matrices with a data array of m-by-n-by-4 array, where m and n stands for the image resolution; and 4 stands for red, green, blue, and exponent components that are defined for each individual pixel. Floating point RGB is calculated from RGBE integer values as follows [57]:

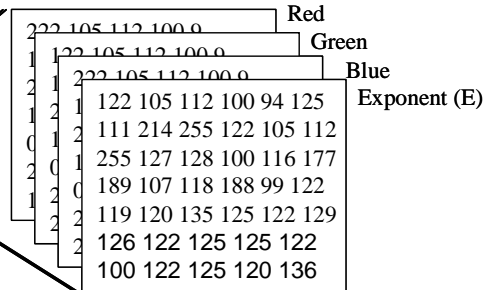
$$red = \frac{R}{255} * 2^{(E-128)}, \quad green = \frac{G}{255} * 2^{(E-128)}, \quad blue = \frac{B}{255} * 2^{(E-128)}$$

The excess '128' notation produces a signed exponent. RGBE values of [1, 1, 1, 1] would yield to RGB values of [2.3E-41, 2.3E-41, 2.3E-41] and RGBE values of [255, 255, 255, 255] would yield to [1.7E+38, 1.7E+38, 1.7E+38].

<sup>11</sup> The RGB-to-XYZ matrix, as denoted 'N' in Fig. 3.6, is constructed with the matrix of RGB chromaticities (denoted by 'K'), which are differentially scaled to achieve the unit white point balance (denoted by 'W') [17].

<sup>12</sup> In calculating luminance (L), CIE Y is multiplied by a constant and divided by the exposure value. The constant is the standard luminous efficacy of equal-energy white light, which is 179 lumens/watt. RGB value of (1,1,1) is equal to a total energy of 1 watt/steradian/m<sup>2</sup> over the visible spectrum; and 1 watt/steradian/m<sup>2</sup> is equal to a photopic luminance of 179 cd/m<sup>2</sup>.

Exposure value is a linear scaling factor applied to pixel values to map the computed luminances to the appropriate display range. The stored pixel values do not encompass gamma correction [57, 60].



CIE chromaticity coordinates for Radiance primaries and equal energy white point [60]

	x	y	z
R	0.640	0.330	0.03
G	0.290	0.600	0.11
B	0.150	0.060	0.79
w	0.333	0.333	0.333

Conversion from RGB to XYZ:

$$K = \begin{bmatrix} r_x & r_y & r_z \\ g_x & g_y & g_z \\ b_x & b_y & b_z \end{bmatrix} = \begin{bmatrix} 0.64 & 0.33 & 0.03 \\ 0.29 & 0.60 & 0.11 \\ 0.15 & 0.06 & 0.79 \end{bmatrix}$$

$$W = \begin{bmatrix} X_n & 1 & Z_n \\ Y_n & & Y_n \end{bmatrix} = [1.0 \quad 1.0 \quad 1.0]$$

$$V = WK^{-1} = [0.8034 \quad 1.1168 \quad 1.0798] = [G_r \quad G_g \quad G_b]$$

$$G = \begin{bmatrix} G_r & 0 & 0 \\ 0 & G_g & 0 \\ 0 & 0 & G_b \end{bmatrix} = \begin{bmatrix} 0.8034 & 0 & 0 \\ 0 & 1.1168 & 0 \\ 0 & 0 & 1.0798 \end{bmatrix}$$

$$N = GK = \begin{bmatrix} 0.5142 & 0.2651 & 0.0241 \\ 0.3239 & 0.6701 & 0.1228 \\ 0.1620 & 0.0648 & 0.8530 \end{bmatrix} = \begin{bmatrix} X_r & X_g & X_b \\ Y_r & Y_g & Y_b \\ Z_r & Z_g & Z_b \end{bmatrix}$$

$$\begin{bmatrix} X \\ Y \\ Z \end{bmatrix} = \begin{bmatrix} X_r & X_g & X_b \\ Y_r & Y_g & Y_b \\ Z_r & Z_g & Z_b \end{bmatrix} \begin{bmatrix} R \\ G \\ B \end{bmatrix} \quad \begin{aligned} X &= 0.5142 * R + 0.3239 * G + 0.1620 * B \\ Y &= 0.2651 * R + 0.6701 * G + 0.0648 * B \\ Z &= 0.021 * R + 0.1228 * G + 0.8530 * B \end{aligned}$$

$$L = 179 * (0.265 * R + 0.670 * G + 0.065 * B) / \text{exposure} \quad (\text{cd/m}^2)$$

Fig. 3.6 Mathematical model for the virtual luminance meter

In virtual photometry, the input and algorithmic capabilities of the rendering software determine the measurement uncertainty. As discussed in Chapter II, every algorithm is a simplification of physical phenomena. Validation studies determine whether the simulation results represent the actual scenes with reasonable accuracy. The Radiance software has been validated through many qualitative and quantitative studies. The validation studies involve comparing the software results with full-scale and scale model measurements, theoretical values, and/or other lighting calculation programs. In all of these studies, the simulation results were highly accurate [22, 74-78]. The relative error for a majority of the predictions has been found to be proportionate to the precision of physical measurement instruments [22].

### **Virtual Illuminance Meter**

Illuminance meters are used to measure the luminous flux density incident on a surface or an imaginary plane [2]. In physical photometry, illuminance is measured at a point by cosine corrected illuminance meters. Spatial measurements, i.e. measuring a surface or space point by point, require time and effort; and measurements are usually limited to the equipment availability. Extensive time-series measurements are required to capture the temporal variations of daylight. The expected errors in physical illuminance meters add up to 6.3%:  $V(\lambda)$  match (2%), UV response (0.2%), IR response (0.2%), cosine response (1.5%), linearity error (0.2%), fatigue (0.2%), and polarization (2%) [73].

Cosine correction is an important feature in illuminance meters. Light reaching the photocell at angles other than the normal are partially reflected by the photocell surface, or obstructed by the rim of the case surrounding the photocell. The resultant error increases as the incidence angle increases. Thus, the illuminance level can be undermeasured by as much as 25%. Physical illuminance meters address this problem by

placing a flashed opal glass, diffusing acrylic disc or integrating sphere over the sensor. Thus, illuminance is scaled in proportion to the cosine of the incidence angle [2].

In Virtual Photometry, there are two ways to calculate illuminance. In the first approach, illuminance is derived from the average luminance values in hemispherical fisheye images. In the second approach, illuminance is calculated on a pixel scale.

Hemispherical fisheye projection is a half sphere projected such that each differential area corresponds to the original area multiplied by the cosine of the polar angle. In other words, it is a parallel projection of the hemisphere onto a planar circular area on the image plane [60, 79]. In practice, this is a very convenient projection method for lighting calculations.

Theoretically, all lighting calculations are based on the prediction of luminous flux transport from a source to a receiving surface. Some of the light incident on every surface is reflected, so all surfaces can be treated as virtual light sources. As explained in Chapter II, a form factor is a geometric quantity that describes the fraction of flux leaving the source that reaches the receiving surface [2]. It can be described with the Nusselt Analog, where the form factor for a finite area is equivalent to the hemispherical fisheye projection [61]. Hemispherical fisheye projection (thus, the Nusselt analog) effectively incorporates the cosine term (Fig. 3.7); therefore, it precisely compensates for the cosine correction applied in the physical illuminance meters. As a result, illuminance is equal to the product of  $\pi$  and the uniform sampling of luminance over the hemispherical fisheye projection [60]. The uniform sampling of luminance is achieved by averaging the luminance quantities within the circular area of the fisheye images.

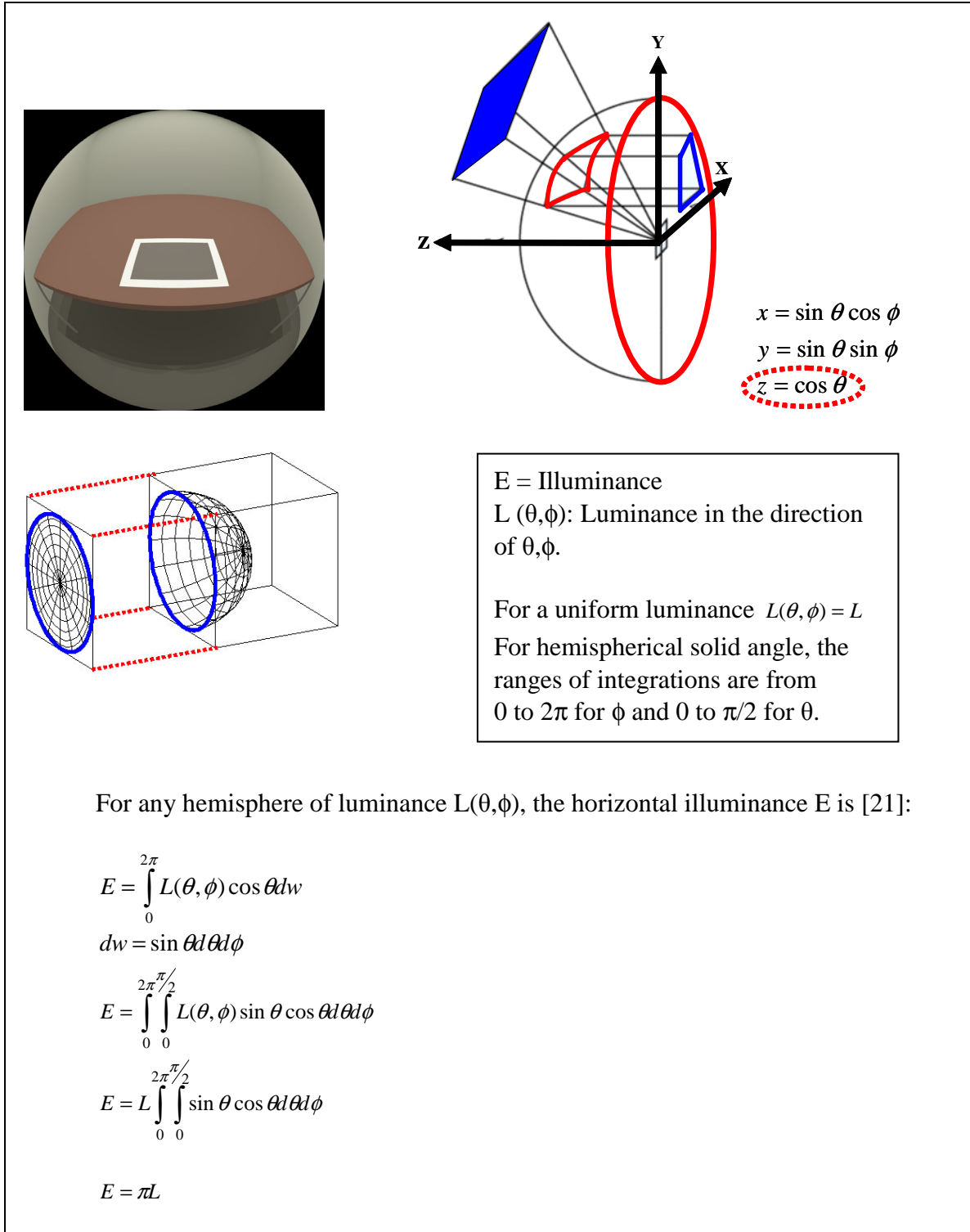


Fig. 3.7 Mathematical and geometric model for the virtual illuminance meter and the Nusselt Analog: illuminance is calculated from hemispherical fisheye images

Camera coordinates determine the illuminance meter position. If the image is generated from the viewer's point (Fig. 3.8a), the calculated quantity is the illuminance value that reaches the viewer's eye. The image incorporates the human field of view as the viewer is performing the task; and it demonstrates the volume seen by an illuminance meter if physical measurements were to be taken at the viewer's forehead. Hence, it can be used to study the characteristics of light that reach the eye. If the images are generated to demonstrate the volume seen by the horizontal or vertical illuminance meters on any task or surface (Fig. 3.8b and c), they can be used to study the characteristics and quantity of light on the task.

Alternatively, illuminance at a certain point (pixel) can be calculated by temporarily replacing the material of the surface (pixel) by a Lambertian material with reflectivity equal to  $\pi$  [60].

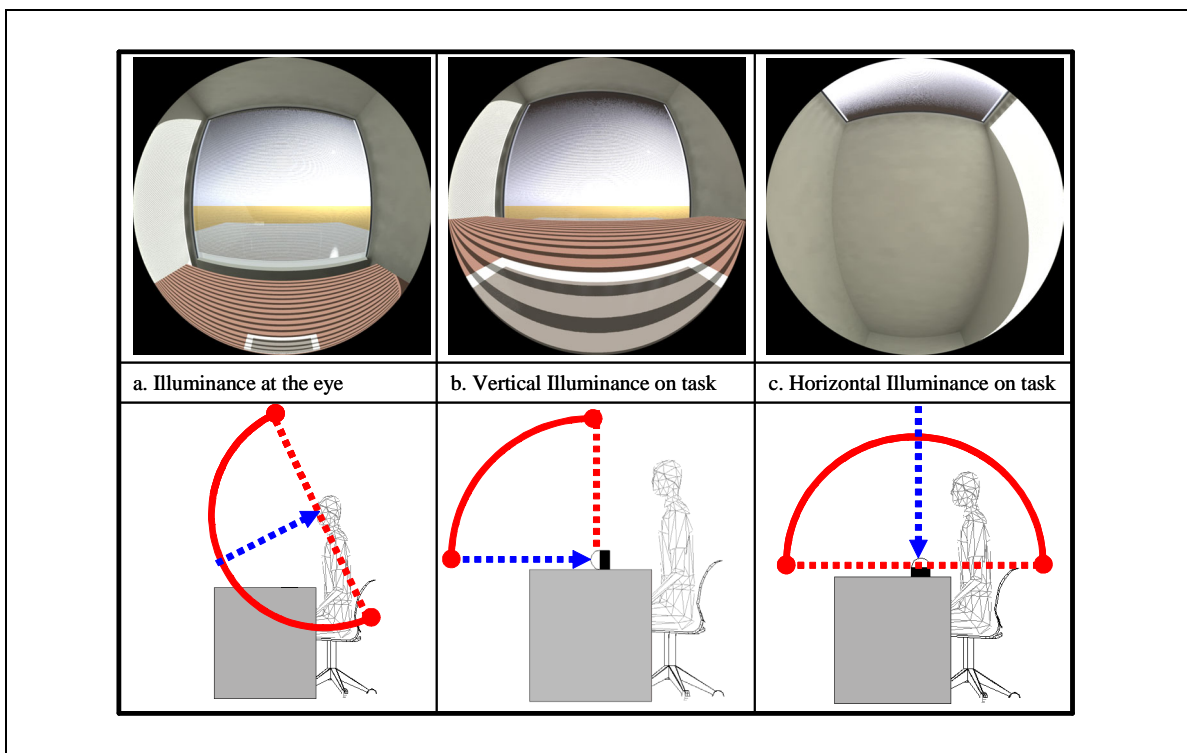


Fig. 3.8 Hemispherical fisheye images used to calculate the illuminance at the eye, vertical and horizontal illuminance values on the task

## Virtual Contrast Meter

Luminance contrast is a metric for studying the relationship between the luminances of an object and background [60]. Luminance contrast is dependent on the object, lighting conditions, and viewing angle. In order to be able to do repeatable contrast measurements under different lighting conditions, it is necessary to use a standardized object and viewing angle [80].

In physical photometry, contrast is determined by a meter, such as the Bruel and Kjaer (B&K) contrast meter. It has a standardized reflection object and an elaborate viewing angle protractor. The reference reflection object consists of black and white surfaces, which are based on the typical reflection properties of task and background in plane visual tasks, such as a paper and printed details. These two surfaces are covered with a glass layer to allow specular reflections that might become veiling reflections from certain viewing angles.

In the B&K contrast standard, the properties of all surfaces have been well defined in terms of specular and diffuse reflections. The glass layer has a refractive index of 1.55; and its surface is composed of multifacets to facilitate the scattering of light into a certain angular range. The black circle is made from a glass material that contains metal particles; it has a diffuse reflectance of 0.015 and a strong and narrow peak of specular reflection; and it has the same index of refraction as the covering glass layer. The white circle has a diffuse reflectance of 0.80, and a weak and broader peak of specular reflection. During measurements, the surfaces are turned one by one into the measuring position. The contrast measured under reference lighting conditions (i.e. isotropic conditions of an integrating sphere) is given as 0.91 for a 25° viewing angle on the task plane [81]. The 25° viewing angle is the CIE recommendation for the reference reflection standard [82].

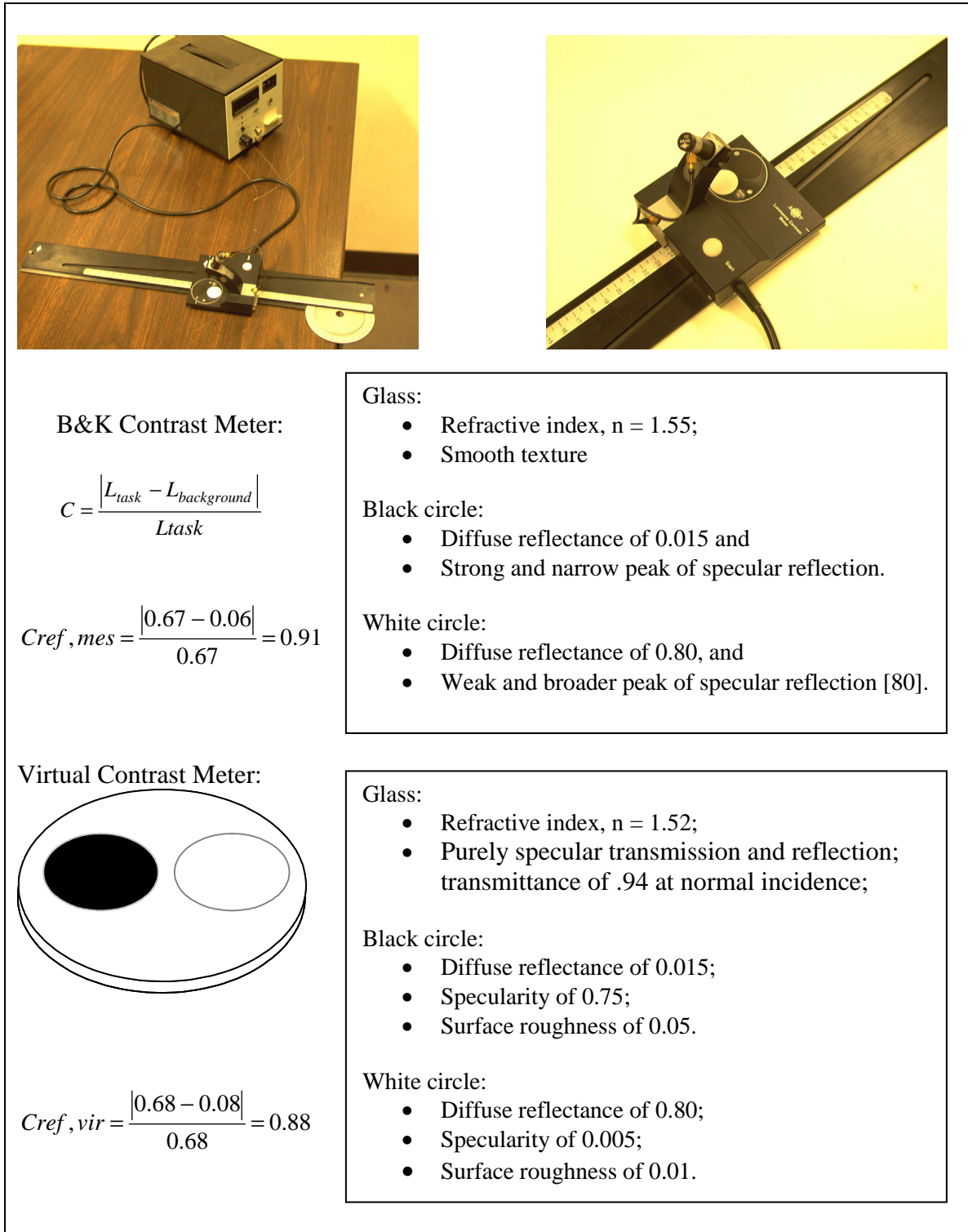


Fig. 3.9 Mathematical, geometric, and material model for the virtual contrast meter

The virtual contrast meter mimics the reference reflection object with similar geometry and representation of the physical materials (Fig.3.9). The calculated virtual contrast under reference lighting conditions is 0.88, which is reasonably close to the physical B&K reflectance standard of 0.91. One major difficulty in developing virtual contrast meter arises from the goniometric properties of reflection. For the physical B&K reflectance standard, reflection properties have been expressed in the form of tables as a function of the viewing angle, azimuth angle, and incidence angle. The reflection properties (specular and directional diffuse) rapidly change as a function of these three angles [81]. Theoretically, it is possible to approximate these properties through microfacet distribution and Fresnel reflection. As explained in Chapter II, microfacet distribution and Fresnel reflection are taken into account as the two key components in BRDF modeling. Yet, the virtual contrast meter should not be considered as the exact match of the physical one. Rather, it is a virtual counterpart of the standard reflection object, which has similar properties.

### **Virtual Integrating Sphere**

An integrating sphere is a hollow sphere coated with a diffusing material with uniform nonselective reflectance. It creates an isotropic luminous environment. The theory of the integrating sphere is based on the principles of flux transfer from a diffuse area source to a receiving area within an enclosure (a.k.a. form factors). The form factor can be easily calculated from a spherical geometry. The fraction of the flux received by a surface is equal to the fraction of the surface area it covers within the sphere (Fig. 3.10). The luminance of any part of the spherical surface due to the direct and interreflected light is the same; and it is proportional to the total flux emitted by the light source regardless of its candlepower distribution. In other words, the reflected flux is independent of the position of the source and the distribution of the light [2, 9, 83].

Integrating spheres are universally used for lighting measurements. Typical usage of integrating spheres includes [2, 9, 83]:

- Measurement of the total luminous flux measurements from a lamp or luminaire;
- Measurement of the uni-directional/hemispherical reflectance or transmittance of materials;
- Formation of a large area source that provides uniform luminance and illuminance as a reference environment.

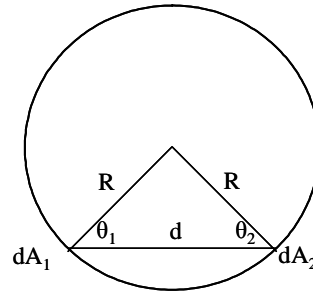
The virtual integrating sphere is created as the reference environment. The theory of form factor calculation is the underlying algorithm for the radiosity calculations, therefore virtual integrating spheres can be generated with any radiosity based rendering software. In VLL, it is created with a different approach: The surfaces are modeled as lambertian emitters with a luminance of  $100 \text{ cd/m}^2$ , and no additional light source is utilized.

Having a virtual integrating sphere turns out to be a very rational approach both economically and theoretically:

- Physical integrating spheres are expensive equipment and are available in some national laboratories and few research universities. Virtual integrating spheres provide access to a larger user group.
- The theory of the integrating sphere assumes a perfectly diffuse and uniform nonselective reflectance inside the sphere [9]. While special materials are used for sphere interiors, no material or coating in real life exhibits the ideal properties of perfect diffusivity and spectral nonselectivity. On the other hand, simulating the perfectly diffuse materials is practical in computer graphics.



[84]



Theoretical calculations of form factors within integrating sphere [83]:

$$dF_{d1-d2} = \frac{\cos \theta_1 \cos \theta_2}{\pi d^2} dA_2$$

$$d = 2R \cos \theta_1 = 2R \cos \theta_2$$

$$dF_{d1-d2} = \frac{dA_2}{4\pi R^2}$$

$$dF_{d1-d2} = \frac{dA_2}{4\pi R^2}$$

$$dF_{d1-d2} = \frac{A_2}{A_{sphere}}$$

$dA_1, dA_2$ : Lambertian, differential area patches on the sphere

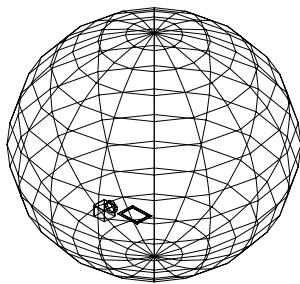
$d$ : distance between the patches

$R$ : the radius of the integrating sphere

$\theta_1$  and  $\theta_2$ : angle measured from the surface normal

$dF_{d1-d2}$ : Differential area form factor

Virtual Integrating Sphere: walls are constructed with self luminous material, which is defined as a RGB value (watts/steradian/m<sup>2</sup>).

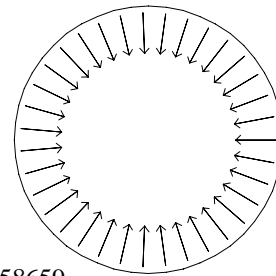


void light sphere\_walls

0

0

3 0.558659 0.558659 0.558659



$$L = 179 * (0.265 * R + 0.670 * G + 0.065 * B) = 100 \text{ cd/m}^2$$

Fig. 3.10 Mathematical, geometric, and material models for the virtual integrating sphere

- There are practical problems associated with the physical integrating spheres. For instance, the sphere has to be perfectly empty in order not to interfere with the reflected flux distribution by the presence of objects within the sphere. However, physical requirements, such as the existence of a light source and necessary shields and baffles are in violation of this condition to a certain extent [9]. In a virtual integrating sphere, neither causes disturbance. The walls are constructed as self emitting, so there is no visible light source. There is no need to be concerned about accessories such as tools to hold sample materials, since gravity is not an issue in a virtual integrating sphere.
- In physical integrating spheres, there are entrance and exit ports on the sphere wall for measurements purposes. The number and size of the ports have an important impact on the selection of the sphere size and sphere coating. Port diameters are usually determined by the size of the measuring devices and the geometric constraints. The sphere size is driven by the size of the ports such that port coverage not to exceed 5% of the sphere wall. The port areas have different reflectance properties than the rest of the sphere. Therefore, the nature of the sphere coating must be chosen accordingly. In virtual integrating spheres, there is no need for an aperture for the measuring equipment. Therefore, the size of the virtual integrating sphere can be flexibly determined. It is also important to note that the initial cost of the physical integrating sphere grows significantly with the size; and adequate physical space is need [9, 83].

The utilization of the virtual integrating sphere is limited here to provide reference conditions. It is not useful to utilize the virtual integrating sphere for measuring the total luminous flux of lamps and luminaires or reflectance and transmittance of materials. These parameters are specified by the user as an input. However, an interesting application may be to use the virtual integrating sphere for measuring the total flux from complex fenestration systems, such as windows with venetian blinds. Physical integrating

spheres have been successfully used to determine the uni-directional/hemispherical transmittance of fenestration systems [85]. Nevertheless, virtual integrating sphere should be cautiously utilized for such applications. The image generation process should employ either a forward ray tracing technique or a backward ray tracing technique with a large number of reflections in order to be able to accurately model the interreflections between surfaces such as the venetian blinds.

### **Virtual Colorimeter**

Although the photometric quantities and meters described have been derived from RGB values of pixels, they do not necessarily provide information about the colorimetric properties of light. It is possible for two light patches to have the same luminance, and yet incorporate totally different spectral power distributions or RGB values. Colorimetric instrumentation provides information about the color properties of light. They can be grouped as the spectro-radiometer/photometer and tristimulus-filter colorimeter. Spectro-radiometers/photometers measure radiometric/photometric quantities as a function of wavelength. Tristimulus-filter colorimeters measure the CIE XYZ values and chromaticity coordinates through CIE Color Matching Functions [9].

In the lighting industry, it is a common practice to quantify the color properties of light sources by color temperature (CT) or correlated color temperature (CCT). The CT quantifies the color appearance of the light from the chromaticity coordinates. The metric is generated from the absolute temperature of a blackbody radiator having a chromaticity value equal to the chromaticity of the light source. A Planckian locus illustrates the locus of blackbody radiator chromaticities on the CIE chromaticity diagram (Fig. 3.11). The CT should only be used to specify the light sources that have equal chromaticity values as the Planckian locus. Otherwise, CCT, which is an approximation to the absolute temperature of a blackbody whose chromaticity is closest that of the light source, is used.

Iso-temperature lines, which are short straight lines that cross the Planckian locus, facilitate the estimation of the CCT for any light source that does not lie on the Planckian locus. The metric becomes ineffective, as the chromaticity of the light source gets distant from the planckian locus [2, 10].

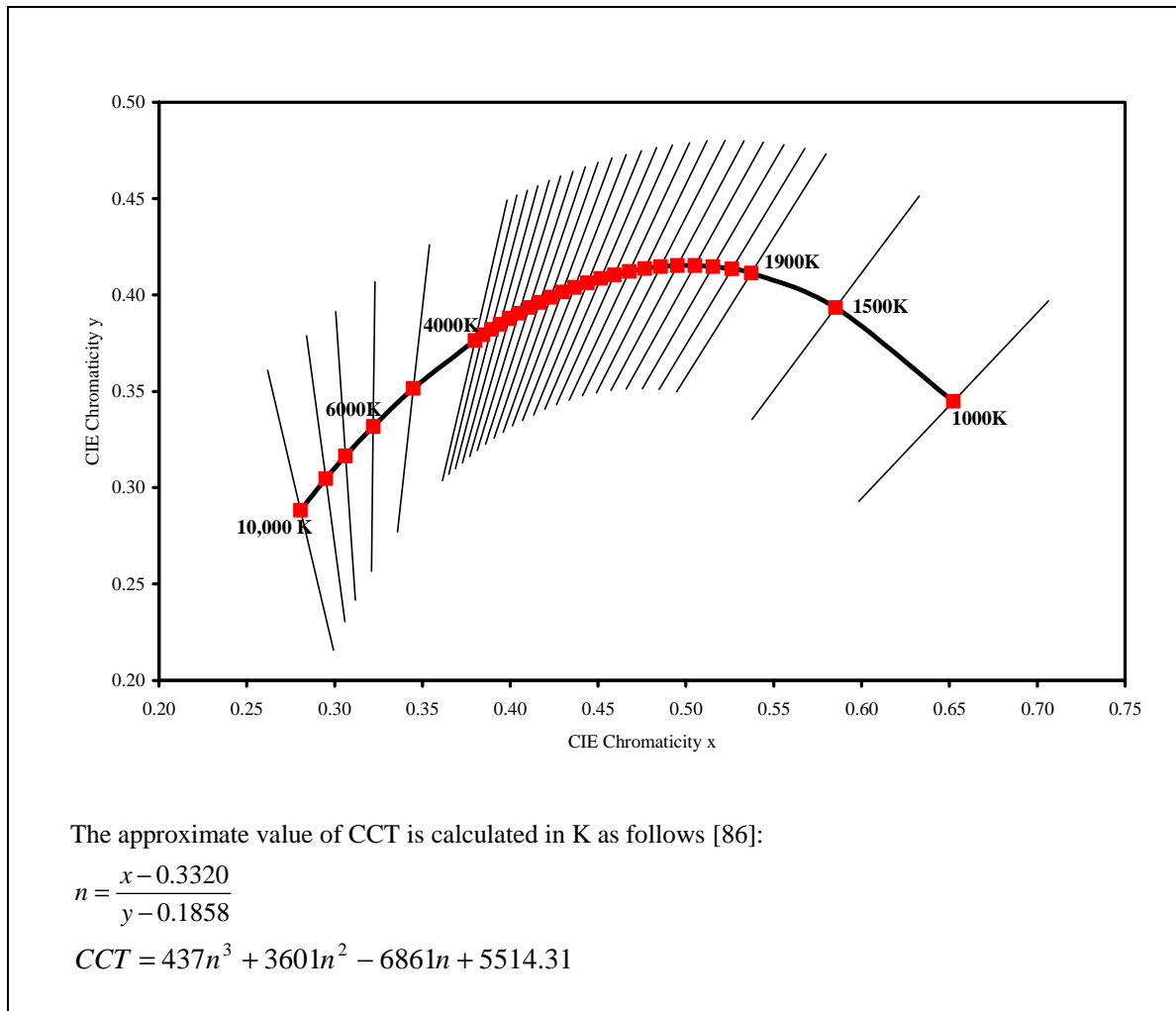


Fig. 3.11 Mathematical model and CIE chromaticity diagram for the virtual CCT<sup>13</sup>

<sup>13</sup> The Planckian locus and iso-temperature lines for Graphs 3.11 and 3.20 are generated with data from [87]. The chromaticity coordinates are used to plot the Planckian locus in the CIE chromaticity diagram. The chromaticity coordinates and the reciprocals of the slopes are used to calculate and plot the iso-temperature lines. The CCT is determined as a function of the intersection of an iso-temperature line with the Planckian locus.

In physical photometry, CCT and chromaticity coordinates can be measured by colorimeters or spectrophotometers. A major discrepancy in a physical tristimulus-filter colorimeter results from the maladjustments of the three photocells in proportion to the CIE 1931 Standard Color Matching Functions. Specifically, it is difficult to fit  $\bar{x}(\lambda)$  with its two peaks. Considerable inconsistencies among commercial meters are common [10, 11].

Virtual Tristimulus-filter Colorimeter measures the CCT and chromaticity coordinates based on the computed CIE XYZ values. Special attention should be paid for determining the chromaticity of the light source in relation to the Planckian locus. The mathematical model for calculating CCT from the CIE XYZ data is given in Fig. 3.11.

### **Virtual Scotopic Meter**

A more recent metric on light source color characteristics is the scotopic/photopic (S/P) ratio [88]. Scotopic luminance is measured by weighing the spectral power distribution of the radiation by the 1951 CIE scotopic observer,  $V'(\lambda)$ . The current lighting practice is to define scotopic/photopic measure as the S/P ratio for lamps and luminaires.

In physical photometry, scotopic luminance is measured by scotopic meters. In principle, it is possible to compute the scotopic luminance by virtual meters. A mathematical model is needed to derive the scotopic luminance values from CIE XYZ, in the same manner that photopic luminance is obtained. However, such a model is not readily available. In computer graphics, tone-mapping algorithms employ both photopic and scotopic luminance values. The commonly used algorithm to derive scotopic luminance from CIE XYZ data is given in Fig. 3.12. It is an approximation that is based on a least square fit to the colors on the Macbeth ColorChecker Chart [52]. This model should be used with caution since it is not based on an accepted standard and it might not

be plausibly accurate for various lighting analysis purposes. Therefore, more research and better algorithms are needed to reliably derive the virtual scotopic metric.

An approximation of scotopic luminance calculation [52]:

$$Y_{\text{scotopic}} = Y \left[ 1.33 \left( 1 + \frac{Y+Z}{X} \right) - 1.68 \right]$$

Fig. 3.12 Mathematical model suggested for the virtual scotopic luminance meter

### **Application Examples on Virtual Photometry**

The first example is a Contrast Rendering Factor (CRF) analysis that is used to demonstrate the application of four virtual meters: luminance meter, illuminance meter, contrast meter and integrating sphere. CRF is an index used to study the effects of veiling reflections in reducing the task contrast. Task contrast is measured by the contrast meter and calculated by comparing the contrast in the analyzed environment with the contrast in a reference environment, i.e. integrating sphere [2].

Researchers have studied CRF through full-scale photometric measurements [89, 90]. Various lighting and furniture configurations have been used to determine the luminance contrast variation on the task plane as a function of luminaire position. In their study, the task station is composed of a table and full-scale body shadow profile. This station is positioned relative to a single luminaire mounted on the ceiling and 11 different source-task geometries have been obtained by moving the task station. For each luminaire position, measurements have been done by an adjustable B&K luminance contrast meter. CRF has been determined by comparing the field measurements with the contrast under isotropic conditions of an integrating sphere. Additionally, horizontal and

vertical illuminance values have been measured for determining contrast potential (CP). CRF and CP values have been analyzed to identify the effective task-source geometry.

VLL has been used for computing the CRF and CP for a similar setting (Fig. 3.13). Surface geometries, materials, light source, and body shadow profile are modeled. The simulation is repeated for all the different luminaire positions (Fig. 3.14). Figures 3.15.a-c illustrate the veiling reflections from the viewer's point. In Fig. 3.15.a, the glass layer is totally washed by the light so it is not possible to see the black and white circles under the glass. If the task were a glossy magazine, it would not be possible to read the text. In Fig. 3.15.b, there are some veiling reflections. Visibility is totally restored in Fig. 3.15.c.

Luminance, luminance contrast, CRF, vertical illuminance, horizontal illuminance, and CP are determined through the virtual meters. Fig. 3.16 shows the variations in CRF and CP as physically and virtually measured in relation to the light source position. In general, forward positioning of the luminaire relative to the viewer reduces the luminance contrast by causing veiling reflections [89, 90]. In physical measurements, CRF and CP contrast steadily increases as the source position changes from 1 to 11. The same dynamics is observed through the virtual measurements, with the exception that the CRF increment is limited to the first four source positions, and it is approximately constant for the other source positions. The differences can be attributed to rendering algorithms, such as the modeling of materials used in the environment and in the contrast meter; material input; light source differences, such as the candlepower distribution of the simulated light source versus the physical source; and/or the physical measurement conditions. Yet, the results indicate that similar dynamics have been obtained using the physical and virtual measurements in terms of identifying the effective task-source geometries.

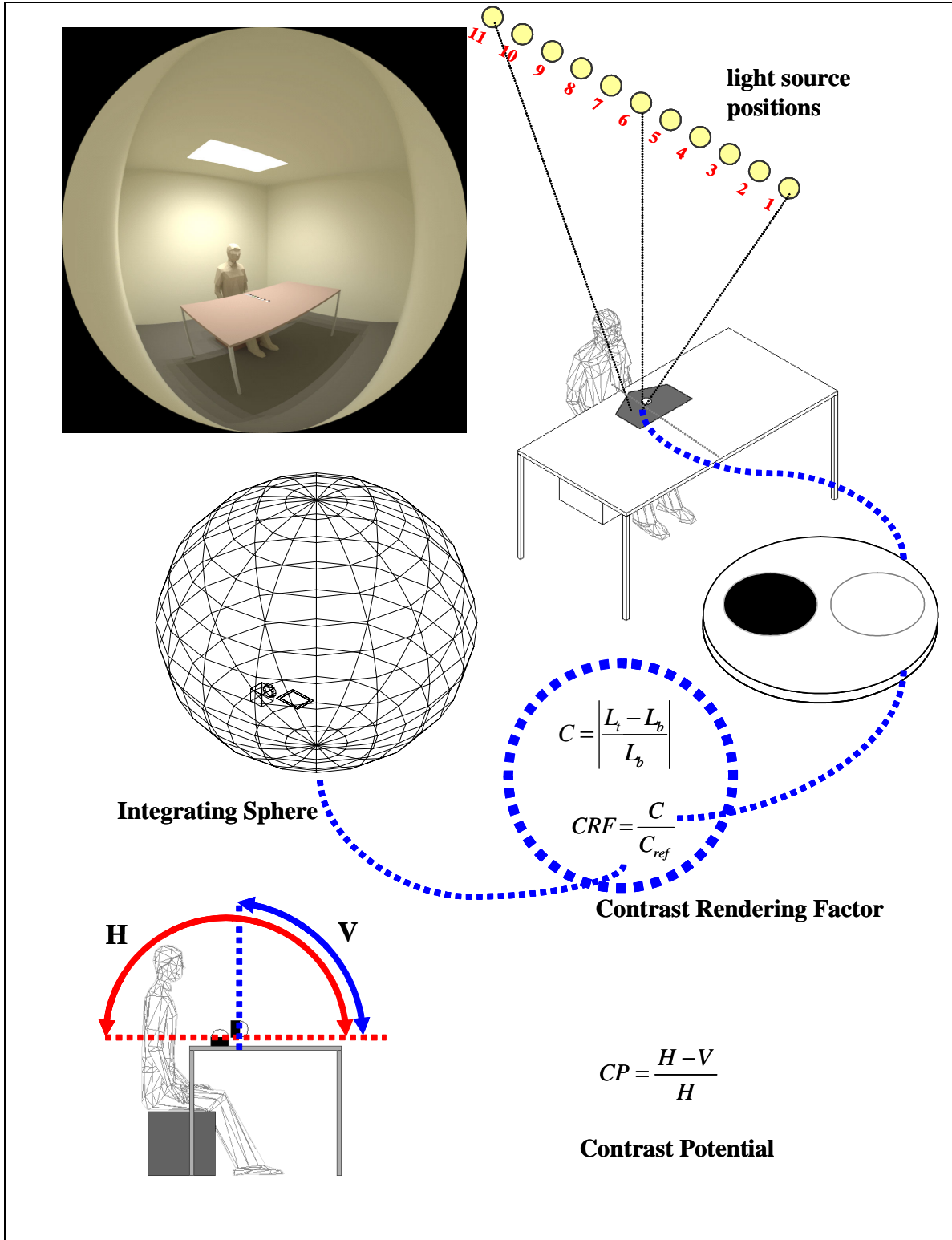


Fig. 3.13 Virtual laboratory for CRF measurements

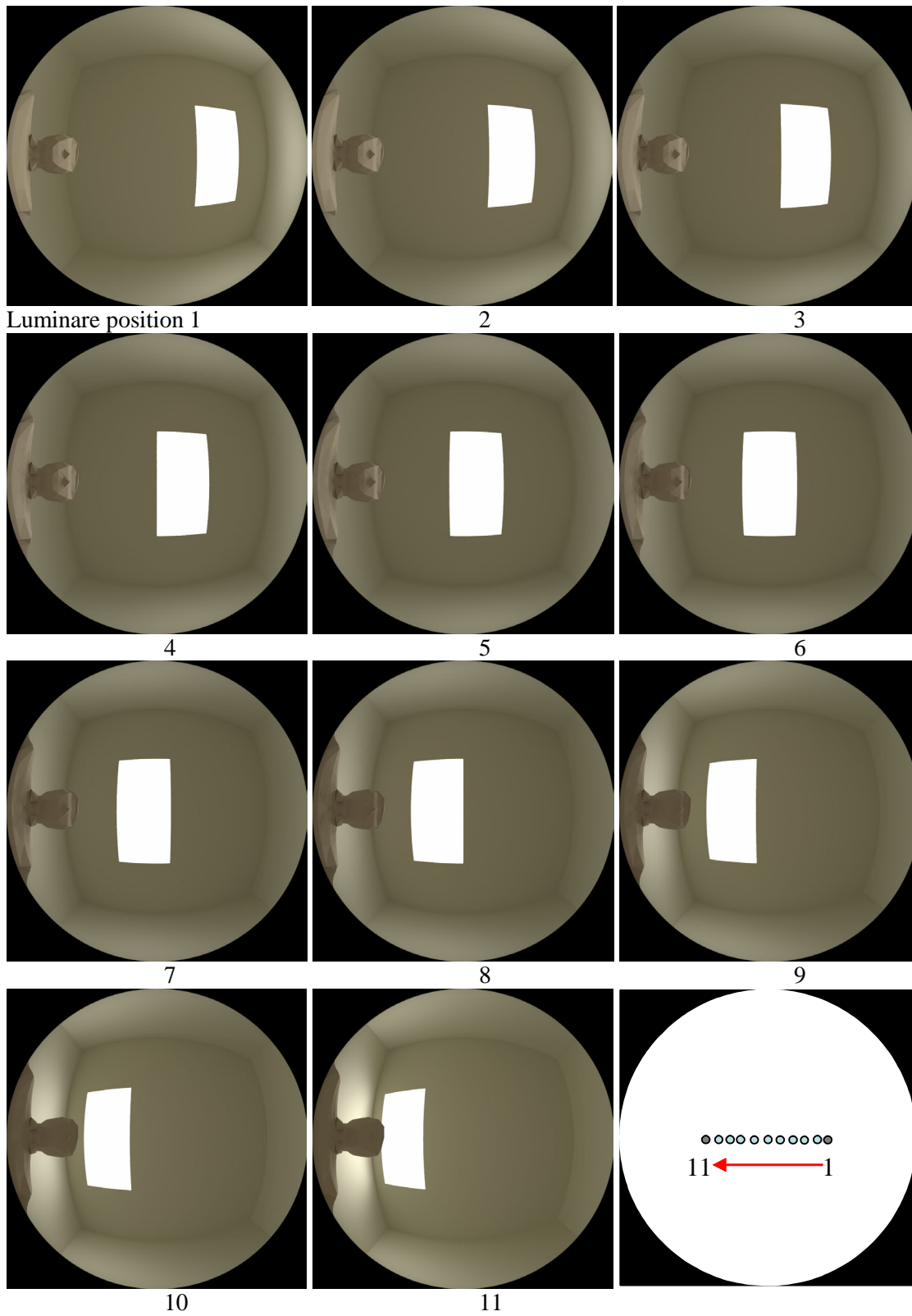


Fig. 3.14 Ceiling views as seen by the illuminance meter while measuring the horizontal illuminance on the table

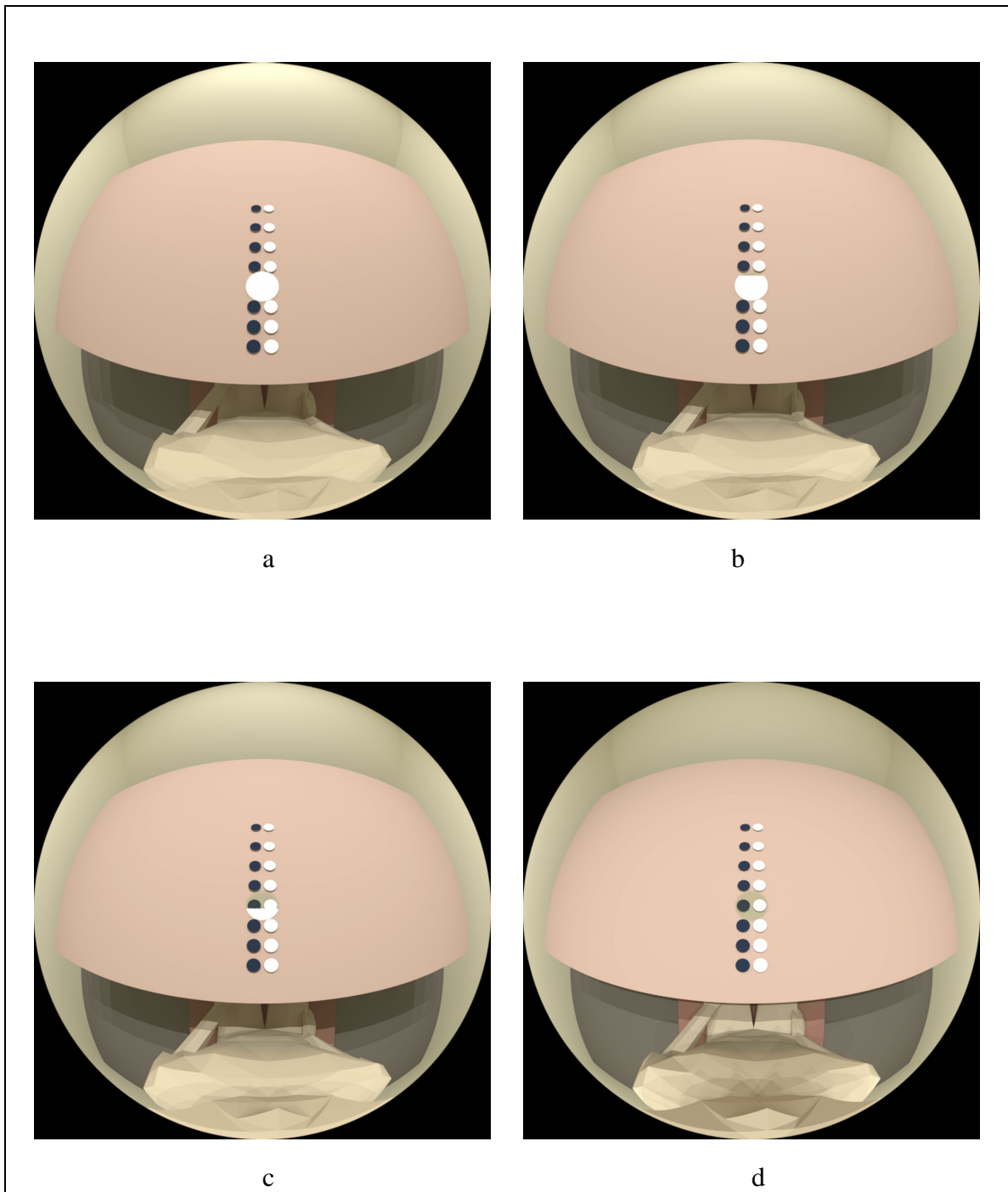


Fig.3.15. Viewer's sight as the luminance contrast variability is determined for the different source positions

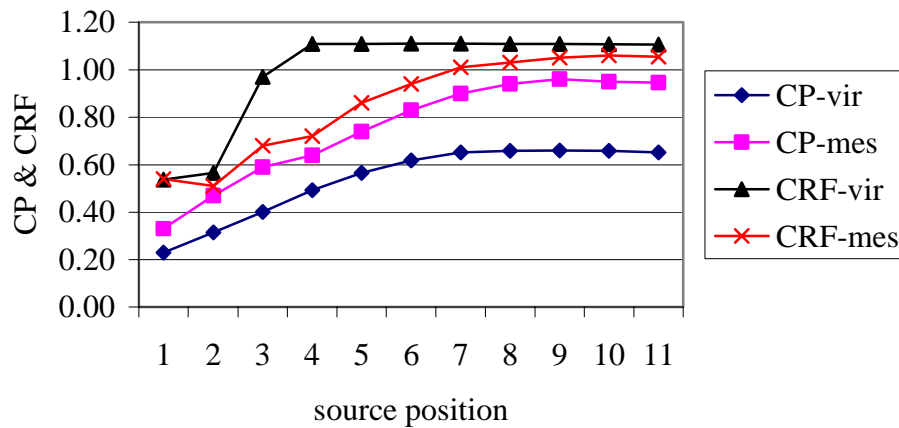


Figure 3.16 CRF and CP variation with respect to the source position in physical and virtual environments

Flexibility is a very powerful feature in the VLL. An extension of this example may incorporate a table that is covered by multiple contrast meters. This approach allows mapping the contrast variation across the task. Another approach would be to incorporate the comparison of the contrast standard with the real world materials. As discussed in the development of the contrast meter, it is important to have a reference object. Yet, it might be useful to simulate the actual tasks (for instance, paper tasks ranging from matt to glossy) and determine their behavior in reference to the contrast standard.

The second example demonstrates the application of the virtual colorimeter and scotopic meters. The effect of interreflection on the color properties of light is discussed. The color scheme of a space is determined by the color properties of the light source as well as the color properties of the surface finishes. Therefore, it could be deceptive to use luminare properties such as the CCT or S/P ratio as design decision criteria. Although the properties of the light sources should not be ignored, it is important to realize that the properties of the light emitted by these sources will be predominantly modified by the spectral transmission and reflection properties of the surrounding architectural surfaces.

The space has width, length, and height of 3 meters (10 feet). The task is white paper positioned horizontally on a table. The light source is recessed fluorescent lensed troffer. The source is kept constant, but the material of one wall has been changed from a scotopically poor color (yellow) to a neutral color (grey), and a scotopically rich color (blue). Yet, all materials have the same photopic reflectance (Fig. 3.17).

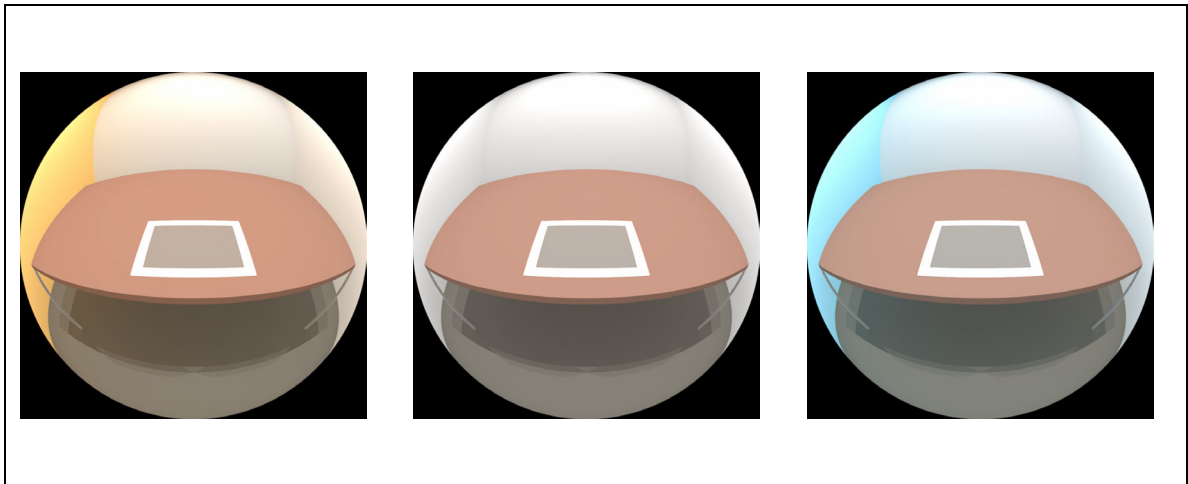


Fig. 3.17 Left wall material as varied from a scotopically poor color (yellow) to a neutral (grey), and a scotopically rich color (blue)

The images are analyzed in terms of CCT and S/P ratio. Fig. 3.18 shows the virtual photopic and scotopic luminance values. The results indicate that photopic luminance does not change much among the three cases. This is expected because the photopic reflectances of materials are deliberately kept same. However, the scotopic luminance changes drastically favoring the scotopically rich blue material. Interreflections (color blending) from the blue wall affect the spectral content of the light within the environment.

Fig. 3.19 illustrates the CCT values in these three rooms. Again, the results indicate that CCT increases, favoring the blue material. Although the light source is kept fixed, color properties of the light within the room varies distinctly with the spectral

properties of the surface materials. The chromaticity coordinates for all pixels are presented in Fig. 3.20. They are in reasonable proximity of the Planckian locus, therefore the CCT values can be reliably calculated from the data.

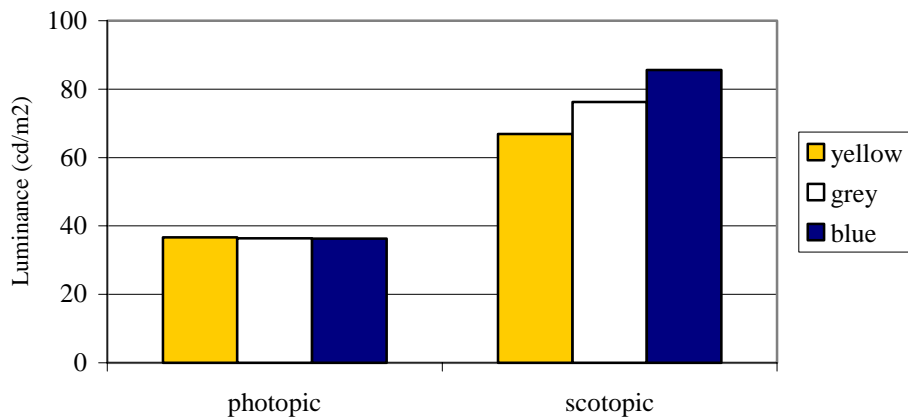


Fig. 3.18 Photopic and scotopic luminance variations in relation to the yellow, grey, and blue wall materials under the same light source

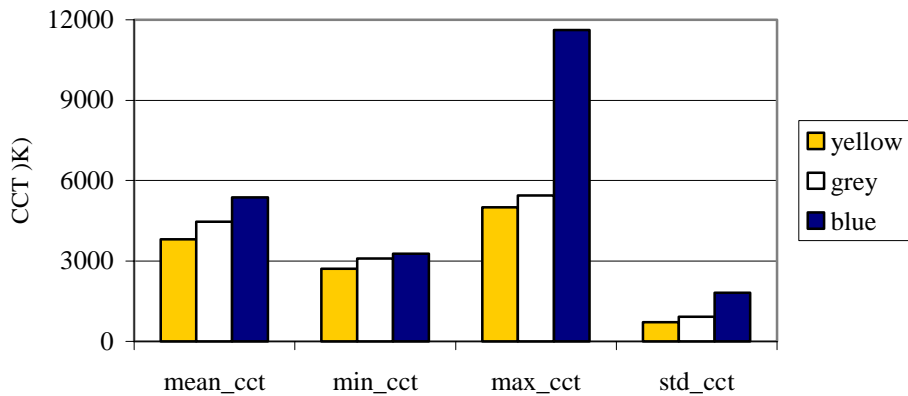


Fig. 3.19 CCT variations in relation to the yellow, grey, and blue wall materials under the same light source

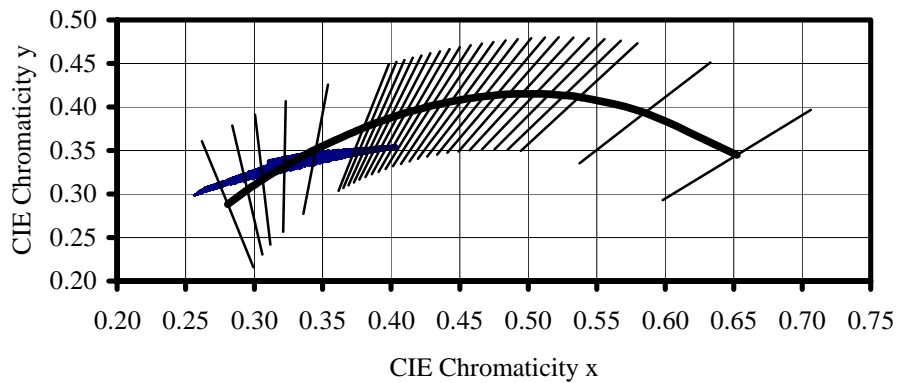
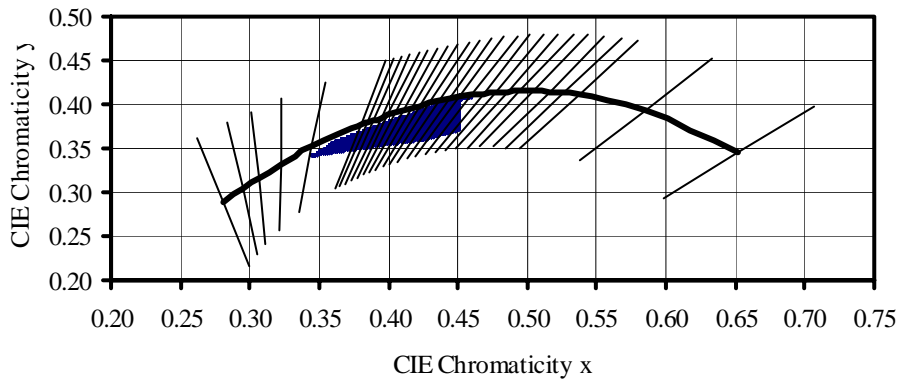
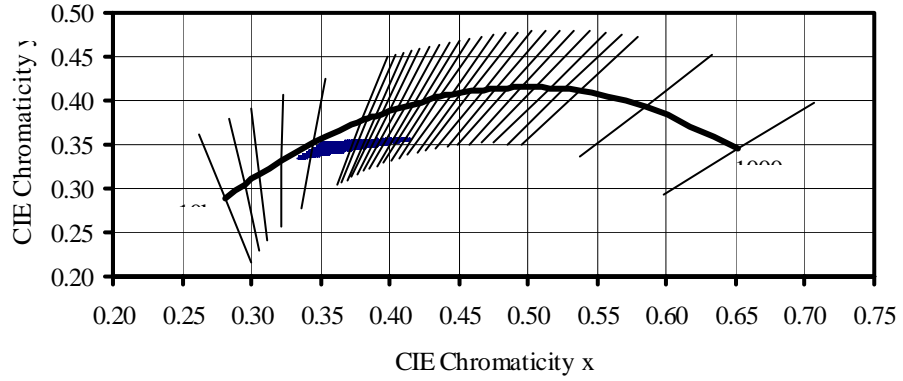


Fig. 3.20 Chromaticity values of pixel data from scenes with the yellow, grey, and blue wall materials

## Remarks

The factors affecting the measurement accuracy in physical photometry include the photometer calibration, ambient temperature, luminaire voltage, ballast-lamp photometric factors, light loss factors, and surface reflectances [2]. As a result, there is an expected amount of error and uncertainty associated with the measurement process. As discussed before, the error and uncertainties in physical photometry can correspond to the errors and uncertainties in virtual photometry through appropriate modeling and rendering approaches.

It is always possible to implement new photometers as long as the researcher understands the assumptions and limitations of the algorithms that are used in the image generation process. Two photometer systems that are deliberately not included among the virtual meters are goniophotometer and spectrophotometer. A goniophotometer is a device that measures the luminous intensity of light sources from different directions [2]. It is not implemented in the VLL because it is better simulated with a forward ray tracing algorithm rather than backward ray tracing. A spectrophotometer is a device that measures the transmittance and reflectance of surfaces as a function of wavelength [2]. It is not included because the simulation is based on RGB combinations, rather than the spectral power curves of light. However, it is important to note that these are not the restriction of the VLL. Rather, they are bounded by the image generation process. With more capable image generation tools and algorithms, it is theoretically possible to create any physical photometer in a virtual environment.

The advantages of the virtual meters are summarized here as follows:

- The images provide lighting values on a pixel scale. For a 1024 by 1024 resolution, the image is equivalent to a physical laboratory where 1,048,567 lighting sensors. Obviously, this is not feasible in any physical laboratory.

- The studies and experiments do not require laborious measurements, especially to map the lighting variation across the task and space, because it is possible to achieve several measurements from one image.
- The studies and experiments do not require physical space and expensive equipments.
- The measurements are free from operator, who could screen off the parts of the environment during measurements.
- The most important feature of the VLL is flexibility. The researcher has the ability to control the extraneous variables; systematically manipulate the independent variables, and measure and compare the dependent variables. The equipment in the laboratory can be expanded or reconfigured as needed through virtual modeling of the set of physical and operational conditions.

**CHAPTER IV**  
**DATA ANALYSIS TECHNIQUES IN THE VIRTUAL LIGHTING**  
**LABORATORY**

In general, architectural lighting analysis is dominated by the investigations of five broad matters to achieve the intended visual effect, performance, and comfort. They are listed as follows [91]:

- Adequate quantity of light;
- Suitable spatial distribution of light;
- Sufficient directionality of light;
- Absence of glare; and
- Sufficient spectral content of light.

This chapter provides a general overview of the data analysis techniques in the VLL. Virtual meters supply the lighting data for analysis. Mathematical operations and statistical analysis can be performed with these quantities. The VLL is capable of performing the lighting analyses listed above, with detail, flexibility and rigor that may be infeasible or impossible with traditional architectural lighting analysis approaches. These capabilities are exemplified.

From a procedural perspective, the data analysis techniques in the VLL can be categorized into three as ‘total data analysis’, ‘regional data analysis’, and ‘per-pixel data analysis’. Fig. 4.1 demonstrates a conceptual overview of these techniques. The analyzed image is a hemispherical fisheye projection, which not only accounts for the cosine correction, but also covers the total human vision. Images are decomposed into elements

by selecting and isolating (masking) a portion that contains a region of interest for the architectural lighting analysis<sup>14</sup>.

*Total data analysis* is performed to provide information about average quantities, standard deviations, minimum and maximum values in the whole scene. To analyze the total data, it is necessary to apply the fisheye mask to filter the pixels in the hemispherical projection (circular part) from the rest of the image, which is composed of null pixels (Fig. 4.1.a). The quantity, basic distribution pattern, directionality, and spectral content of light can be investigated.

*Regional data analysis* is performed on various elements in the scene, generally to provide information about the task and the surrounding. To perform regional data analysis, it is necessary to decompose the scene into regions such as the task and the surrounding surfaces (walls, ceiling, table, and so on). Then, the quantities and ratios in these regions can be studied. The first diagram in Fig. 4.1.b shows the isolation of the computer screen from the rest of the scene. Similarly, the scene can be decomposed into different parts of the human field of view (foveal, binocular, and peripheral vision). The second diagram in Fig. 4.1.b shows the isolation of the scene that is seen as the binocular vision, when the viewer is fixated at the computer screen. Field of view analysis is a

---

<sup>14</sup> Masking is done by filtering the original image by a binary image that has the same resolution. The binary image contains 1's for pixels that are part of the region of interest and 0's for the rest of the image [92]. The filtered values are the quantities in the original image (essentially, the lighting matrix) that correspond to pixel coordinates with 1's in the binary image. They are stored in a separate matrix, in which each element of the matrix corresponds to a lighting quantity (such as luminance, illuminance, and CCT) of a single pixel. Therefore, VLL functions, user-defined functions, in-built mathematical and statistical operations can be applied to inquire various properties of the region of interest.

There are multiple ways of creating the binary masks. For instance, Matlab Image Processing Toolbox<sup>®</sup> offers several useful functions [92]. Polygon-based region of interest is specified by supplying the pixel coordinates or simply clicking on the vertices of a polygon in the image. It is effective when the region of interest has an uncomplicated geometry. Intensity-based region of interest is specified by supplying a range of intensities for pixel values. It is effective when the intensity changes rapidly between different objects in the image. The third option is to employ edge detection functions to detect various object boundaries in an image. This function returns a binary image that contains 1's for edges and 0's in the rest of the image. Therefore, further processing would be required to create the region of interest.

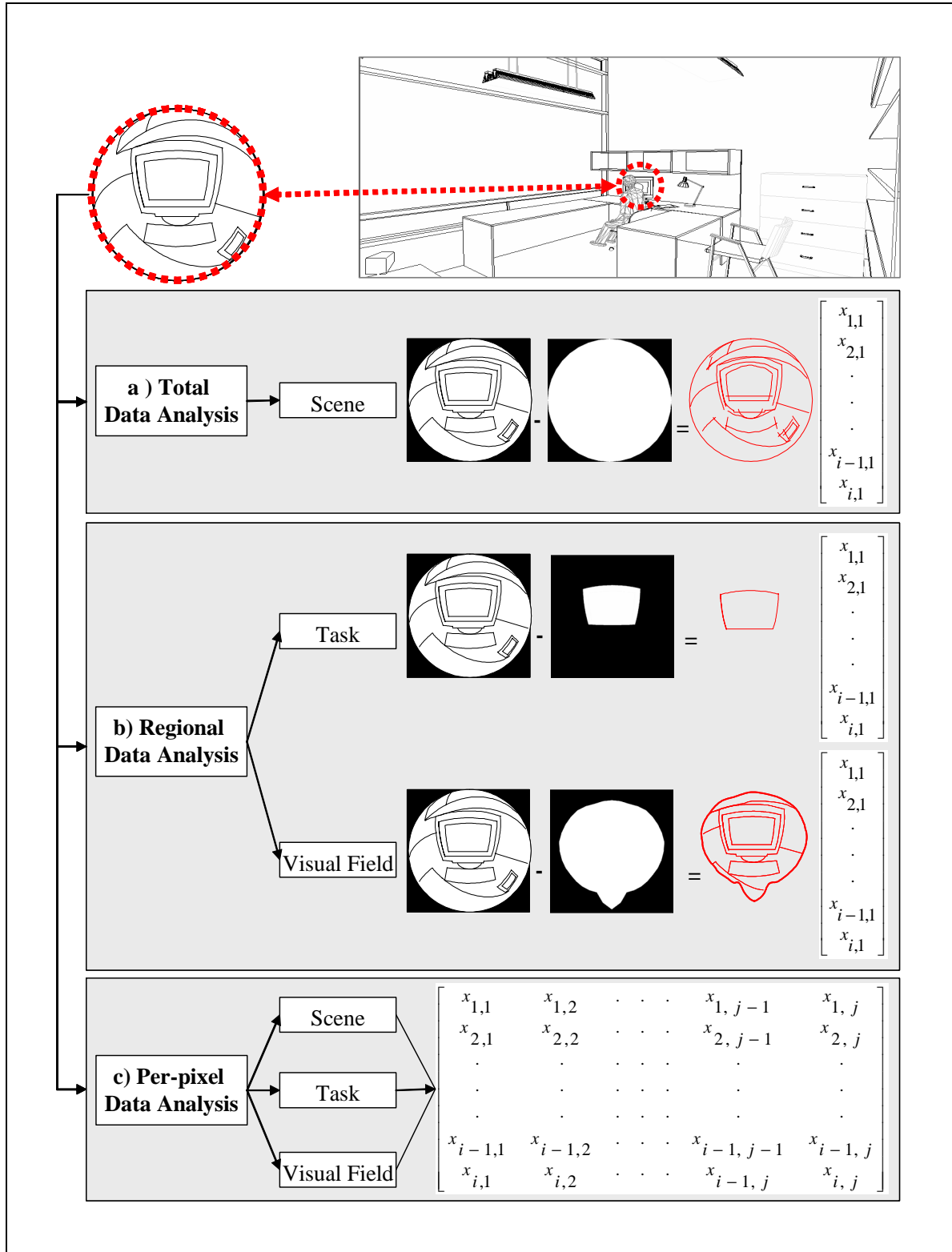


Fig. 4.1 Data analysis techniques in the VLL

special analysis method, which is not attainable with traditional physical photometry techniques. It is performed with an appropriate masking application in the VLL.

*Per-pixel data analysis* is also pertinent to VLL and cannot be done with the traditional techniques. It provides remarkably detailed information about the temporal and spatial dynamics within an environment.

The underlying idea is that the single quantities (such as luminance, illuminance, visual comfort and performance indices) are not very informative about the quantitative and qualitative dynamics of lighting throughout the entire space. Luminous environment dynamics occurs with both daylighting and electric lighting. Temporal dynamics in daylighting is attributed to the movement of sun and the sky conditions. Dynamics in electric lighting can be attributed to factors such as dimming and switching between different lighting configurations. The spatial lighting dynamics results from the spatial distribution of light source as well as the viewer's fixation point and movement in the environment. Per-pixel information is appropriate to study such dynamics and the analysis can be performed on the whole scene, on a specific task, or on a part of the human field of view.

### **The Design Scenario**

An office located in Ann Arbor, Michigan (42°13' North latitude and 83°45' West longitude) has been studied. The room dimensions are 3.7 meters by 3.7 meters (12 feet by 12 feet); it has an inclined ceiling (15°) with an average height of 3.4 meters (11 feet). It is located on the fourth floor of an office building. The wall, floor, and ceiling materials are matte and polished with 57%, 71%, and 30% reflectivity. The office has integrated daylighting and electric lighting.

Daylighting comes from a south facing window with generic monolithic clear glass of 89.9% transmittance (approximately 10.2 m<sup>2</sup> - 110 ft<sup>2</sup>). In the base case, there is

not any daylight admission control system on the window. Electric lighting is supplied by both ambient and task lighting. There are two direct/indirect luminaires on the ceiling. Luminaires are made of extruded aluminum, which provides uplight from a white painted reflector; and downlight from white lightvent openings. There are three fluorescent lamps rated at 2850 lumen output. The task lighting is a table lamp with an incandescent lamp rated at 1200 lumen output. The task and ambient lighting combination is chosen to provide approximately 500 lx on the table during nighttime. Base simulations are done for the 21<sup>st</sup> of December from 9:00 to 17:00 with the CIE Clear Sky. In the base case, the outside is kept simple without any obstruction. Ground reflectivity is 12%.



Figure 4.2 The office space during the daytime and nighttime

Three visual tasks have been specified for an optimum performance in the office:

- The first task is reading a text displayed on the computer screen and recognition of the letters on the keyboard;
- The second task is reading a text on a document placed at a normal reading distance close to the computer;
- The third task is looking through the window.

The computer screen consists of the black and white surfaces that represent the foreground and the background of a task. Both surfaces are self luminous (80 and 10 cd/m<sup>2</sup>, respectively) and the entire screen is covered with clear glass to mimic the luminosity and reflectivity of the physical computer screens. Similarly, the paper task consists of black and white surfaces to represent the foreground (text) and the background (paper). Materials are matte, polished with 10 and 85% reflectivity. A 25° viewing angle is maintained on the task plane.

Figures 4.3.a-c are generated to demonstrate the viewer's sight for the specified visual tasks. The exact position of the viewer is important to study the amount and characteristics of the light reaching the eye. Figures 4.3.d-e (computer-view and paper-view) demonstrate the volume seen by the illuminance meter, if physical measurements were to be taken. Four more images (Figures 4.3.f-i) are generated to simulate the vertical illuminance meter on paper for the four cardinal orientations. These images are used to study the characteristics of the light on the tasks. The amount of light reaching the tasks can be derived from these images. It is also possible to identify and study the surfaces and light sources that have direct impact on the task.

It is important to generate the images with a specific scenario and typical work pattern. In the office example, the visual tasks are specified as looking at the computer screen, paper, and window. In another architectural setting, the tasks and, as a result, the viewpoints will be different. This approach investigates the specific requirements of each

space and task. Additionally, conflicting lighting requirements between different tasks can be explored, prioritized, and/or optimized.

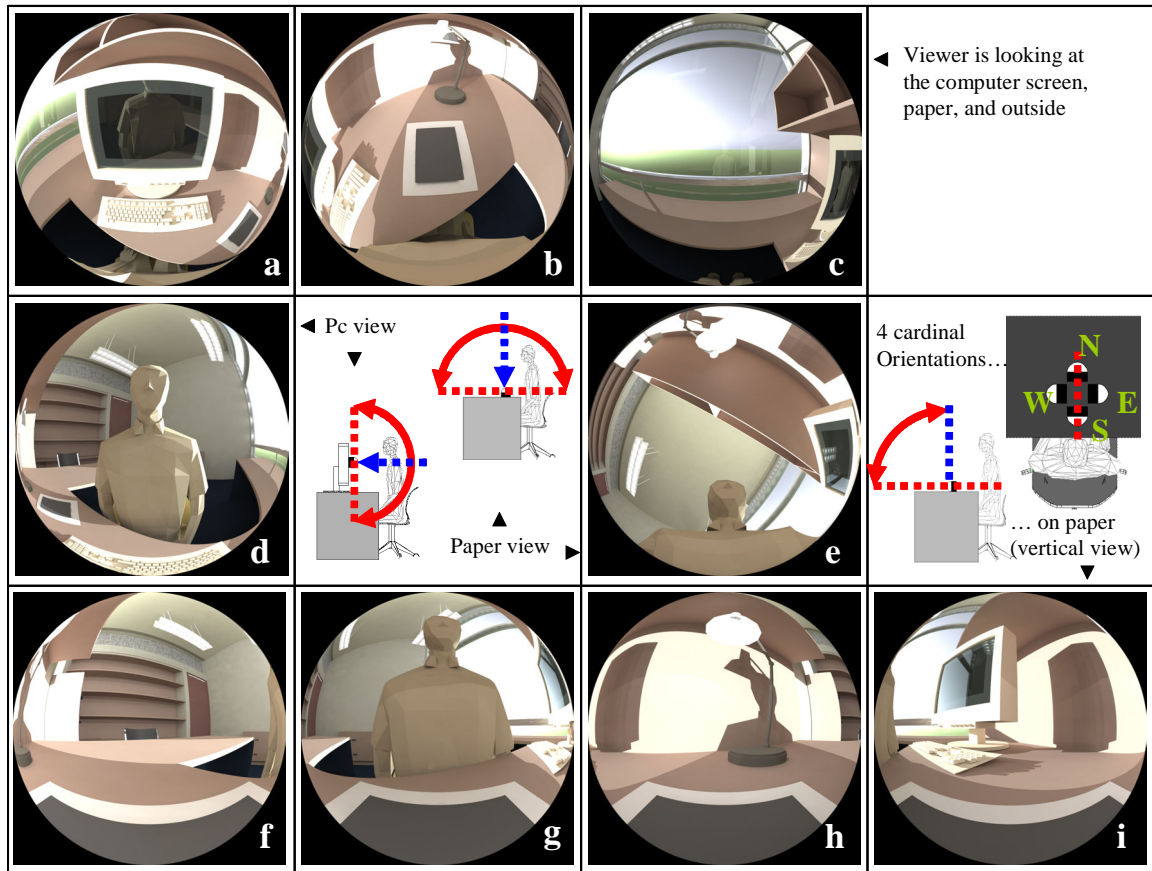


Fig. 4.3 Set of analyzed images in VLL a) viewer looking at the computer screen, b) viewer looking at the paper task, c) viewer looking through the window, d) computer view e) paper view, f) paper: east view, g) paper: south view, h) paper: north view, and i) paper: west view<sup>15</sup>

<sup>15</sup> For the sake of abbreviation in graphs, a) the viewer looking the computer screen is referred as 'eye2pc' view, b) viewer looking at the paper task as 'eye2pap', c) viewer looking through the window as 'eye2win', d) computer view as 'pc', e) paper view as 'pap', f) paper: east view as 'pape', g) paper: south view as 'paps', h) paper: north view as 'papn'; and i) paper: west view as 'papw'.

## Data Analysis

### Quantity

The most common lighting analysis is to check the illuminance level (horizontal, vertical, or both) in accordance with the recommendations from the national and international committees. The IESNA established an illuminance selection procedure. In general, there is a broad range of acceptable illuminance levels which is specified as a recommendation based on the space, task, and occupant characteristics. Ultimately, architects and lighting designers decide on a target illuminance level [2].

Illuminance level in the office space varies spatially as a function of the luminaire location and candlepower distribution, space and surface geometry, and reflection and transmission properties of the surface materials. It varies temporally as a function of the site location, day, time, atmospheric conditions and glazing properties. Therefore, it is useful to study the illuminance at different points and throughout time. The dynamics of the amount of the illuminance is studied throughout Dec 21. The data is supplied by the virtual illuminance meter. As discussed in Chapter III, the virtual illuminance is derived from approximately million pixel values in the scene. In Fig. 4.4, illuminance at the viewer's eye (forehead) is illustrated when the viewer is looking at the computer screen, paper, and window. The illuminance ratios between the tasks are also extreme. Table 4.1 demonstrates the illuminance ratios on the viewer's eye, as he switches between the computer view, paper view, and window view. The nighttime illuminance values are 86, 141, and 58 lx, respectively.

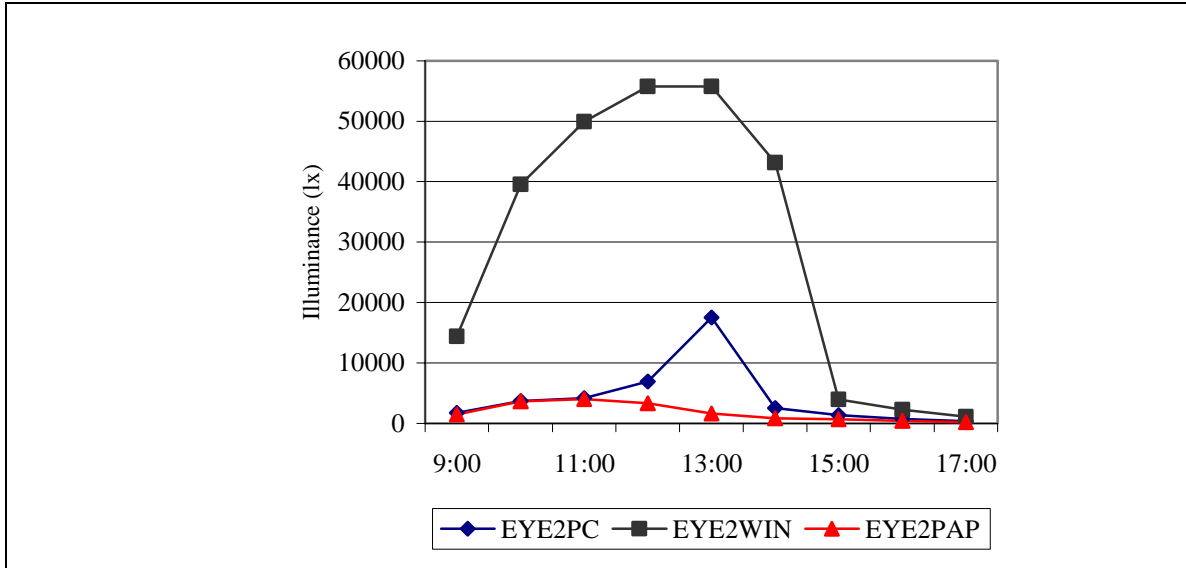


Fig. 4.4 Illuminance reaching the eye throughout Dec. 21 when the viewer is looking at the computer screen, paper, and window

	9:00	10:00	11:00	12:00	13:00	14:00	15:00	16:00	17:00
E2win : E2pc	8.3:1	10.6:1	12.0:1	8.0:1	3.2:1	17.1:1	2.9:1	3.0:1	3.3:1
E2pap : E2pc	0.9:1	1:1	1:1	1:0.5	0.1:1	0.3:1	0.5:1	0.6:1	0.6:1
E2win : E2pap	9.7:1	10.8:1	12.5:1	16.6:1	33.9:1	49.8:1	5.9:1	5.4:1	5.4:1

Table 4.1 Illuminance ratios between the tasks when the viewer is looking at the computer screen, paper, and window

The horizontal illuminance on the paper and vertical illuminance on the computer screen are illustrated throughout the same day in Fig. 4.5. The recommendations suggest that horizontal illuminance values should not exceed 500 lx in office spaces which accommodate both paper and computer based tasks [2]. Although it is known that there is a broad range of light levels that can be tolerated for paper based tasks, exceeding the target illuminance level often results in reduced visibility for computer based tasks. The

analyses from the base case indicate obviously unacceptable values, which would cause visual comfort and performance problems. Fig. 4.5 demonstrates the most troublesome time of the day, which is 12:00 for the paper task. The nighttime illuminance values on the computer screen and paper are 139 and 489 lx, respectively; both are within reasonable range.

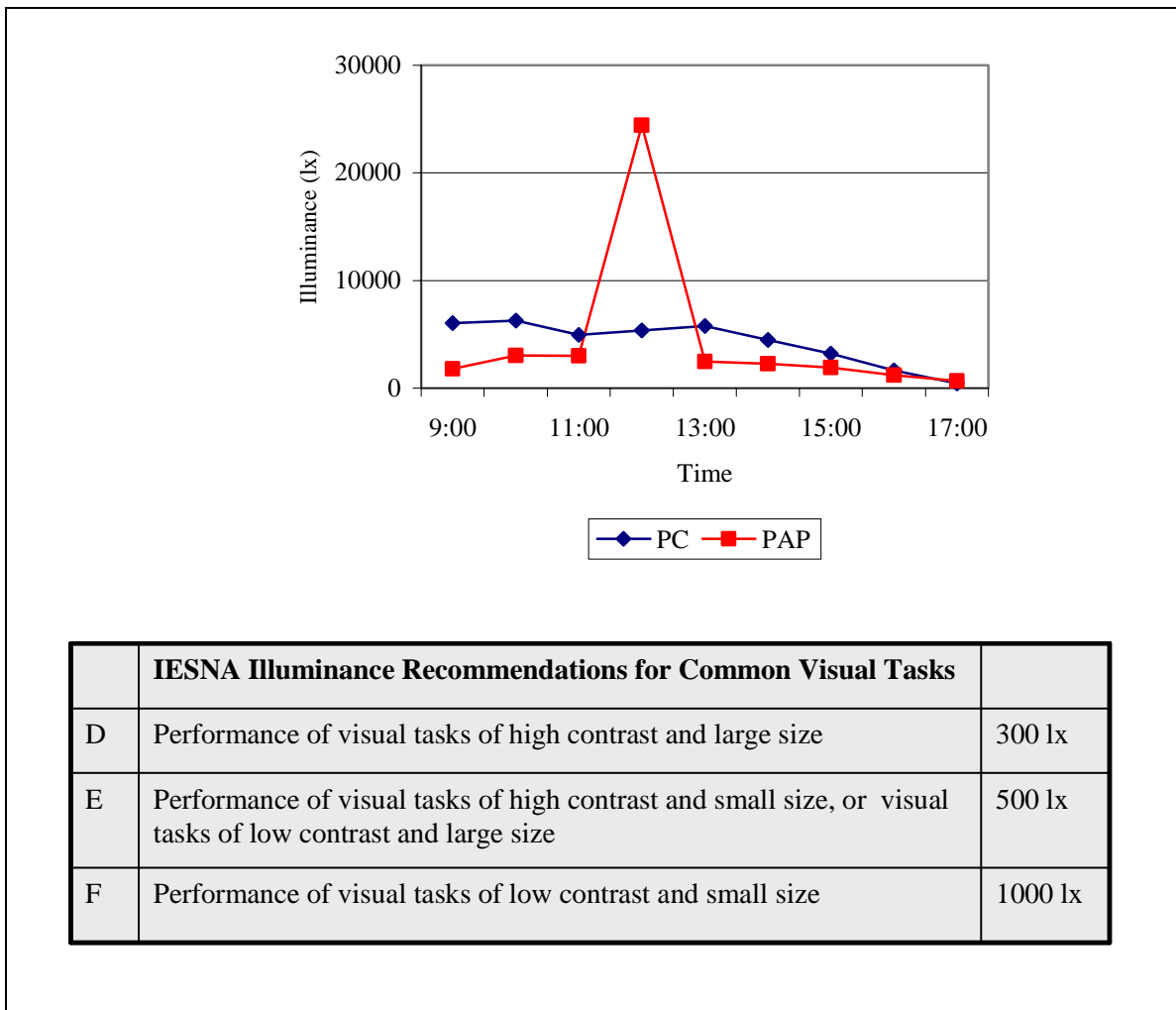


Fig. 4.5 Horizontal illuminance on the paper and vertical illuminance on the computer screen; the IESNA recommendations for common visual tasks

## Distribution

The spatial distribution of light is a measure of luminance and/or illuminance variability across a plane or surface [93]. An adequate amount of variation in luminance and/or color assures good visual comfort and performance, and an aesthetically pleasing environment. The simplest and most crude way is to look at the average value accompanied with the maximum and minimum values. These values can be used as indicators of the quality of lighting design. The quantities that deviate significantly from the target values may indicate poor lighting conditions [2].

In the physical world, spatial distribution of light is determined through multi-point measurements on surfaces. The major drawback is that large numbers of measurements have to be done in a grid pattern to determine the distribution on or across a surface. Obviously, the number of points determines the resolution of the distribution pattern as well as the precision of average calculations. The distributions can also be expressed in terms of the ratio of two quantities, such as the ‘maximum to minimum’, ‘maximum to average’, and ‘average to minimum’. The maxima and minima have to be located in the field of view for this kind of analysis. This is not always a straightforward task. Due to the spatial and temporal variations, measuring one point (or time) versus another could produce different quantities and ratios, which could point to an ambiguous and non-repeatable measuring process.

The VLL is a very convenient environment for studying the lighting distributions. It is a trivial task to calculate the average and locate the minima and maxima from the lighting matrix. The resolution of the data is equivalent to the resolution of the image, which cannot be matched with any physical measurement.

Fig. 4.6 shows the minimum, maximum and average luminance values on Dec. 21 when the viewer is looking at the computer screen. Since the variations are enormous, logarithmic scale is used. It is also an appropriate representation for luminance values

because human vision is sensitive to logarithmic differences. At nighttime, the average luminance is  $27.4 \text{ cd/m}^2$ , with minima and maxima of  $0.0023$  and  $1953 \text{ cd/m}^2$ , respectively.

Fig. 4.7 shows the ‘maximum to minimum’, ‘maximum to average’, and ‘average to minimum’ variations when the viewer is looking at the computer screen. The variations are significant between 11:00 to 14:00 in particular. The ‘maximum to minimum’, ‘maximum to average’, and ‘average to minimum’ values for the nighttime are 51200, 71, and 11917 to 1, respectively.

Average, minimum, maximum, and point values provide a generic idea about the performance of lighting. However, they are not sufficient to describe and evaluate the lighting performance. Specifically, they are ineffective in describing the light distribution pattern over different architectural surfaces. As the next step, various analysis approaches are presented with specific focus on the actual task.

Luminance variations ‘between the task and the immediate background’, ‘across the immediate task’, and ‘between the task and the ambient surfaces’ are very distinct matters that have to be treated differently. The suitable ratios for these luminance variations have to be obtained.

Luminance variation between the task and the immediate background is needed to distinguish the details of the task. Luminance and luminance contrast are the variables that affect the task visibility along with the task size and age of the observer. Adequate luminance variation contributes to the contrast variation by making parts of the task to appear distinct. Excessive luminance variation reduces the contrast through veiling reflections, disability, and discomfort glare.

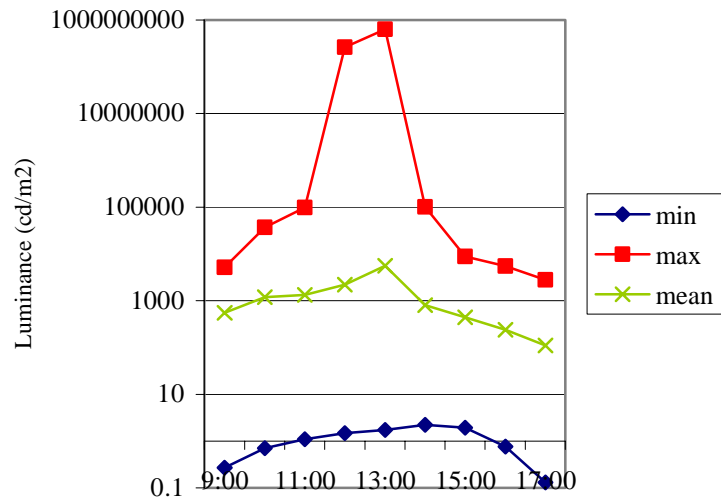


Fig. 4.6 Minimum, maximum, and mean luminance values in logarithmic scale throughout Dec. 21, when the viewer is looking at the computer screen

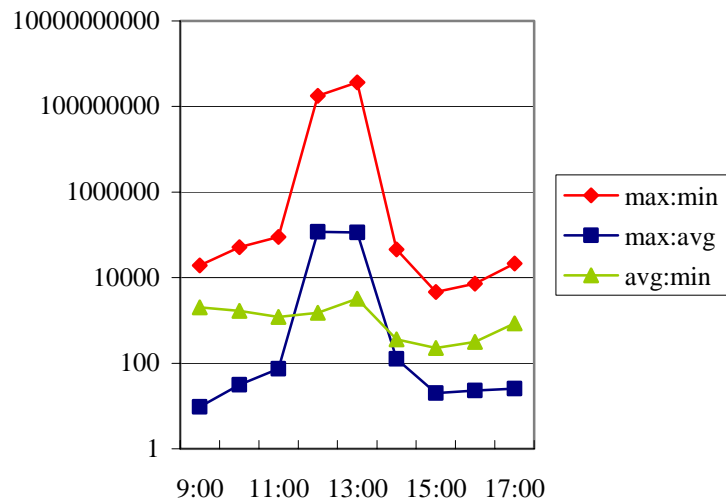


Fig. 4.7 'Maximum to minimum', 'maximum to average', and 'average to minimum' luminance ratios throughout Dec. 21, when the viewer is looking at the computer screen

Luminance variation across the immediate task has to be kept within 3:1 range, where the task luminance is suggested to be higher than the immediate surrounding. Ceiling and walls are recommended to be within a 3:1 luminance ratio. Distant room surfaces are preferred to be within 10:1 luminance range (40:1 maximum). In offices with computer tasks, the maximum allowable ceiling luminance is  $850 \text{ cd/m}^2$ , whereas the desirable ceiling luminance is to be less than  $425 \text{ cd/m}^2$ . Maximum to the minimum ceiling luminance ratios up to 8:1 are acceptable whereas 2:1 ratios are desirable. These recommendations are specified to avoid extreme luminance differences since the human vision cannot adapt to wide range of luminances at once. They are the generalized results of studies that investigate the effects of different lighting variables on visual comfort and performance [2, 93].

The scene in Figure 4.8 is decomposed into elements, which are the computer screen, paper, wall behind the task, table, and the window. Minimum, maximum, and mean luminance values, luminance range and ratios are identified. This analysis again reveals the problems caused by the excessive daylight. The maximum luminance values and the luminance ranges are unacceptably high. Fig. 4.9 demonstrates the identified elements in other scenes, which include various combinations of the task and surroundings.

Contrast on the paper is the quotient of the difference between foreground and background luminance values and the background luminance value [2]. It quantifies the visibility of foreground relative to its immediate background. Contrast on the computer screen is the quotient of the background to foreground luminance. It is the contrast calculation method used for self luminous displays, and quantifies the effect of veiling reflections that occur due to the lighting characteristics of the space and specular reflection characteristics of the computer screen [19, 80]. Virtual luminance contrasts are calculated for the paper and the computer screen through regional data analysis. The formulae are as follows:

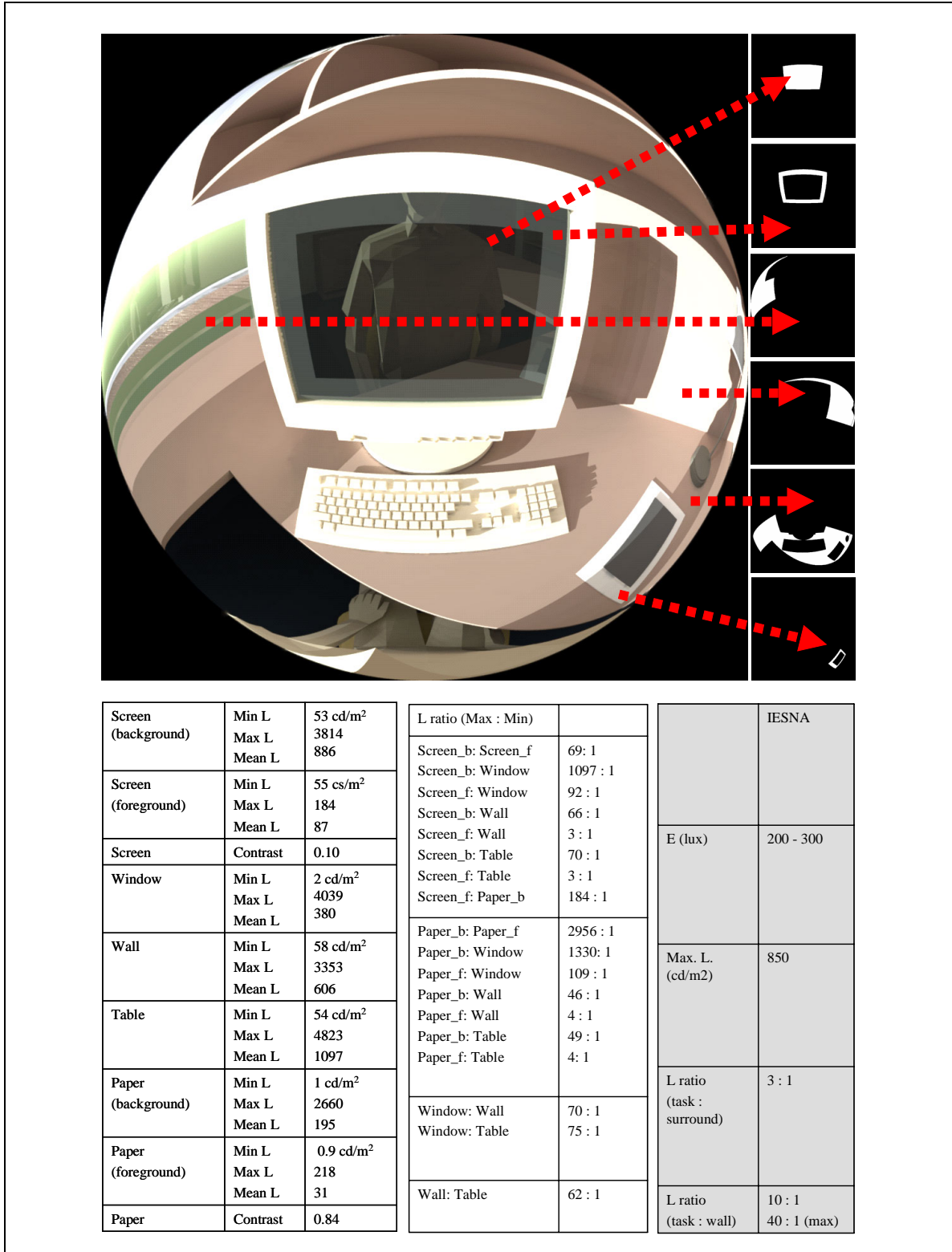


Figure 4.8 The scene is decomposed into architectural elements to study the luminance ratios

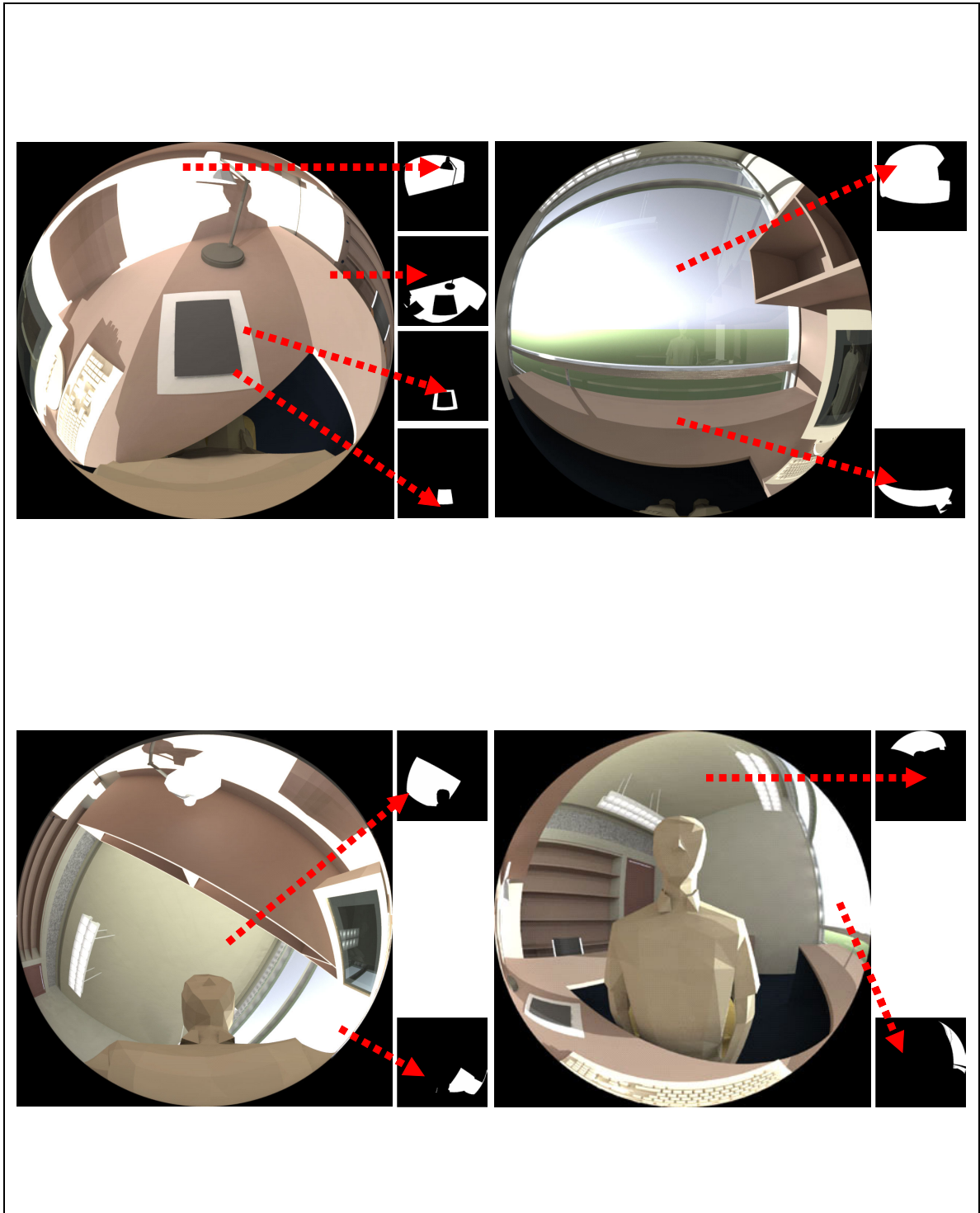


Fig. 4.9 The decomposition of different scenes into architectural elements

$$\text{Virtual Contrast}_{\text{paper}} = \frac{|\text{Avg. L. of background pixels} - \text{Avg. L. of foreground pixels}|}{\text{Avg. L. of background pixels}}$$

$$\text{Virtual Contrast}_{\text{computer screen}} = \frac{\text{Avg. L. of foreground pixels}}{\text{Avg. L. of background pixels}}$$

Figure 4.10 shows the dynamics of the screen and paper contrast throughout the day. Both for the paper and computer tasks, 13:00 is the most troublesome time of the day. Pertinent to the calculation methods, a higher contrast value denotes better visibility conditions on paper and a lower contrast value denotes better visibility conditions on the computer screen. During nighttime, the contrasts on paper and computer screen are calculated as 0.85 and 0.14, respectively.

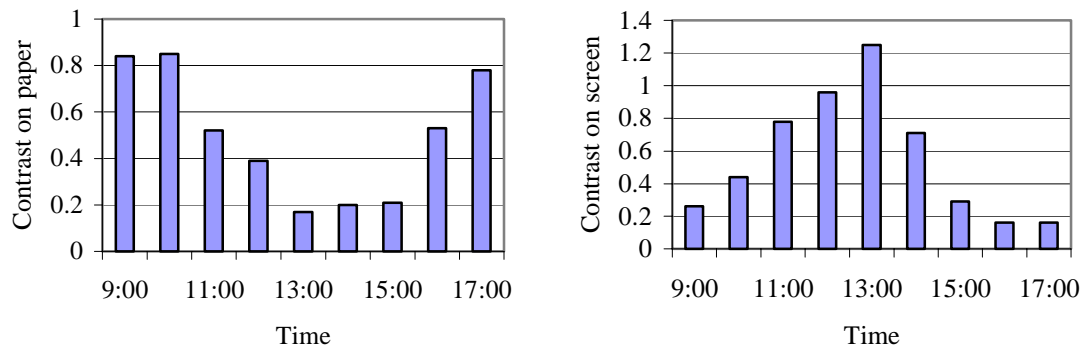


Fig. 4.10 Contrast variation on the paper and computer screen throughout Dec. 21

In the VLL, the scenes can also be dissected into specific regions of the visual field, i.e. foveal, binocular, and peripheral, to have a better understanding of the performance of the human vision (Fig 4.11). The total human vision is 180° horizontally and 130° vertically. Monocular human vision is considered to be approximately 90° temporally, 60° nasally (restricted by the nose), 70° inferiorly (restricted by the cheek) and 50° superiorly (restricted by the brow). The central 120° forms the combined

binocular vision, which is the overlap of two monocular fields. Fovea is the central  $2^\circ$  visual field on visual axis [2]. Note that the boundaries of visual fields in the figure have been modified by the cosine of the polar angle to match the hemispherical fisheye projection. In all images generated from the viewer's point, the task is centered at the fovea, i.e., the viewer is fixated at the task.

Fig. 4.12 demonstrates the average luminance variations in the fisheye view, total vision, binocular vision, and foveal vision. In the scene where the viewer is looking at the computer screen (Fig. 4.12.a), the extremes occur outside the human total vision. Therefore, it might be misleading to process the data from the fisheye view. In the scene where the viewer is looking at the paper (Fig. 4.12.b), the variations occur in the total vision, with major extremes in binocular vision and foveal vision. In the scene where the viewer is looking through the window (Fig. 4.12.c), the variations are notable in the binocular vision. It is very important that these extreme variations are addressed with appropriate design decisions.

It is also interesting to study the luminance differences in different parts of the visual field when the occupant is looking at different tasks. Fig. 4.13 demonstrates the luminance transition occurring when the occupant switches from the computer screen to the paper, and to the window. As a general rule, the occupant should not be exposed to a wide luminance range between consecutive tasks to avoid visual performance and comfort problems. The human visual system can be quite insensitive to large luminance differences in the total field of view, but it is very sensitive to small luminance differences in the foveal region. As seen in the figure, extreme variations occur at the fovea.

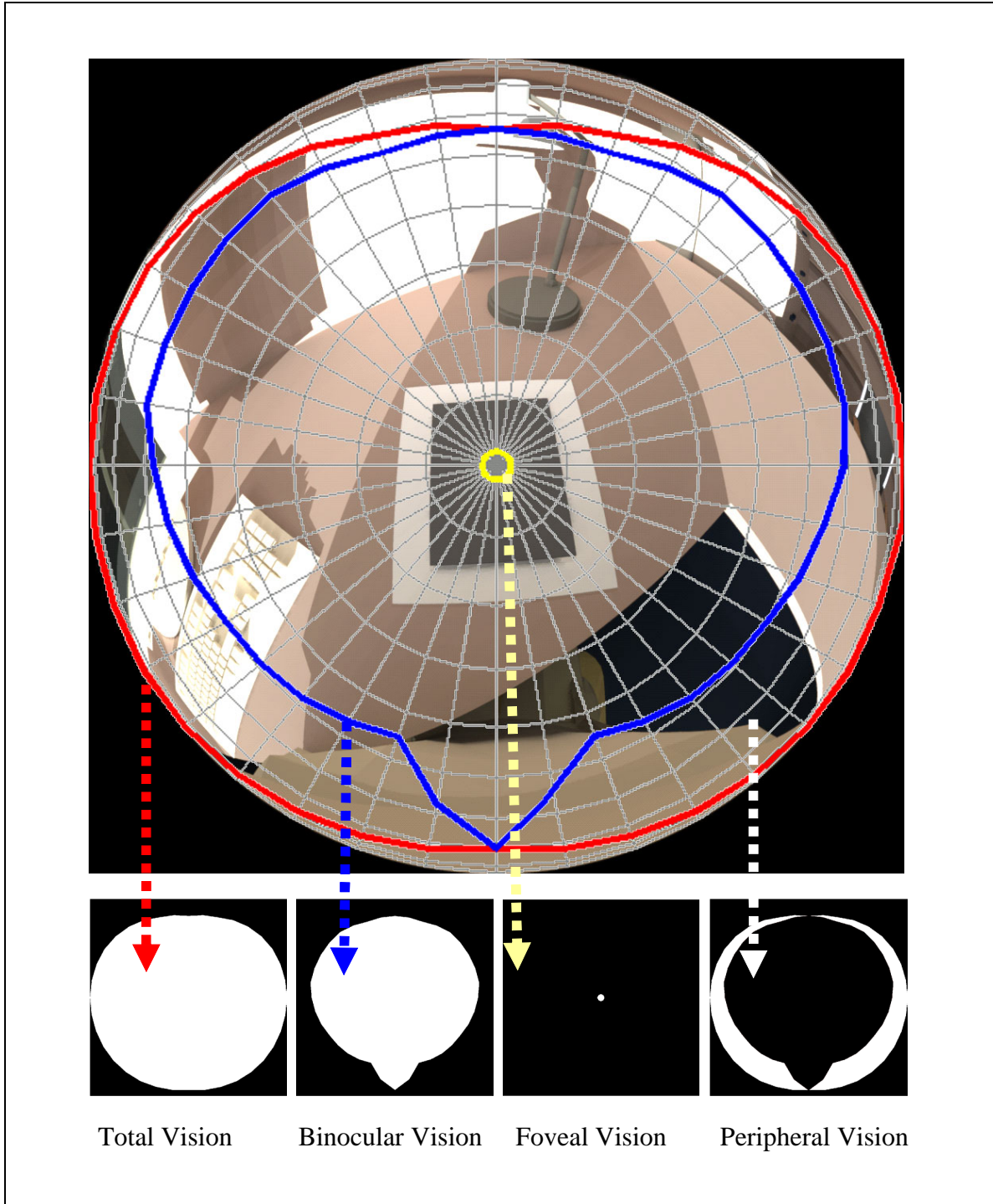
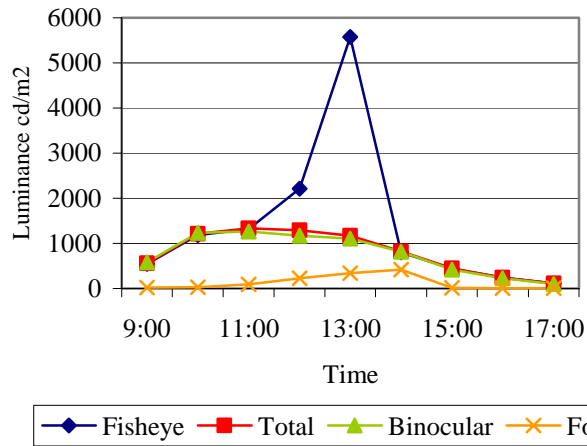
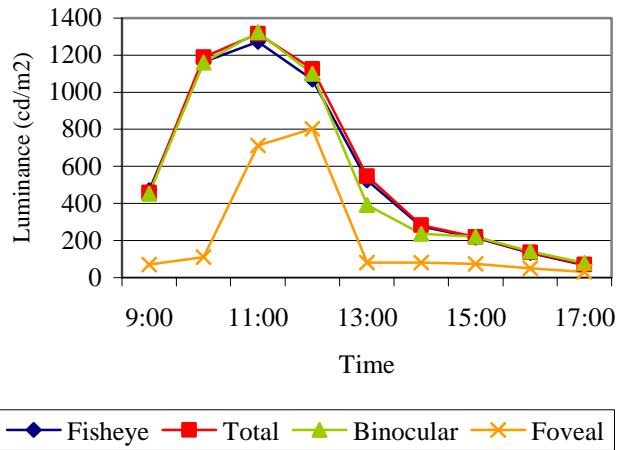


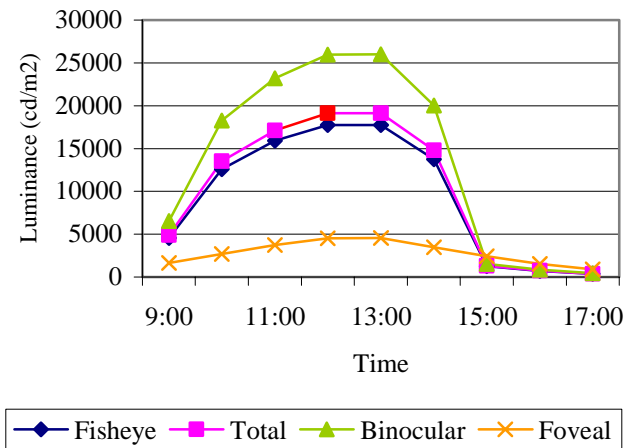
Fig. 4.11 The decomposition of a scene into human field of view



a) Eye2pc



b) Eye2paper



c) Eye2win

Fig. 4.12 Luminance variations in different parts of the visual field throughout

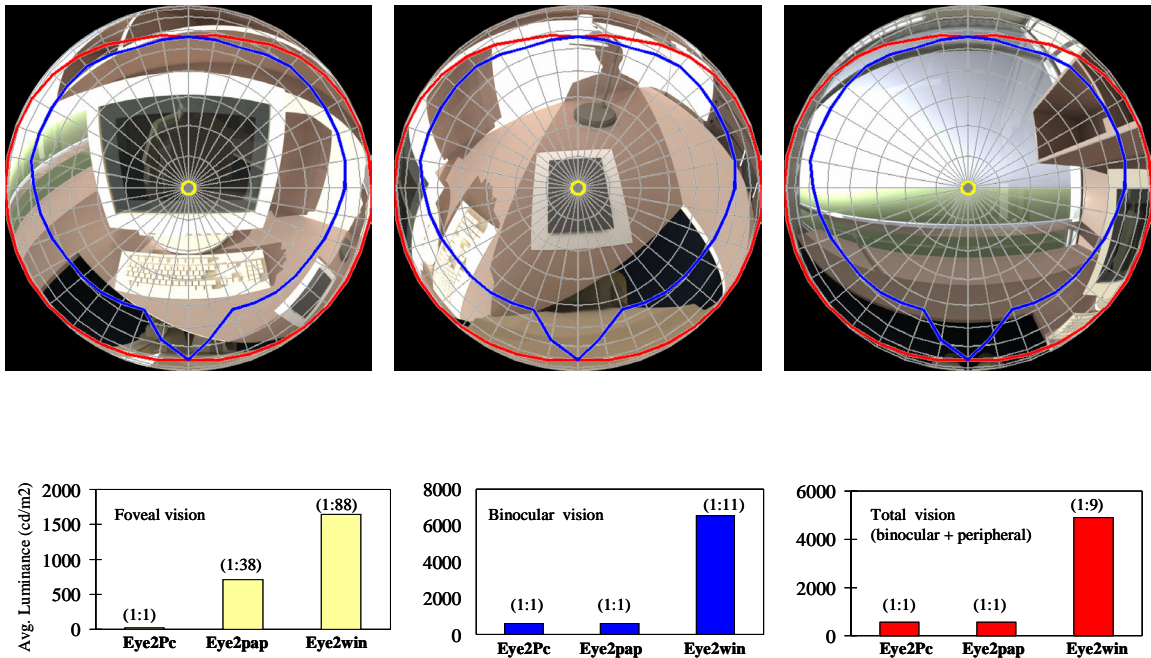


Figure 4.13 Luminance ratios (eye2pc:eye2pc, eye2pc:eye2pap, eye2pc:eye2win) in different regions of the visual field as the viewer switches between the visual tasks (The ratios are given with respect to the computer task).

The luminance distribution patterns play a significant role in determining the adaptation luminance and discomfort/disability glare. Adaptation is the process by which the properties of the visual system are modified according to the luminances in the field of view [82]. One of the reasons why researchers conduct laboratory experiments rather than field studies is that measurability has always been an issue in complex environments. Luminance adaptation affects visual acuity, contrast sensitivity, and color perception. In practice, adaptation luminance is usually taken as the average luminance in the relevant viewpoint, which is a gross simplification. The adaptation luminance is affected both from the average and the variance of the luminance distribution [94]. The response to light is not the consistent over the human retina. The photoreceptors (rods and cones) are unevenly distributed: Cones are concentrated on the fovea and rods rapidly peak outside the fovea, but decrease towards far periphery [2]. Calculating the

average luminance is a nontrivial task. To avoid ambiguity, research studies such as glare indices, originate from physical laboratory environments which provide homogeneous luminance for the surrounding [95]. However, the resultant empirical formulae cannot predict the effect of varying luminance across the visual field.

In the VLL, the luminance values can be studied in relation to their physical position within the total visual field. It can be conveniently utilized as an analysis tool as well as an analysis aid to psychophysical experiments for documenting the photometric properties of complex environments. Therefore, these studies can be shifted from simple laboratory environments to realistic settings. The VLL provides potentially significant contributions to future psychophysical research. One application would be to study the variability of the luminance patterns in the visual field to determine the adaptation luminance and glare assessment<sup>16</sup>. It would also be interesting to study transitional adaptation process<sup>17</sup>. Another application would be to study the occupancy perception and preference in relation to lighting distributions. As discussed, the lighting designer specifies a target illuminance and/or luminance values. It is neither possible nor desirable to achieve a uniform value throughout the entire space or task. However, it is necessary to distinguish variations that are desirable, noticeable, tolerable or disturbing<sup>18</sup>.

---

<sup>16</sup> There is no explicit procedure to calculate the adaptation luminance level in complex settings. The primary obstacle has been to measure the data and relate it to the foveal, binocular, and peripheral visual fields. The ability to achieve such data in the VLL could enable effective methods to calculate the adaptation luminance. Obviously, such a study would require a multi-disciplinary approach and numerous psychophysical experiments.

<sup>17</sup> It has been difficult to account for the effect of the scanning movements of the eye in lighting analysis. These movements can be studied within one fisheye image for solid angles of 2°, corresponding to the foveal vision. The area seen by the fovea would change as the line of sight changes in the visual field. Sufficiently large differences in these areas produce transient adaptation effects. Therefore, it is possible to study these effects by dissecting the field of view into sufficiently small solid angles. The study of the transient adaptation process would require frequent time steps, such as per minute, in daylight environments. Again, this study would require numerous psychophysical experiments; but the capabilities in the VLL enable the collection of the necessary data.

<sup>18</sup> There are many studies on the psychological effect of lighting, perception, and aesthetics. Despite the large number of studies, it has not been possible to quantify these effects. An obstacle has been the inability

Per-pixel analysis allows for a more detailed study of the luminance variations. Per-pixel lighting data provides invaluable information for analysis, but it might also be difficult to process the data. Several techniques are exemplified here. They are not exhaustive in nature; rather, they highlight some of the per-pixel analysis capabilities.

Per-pixel analysis can be used to calculate the criterion rating which quantifies the probability that a specific criterion is met within a defined area [2]. It can be expressed for various lighting quantities such as luminance, illuminance, contrast, and CCT. The Virtual Criterion Rating (VCR) is calculated as follows:

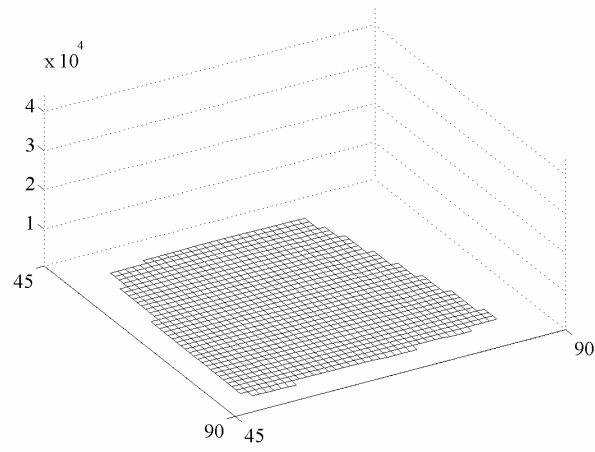
$$\text{VCR (\%)} = \frac{\text{Number of pixels satisfying the criterion} * 100}{\text{Total number of pixels}}$$

The VCR has been applied to the target illuminance value on the paper task. It is necessary to achieve the target illuminance with a sound uniformity level across the task surface. As a guideline, it is suggested to study the task illuminance and luminance values to ensure that they are between 2/3 to 4/3 of the target value. The limits are still flexible and it is suggested to aim for achieving the 2/3 to 4/3 range in 90% of the task locations. Task illumination levels do not have to be maintained throughout the whole space. Ambient lighting can be provided to illuminate the rest of the space and it is advised to be 1/3 of the task illumination level [2, 93]. The variation in the task can be studied on a per-pixel scale by isolating the data as suggested in the regional data analysis techniques.

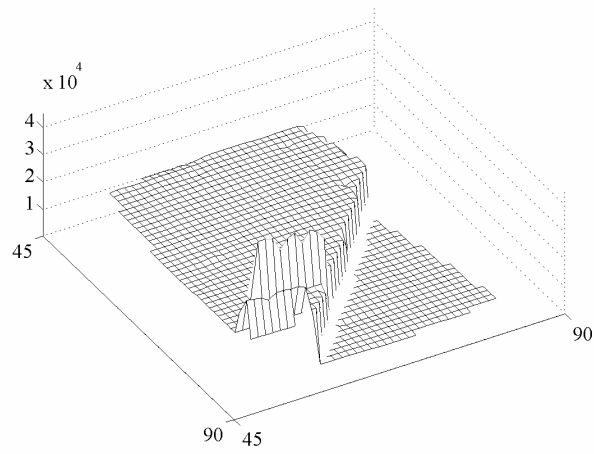
Fig. 4.14 shows the per-pixel illuminance values on the paper on Dec. 21 for selected hours. All graphs are given with the same scale, with values varying between 0 to 45,000 lx, which includes the minimum and maximum data throughout the day. The high values at 11:00 and 12:00 are due to direct rays of sun, where as the sharp drop offs are due to the body shadow of the occupant on the paper.

---

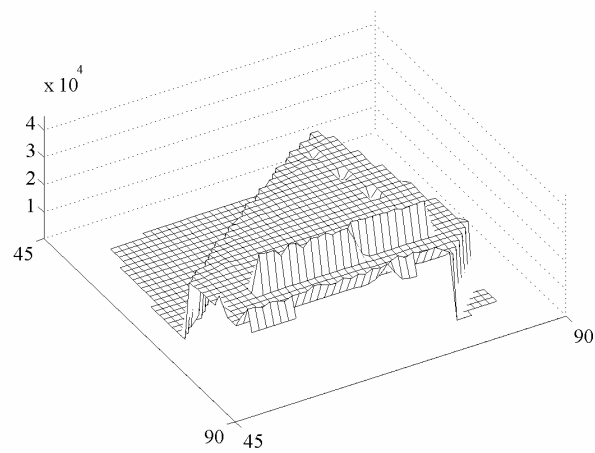
to document the lighting properties of the space in sufficient detail. The VLL provides this ability so that the numerical information of the space could be correlated with the sensation it creates.



10:00



11:00



12:00

Fig. 4.14 Per-pixel illuminance values on the paper for Dec. 21 on selected hours

The pixel values are further studied to check the VCR. The target value for the paper task has been established as 500 lx. Since the paper tasks have flexible limits, the acceptable range is taken as 300-1000 lx, where 300 lx reflects the IESNA recommendation for visual tasks of high contrast and large size, and 1000 lx reflects the recommendation for visual tasks of low contrast and small size [2]. For nighttime, 84% of the pixels that correspond to the paper task satisfy the 300-1000 lx range. During daytime, the criterion rating is quite low since most of the illuminance values are above 1000 lx. In Fig. 4.15, the VCR and the contrast on the paper task are plotted on the same graph. The contrasts on the paper task are good at 9:00 and 10:00 despite the poor criterion ratings, because the body shadow on the paper blocks the excessive daylight on the paper.

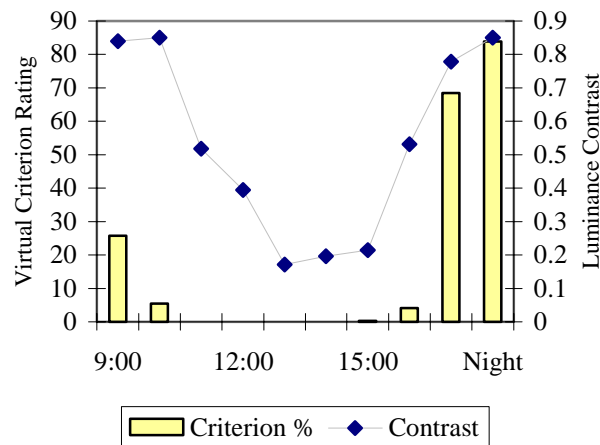


Fig. 4.15 The VCR for illuminance on the paper throughout Dec. 21

Although it is effective to study the visual tasks separately, the ambient and task lighting must work together. The luminance distribution patterns for the nighttime and daytime images are studied in per-pixel detail when the viewer is looking at the computer screen. The nighttime image is selected for relatively low luminance distribution and the daytime image (12:00) is selected for the high luminance distribution pattern. Fig. 4.16

shows the mesh plot for the night scene. In this figure, the first mesh plot illustrates the luminance distribution in the total luminance range. This graph illustrates the location of the high luminance values, which correspond to the task lighting area. The close-up image is done with block processing; i.e. the 1024 by 1024 image has been processed as 128 by 128 blocks, where each block represents an area corresponding to an 8 by 8 matrix. The maximum value of each block has been represented. The data between 0 to 100  $\text{cd}/\text{m}^2$  is presented in the plots which provide insightful information about the luminance distribution. It is apparent from this information that it might be deceptive to study average, minimum, and maximum values to understand the distribution pattern of the luminance data.

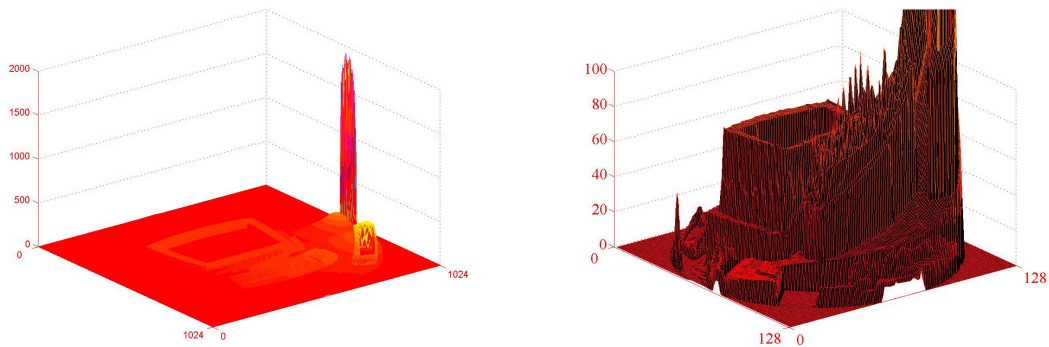


Fig. 4.16 Mesh plots for the luminance distribution at nighttime when the viewer is looking at the computer screen

Another way to visualize this data is provided in Fig. 4.17. The first histogram demonstrates that the data is unimodal and skewed to the left. Although the data spreads from 0.0023 to 1953  $\text{cd}/\text{m}^2$ , 99.67% of the pixels have luminance values between 0 to 200  $\text{cd}/\text{m}^2$ . The second histogram shows the data for this range. The close up view reveals that most of the pixel values lie between 0 to 20  $\text{cd}/\text{m}^2$  (58.81%). These graphs

suggest that the luminance distribution pattern is somewhat in close range throughout the scene with few outlier pixels.

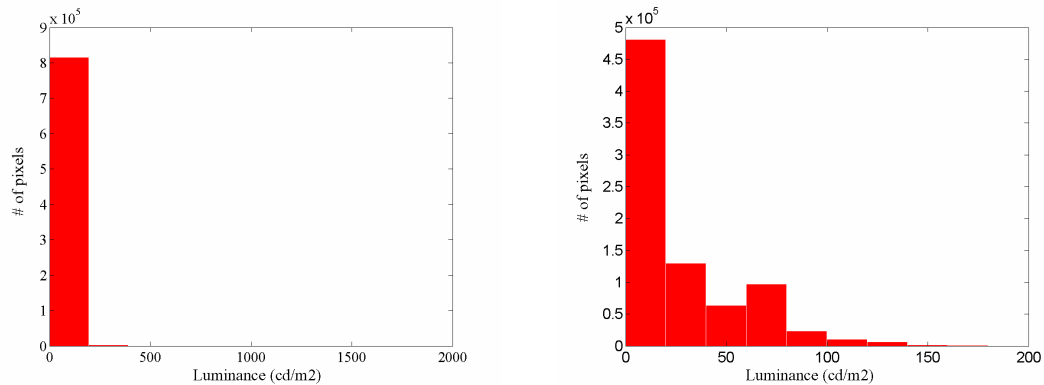


Fig. 4.17 Luminance distribution histograms for the nighttime when the viewer is looking at the computer screen

The mesh plots in Fig. 4.18 show the location and distribution of the variation in different scales. Fig. 4.19 shows the histograms for the daytime. Obviously, the luminance variation is much higher for this scene than the night scene. The average, maximum, and minimum luminance values are 2210, 261,579,980, and 1.5 cd/m<sup>2</sup>, respectively. The data is again unimodal and skewed to the left. Actually, 99.89% of the pixels are less than 10,000 cd/m<sup>2</sup>, 91.10% of the pixels are less than 3000 cd/m<sup>2</sup>, and 52.80% of the pixels lie between 0 and 500 cd/m<sup>2</sup>. These histograms given in different luminance ranges suggest that, although luminance distribution pattern is quite non-uniform throughout the scene, the extreme value suggested by the maxima occurs in few pixels as an outlier.

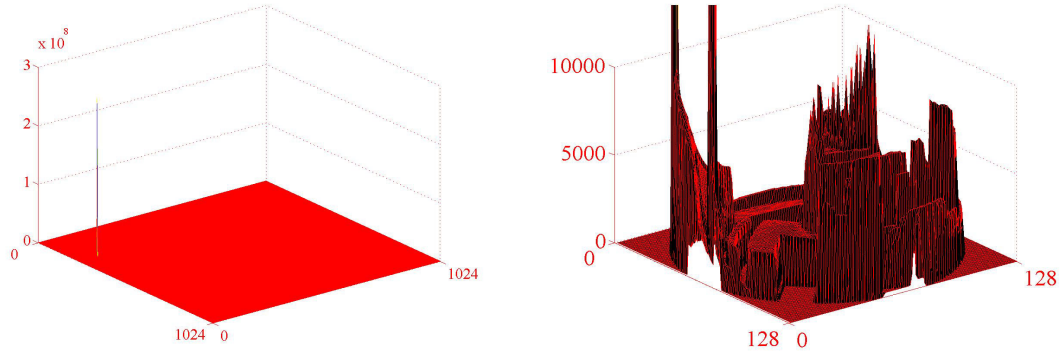


Fig. 4.18 Mesh plots for the luminance distribution on Dec. 21, at 12:00, when the viewer is looking at the computer screen

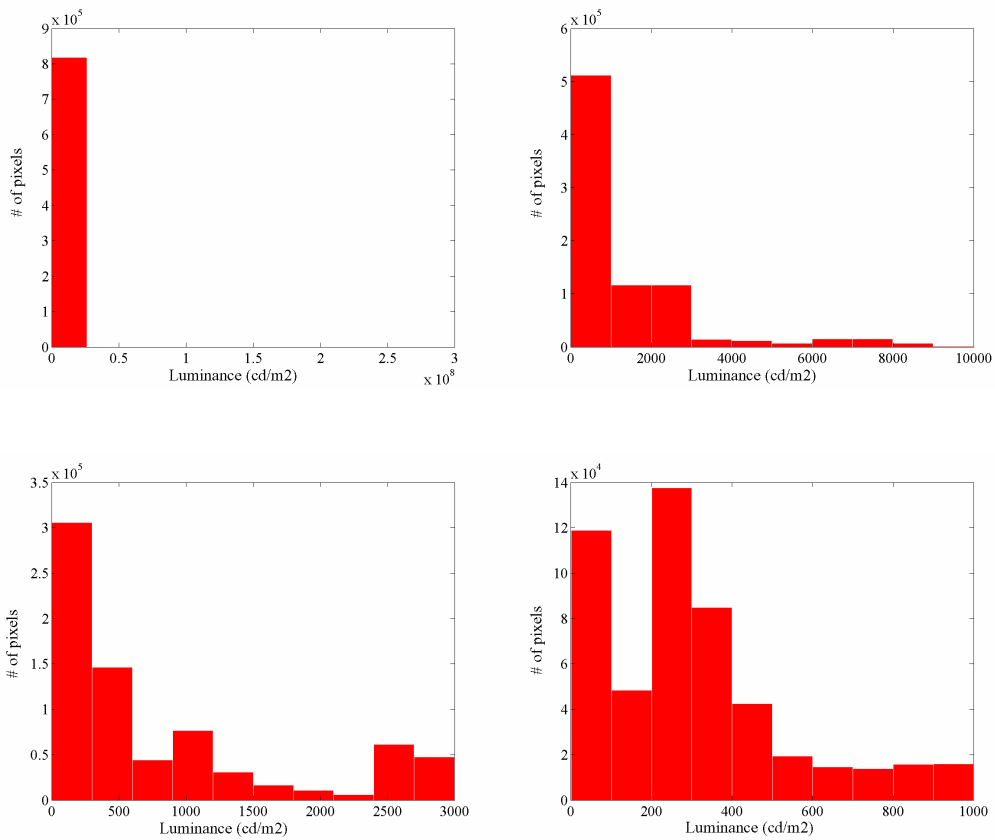


Fig. 4.19 Luminance distribution histograms for Dec. 21, at 12:00, when the viewer is looking at the computer screen

In general, it is difficult to interpret the maximum value since it may indicate bad lighting quality such as poor visibility, discomfort, and visual clutter; or it may indicate good lighting quality such as highlights and sparkles.

There are three distinct variation patterns in a luminous environment: the shadow pattern, the highlight pattern, and the shading pattern [96]. These are actually the outcome of the directionality of light, which will be discussed later in this chapter. Here, they are analyzed within the context of the luminance distributions. From a practical standpoint, the highlights, shadows, and shading patterns, and even the veiling reflections and glare, are all produced in the same way, where the determining factor becomes the angular size of the light source on the surface that has the high luminance (i.e. the size of the light source in relation to its distance to the object or eye) [96]. For example, a circular light, with a semi-subtense angle of  $1^\circ$  or less, creates highlights and sparkles on a dielectric surface; casts shadows with quite sharp edges; and produces a shading pattern with maximum contrast level (the gray levels range from 100 to 0%). A circular light with a semi-subtense angle of  $10^\circ$  creates blurred highlights and shadows; and produces reduced contrast. The circular light, with a semi-subtense angle of  $90^\circ$  and beyond (equivalent of an integrating sphere for a 2D task) creates washed-out lighting; contrast is diminished; shading patterns provide a reduced range of gray levels; shadows are absent; and highlights have spread into veiling reflections [97].

On the positive side, luminance variation patterns create a stimulating and interesting environment which contributes to the well-being of the occupants. Luminance variations are also necessary for visual comfort and performance. Peak luminances may contribute to the contrast variation by making details of the task more visible. They may contribute to the visual comfort by providing visual interest for distant eye focus, which is good for eye muscle relaxation.

Peak luminances which exceed the luminance ratio recommendations in small visual areas are called highlights and sparkles. The highlights can have luminance ratios

of 5 or more logarithmic units. This might seem to be contradicting with luminance ratio recommendations given earlier in this section. The recommendations aim to prevent excessive luminance ratios in large visual areas that might create glare, veiling reflections, and transient adaptation problems. Highlights and sparkles, on the contrary, may provide visual information that contributes to visibility. For example, highlights from a dielectric material such as a shiny glass reveal the shape of the object; whereas the uniform lighting conditions in an integrating sphere cause the object to visually disappear. This is also the reason behind choosing a glossy paper for magazines rather than matte paper, because the specular reflections (which are white -or the color of the light within the environment - rather than the color of the object) increase the contrast on the task. It equates to darkened blacks and saturated colors in comparison to lightened blacks and faded colors with matte surfaces. The highlights and sparkles on the task can easily be avoided by a small movement of the head or task [96].

On the negative side, luminance variation may create a distracting and confusing environment through visual clutter, which is usually manifested by harsh reflections and irregular light-shade patterns in the environment. In the extreme situations, the consequences are veiling reflections, disability and discomfort glare. Large area sources abolish highlights, and create surface reflections that become “veiling reflections” that smear the details of the task, lighten the blacks and un-saturate colors. They are difficult to avoid [98]. These kinds of sources and semi-specular tasks form the underlying assumptions behind CRF calculations, which are discussed in Chapter III.

The above information on the effect of luminance distribution patterns, directs the discussion back to the means of interpreting the maximum luminance value in a scene that may indicate bad or good lighting quality. It is possible to interpret luminance variations with the per-pixel data in the VLL. The interesting information in Figures 4.16 - 4.19 is that the peak luminances occur in few pixels as outliers. The outliers potentially identify the positive peak luminances, rather than troublesome areas when the rest of the

pixels fall into acceptable ranges. Obviously, the location of the peak luminance is of utmost importance and it can be studied with the mesh plots (Fig. 4.16 and 4.18). The highlights and sparkles add to the quality of the scene when they are meaningfully located since the eye is drawn to the bright parts in the scene<sup>19</sup>.

Alternative means of analyzing per-pixel data is provided through an image subtraction operation. The sun positions, shadows, and the depth of each shadow have significant effects on the daytime luminance variation. Two images are generated to study the effect of the sun. In the first image, the viewer is looking at the computer screen on Dec. 21, 12:00. The sky model is CIE Clear Sky. The second image is generated with the exact features, except that the sun is omitted from the clear sky model. The second image is subtracted from the first, and the new image demonstrates the variations caused by the sun (Fig. 4.20). Note that, again, such an analysis is possible only with a physically based rendering approach.

In the first image, the average is 2211 cd/m<sup>2</sup> with a variance of 2.6e+008. In the second image, the average is 394 cd/m<sup>2</sup> with a variance of 10552. In the third image, the average is 1817 with a variance of 2.6e+008. The luminance distribution histograms illustrated in Fig. 4.21 show the data between 0 and 5000 cd/m<sup>2</sup>. The results clearly

---

<sup>19</sup> Another interesting analysis in the per-pixel framework is done by studying the highlights closely in relation to visual acuity. Critical task detail is defined as the 0.5° arc (the angle that it subtends at the eye), which can correspond to the detail differentiating an 'O', from a 'C', or a 'G' when the eye-task distance is fixed at a typical reading distance of 40 cm (16 inch). With per-pixel analysis, it is possible to go into such detail. When the task is located in the middle of the hemispherical fisheye image, 0.5° arc corresponds to 30 pixels, where as the foveal region corresponds to 1002 pixels.

Given that the eye is drawn to the bright parts, it is possible to locate the highlights in the scene when the viewer is performing a certain task. For instance, the eye can switch between a paper task, and a highlight in the scene. In the scenes where the viewer is looking at the paper, the luminance average of the highlight can be calculated in an area corresponding to critical task detail, as the foreground. The luminance average of the paper task can be calculated in the foveal area, as the background. Therefore, it is possible to calculate the resultant contrast on the eye. This kind of analysis illustrates the further contribution of the VLL that can be used in the vision studies.

demonstrate that the high luminance variations are caused by the direct rays of the sun and a design goal should be to limit them within the office space.

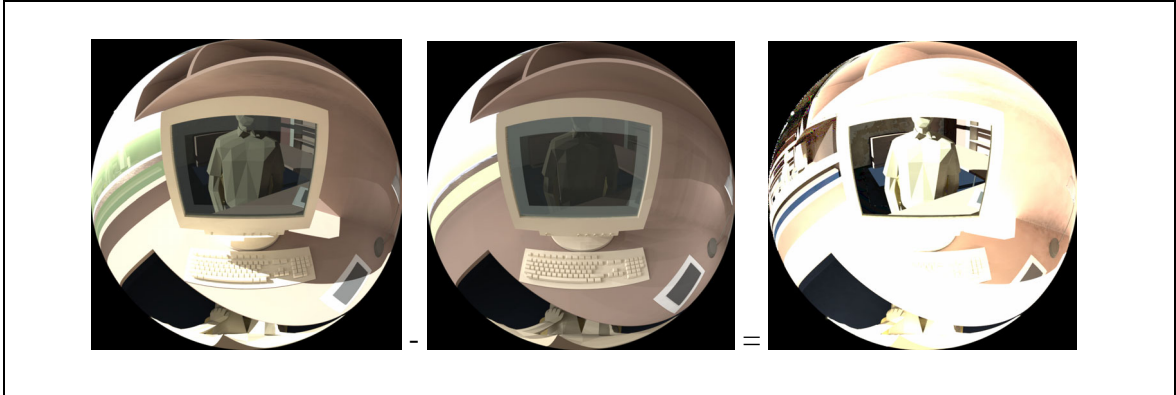


Fig. 4.20 Viewer's sight of the computer screen a) Clear sky with the sun b) Clear sky without the sun: the 'skylight' c) Difference of a and b: the effect of the 'sun'

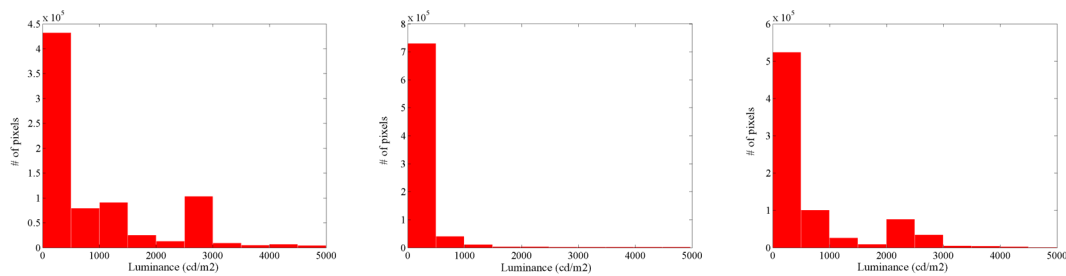


Fig. 4.21 Luminance distribution histograms analyzing the viewer's sight of the computer screen a) Clear sky with the sun b) Clear sky without the sun: the 'skylight' c) Difference of a and b

It is also useful to study the per-pixel information to determine the 'rate of change'. For instance, the rate of change can be determined for a series of images to demonstrate the temporal dynamics. In Fig. 4.22 the rate of hourly change is plotted for Dec. 21, when the viewer is looking at the computer screen. All graphs are plotted in the same scale to compare the hourly rate of change.

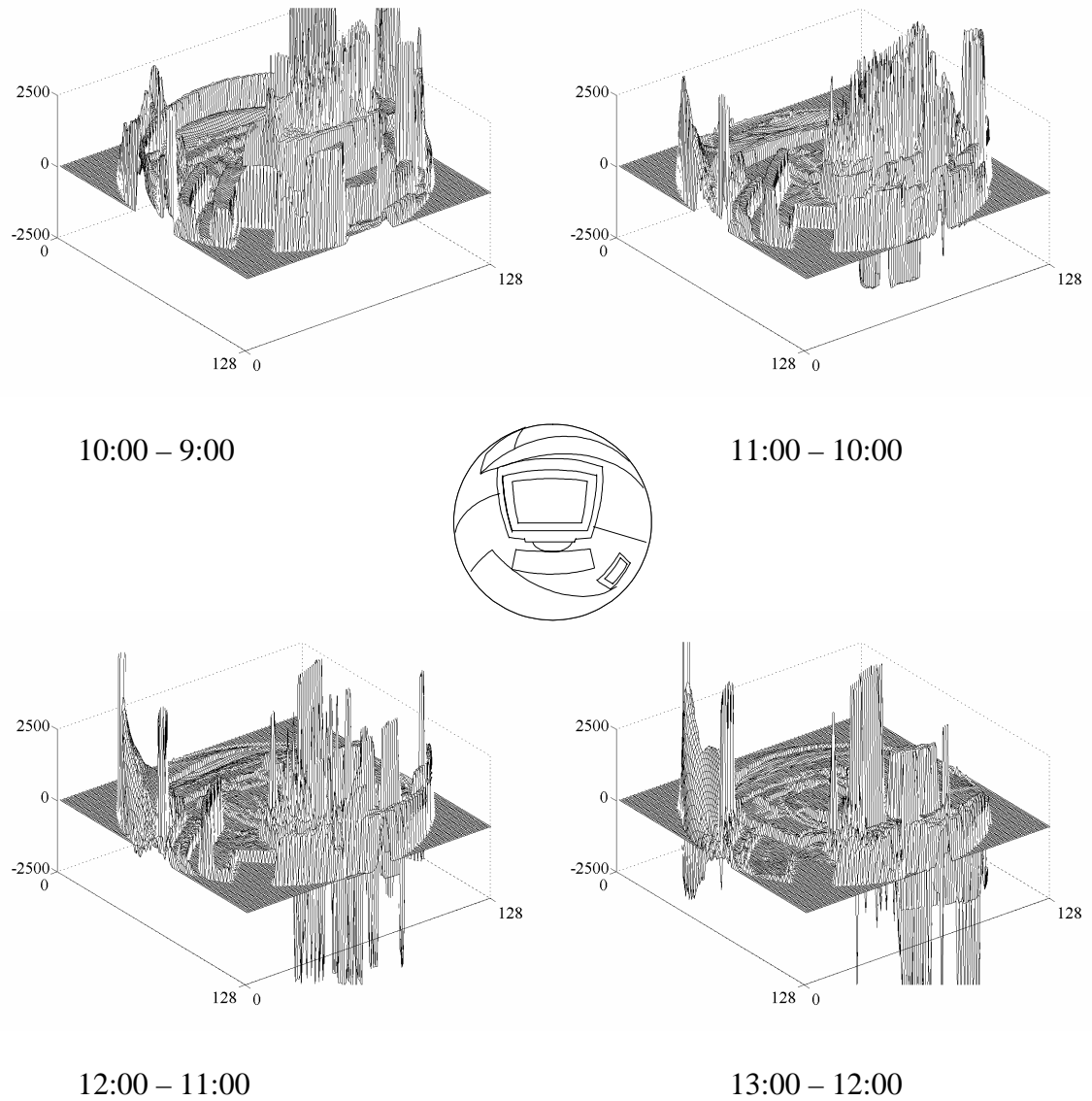


Fig. 4.22 Rate of change in the luminance values between hourly images on Dec. 21, when the viewer is looking at the computer screen

## Directionality

The directionality of light is a balance between the diffuse and directional components within the luminous environment. It gives an indication about the spatial distribution of light flow onto an element or into a space. On one hand, poor directionality may create shadows on the task or veiling reflections towards the viewing angle. On the other hand, adequate directionality may distinguish the details of a task, reveal the surface textures, and model the 3D surfaces [82].

Vertical to horizontal illuminance ratio (V/H ratio) is one of the performance indicators used for assessing the directionality of light. It is based on the ratio of the intensity of light coming from side to the intensity of light coming from the top [99]. Fig. 4.23 shows the V/H ratio for outside and for the paper task. Since the V/H ratio is subject to substantial variations for different orientations, it is useful to study it in the four cardinal directions (east, west, south, and north). In general, the V/H ratio is less than 1.0 for dominant downlighting, and greater than 1.0 for dominant lateral lighting [99]. As seen in the figure, south and west facing V/H ratios point to strong lateral emphasis by daylight, specifically at 11:00. The V/H ratios during the nighttime for east, west, south, and north facing directions are 0.40, 0.31, 0.26, and 1.73, respectively. The north facing V/H ratio points to the anterior emphasis by the task lighting. In all other orientations, the electric lighting from the ceiling poses a downward emphasis and the small amount of lateral illumination originates from the interreflected light.

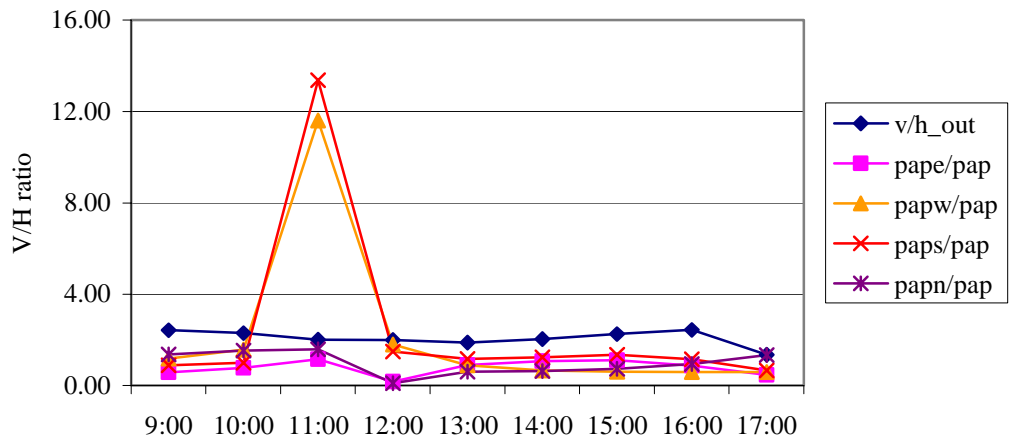


Fig. 4.23 V/H ratio for Dec. 21 on the paper in four cardinal directions

Other directionality indicators developed in the past include mean cylindrical and semi-cylindrical illuminance, scalar (mean spherical) illuminance and semi-scalar (mean hemispherical) illuminance, vector illuminance, vector-to-scalar illuminance ratio, and cubic illumination [96, 100-102]. Some of these techniques have been implemented in physically based rendering tools [102]. In the VLL, a more direct approach is adopted, based on the definition of directionality: The diffuse and directional components of the luminous environment are separated as a unique feature of virtual photometry (Fig. 2.24); and the ratio of the directional-to-diffuse lighting is suggested as a new indicator.

The directional components in Radiance include the light sources and specular reflections, which refer to all non-Lambertian reflections and transmissions (including refraction, ideal reflection and directional scatterings). Contribution of light sources is calculated through the ‘direct calculation’ method. Calculations of specular component is more complicated: The reflected component can be divided into components and some part of it could be handled in the ‘direct calculation’ as part of the BRTDF evaluation in the direction of each light source; while other parts are computed in the ‘indirect calculation’ [60].

The diffuse reflections refer to the Lambertian components from all surfaces other than the light sources. The diffuse component is separable from the rest of the reflections<sup>20</sup>. The components removed from the environment includes 1) skylight, 2) diffuse reflection of solar radiation from outside surfaces, 3) diffuse reflection of skylight from outside surfaces, 4) diffuse interreflections within the interior space [12, 60].

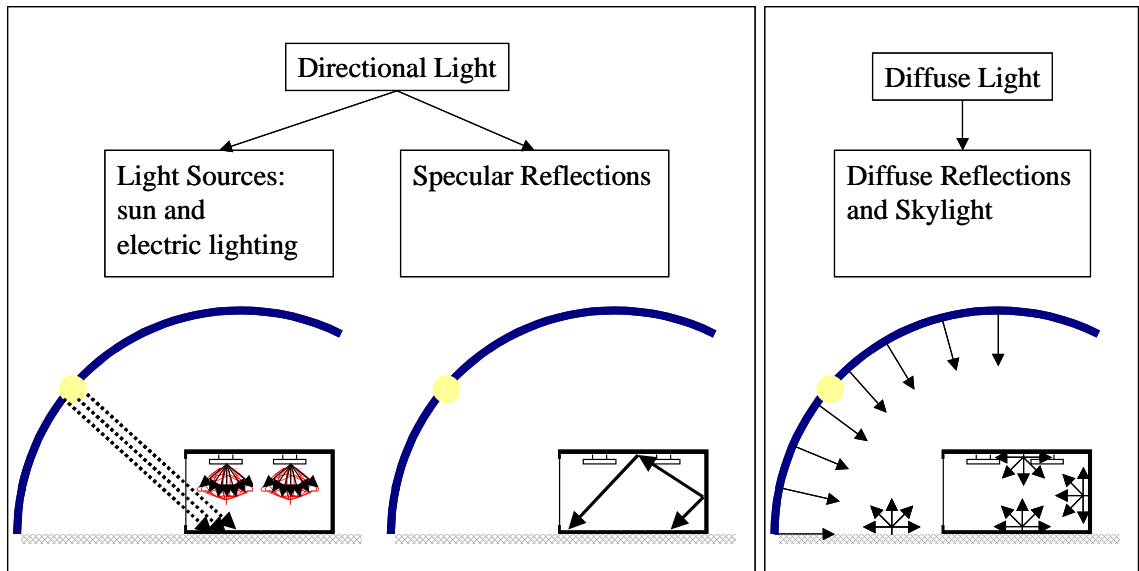


Fig. 2.24 Dissection of light into the directional and diffuse components

The diffuse and directional components of light are separated through image subtraction method. The first image includes the directional (direct light and specular reflections) and diffuse components of the luminous environment. In the second image, the diffuse component is removed by setting the ambient calculation parameters (ambient bounces and the ambient value approximation) to 0. The ability to isolate the diffuse

<sup>20</sup> In Radiance, it is possible to treat windows either as light sources or transmitting surfaces. When the windows are considered as light sources, the diffuse component of light passing through the glazing is computed a priori during the direct calculation instead of the indirect calculation. Therefore, it may not be possible to isolate all diffuse components from the rest of the scene. On the other hand, when windows are treated as transmitting surfaces, the diffuse component of light passing through the glazing is calculated in the indirect calculation and can be eliminated through the ambient calculation parameters. Despite the fact that skylight is removed, the sky will remain visible through the window [42, 60].

component is essential for the directional-to-diffuse metrics. The subtraction of the first image with the second one produces the directional component (Fig. 2.25). The ratio of the directional and diffuse components is calculated with the average luminance values.

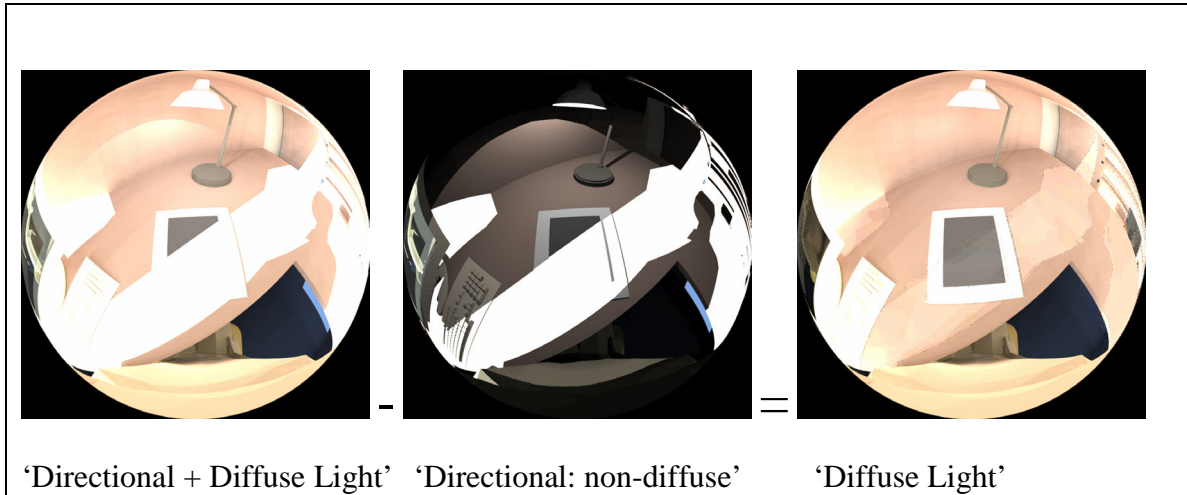


Fig. 2.25 Image subtraction method for determining the directional-to-diffuse ratio

Fig. 4.26 shows the directional-to-diffuse ratio when the viewer is looking at the paper task throughout Dec. 21. The sensitivity of the indicator is apparent when it is viewed side by side with the visual information, which illustrates the light and shade patterns of the direct sunlight in the scene. A typical assessment of the directional-to-diffuse luminance ratio should be studied in real world examples to relate the perceived directionality with the calculated ratio. Yet, the higher values point to strong directionality, and the lower values point to weak directionality. The time period between 9:00-12:00 has an increasingly strong directionality when the direct rays of sun are present in the scene and the time period after 14:00 has a weak directionality indicator when the scene is under shade. Note that there is an increase in the indicator after 15:00, which points to an increased effect of the directionality from the task lighting since the directionality from the opposite direction (window) is fading after this point. The scene

at 12:00 has also been rendered with the CIE Overcast Sky, and as expected, the directional-to-diffuse ratio dropped to 1.4, which is 2.5 with the CIE Clear Sky with sun.

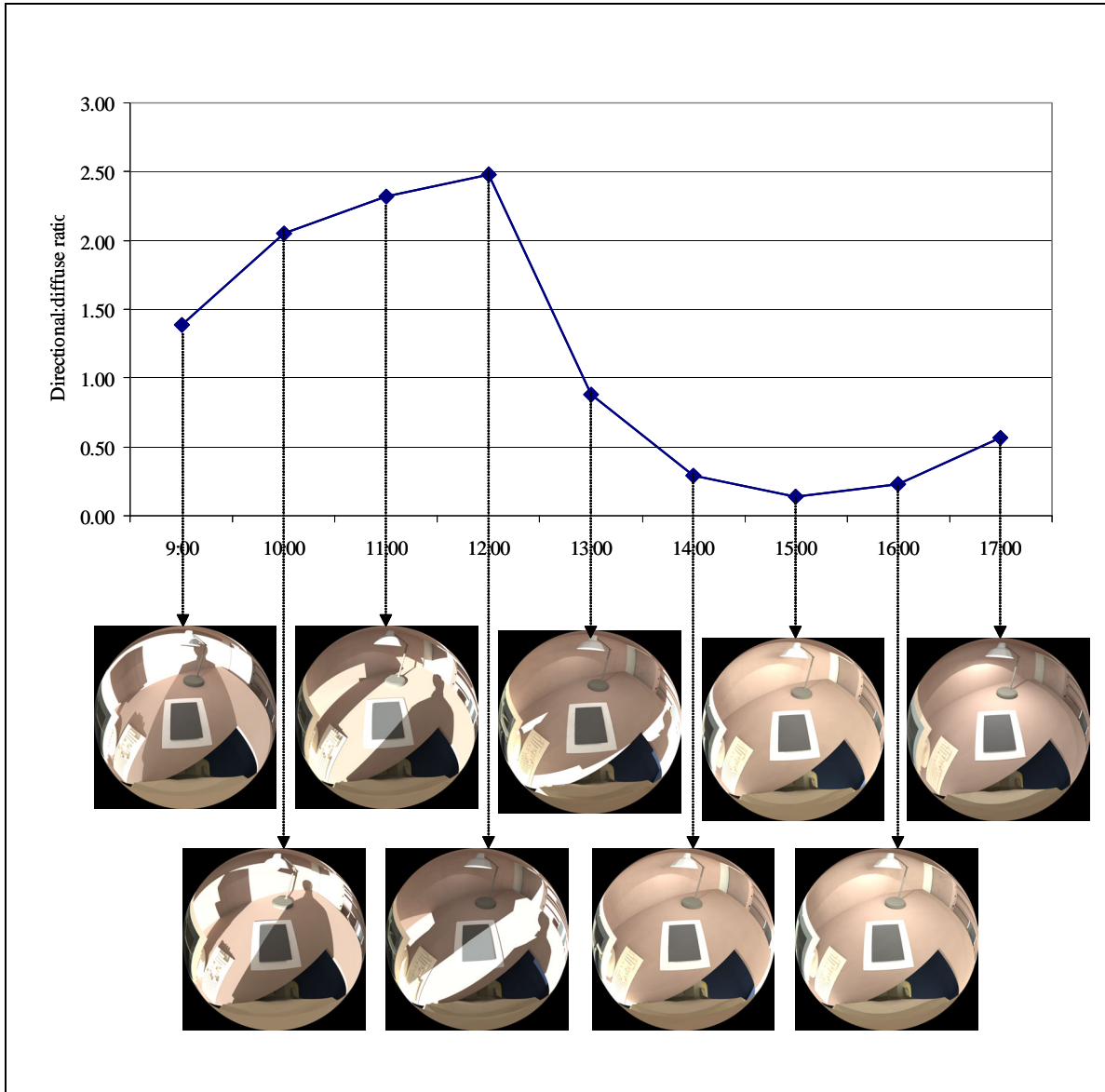


Fig. 2.26 Directional-to-diffuse luminance ratios for Dec. 21 when the viewer is looking at the paper task

## Glare

Glare is the effect produced when luminance in the field of view is sufficiently greater than the adaptation luminance to cause annoyance, discomfort and/or poor visibility [2]. The glare index used in North America is Visual Comfort Probability (VCP) [2]; the rest of the world uses Unified Glare Rating (UGR) [103] to compute glare possibility from electric light sources. For daylight, the Daylight Glare Index (DGI) [95, 104] is employed. The factors that are involved in the determination of discomfort glare are the luminance of the source, location and direction of the source, size of the source, number of glare sources, and the adaptation luminance [2].

The main problem with these glare studies is that the glare indices have been generated from experiments under certain lighting layouts and room geometries. It is not easy or possible, in most cases, to measure the parameters required for the calculation with the traditional measuring devices. Therefore, the common practice is to take few luminance measurements in relevant viewing directions within the space [105], which may not be necessarily enough to inform about the absence or presence of glare. Glare calculations are implemented in the Radiance software to locate and quantify the glare sources with a selected discomfort glare index [62]. Accordingly, the same indices have not been implemented in the VLL. The locations of glare sources are identified for Dec. 21 12:00, when the viewer is looking at the paper through the Radiance glare module (Fig. 4.27). The chart displays the DGI values for the same position and time. In the DGI, a value of 16 is perceived as “just imperceptible”, 19 as “just acceptable”, 24 as “just uncomfortable”, and 28 as “just intolerable” [104].

Implementation of new glare indices is always possible with the per-pixel data. However, as it has been discussed in the luminance distribution framework, it would be very useful to have better glare indices that have the predictive power for the absence or presence of glare with environments that have complex luminance distribution patterns.

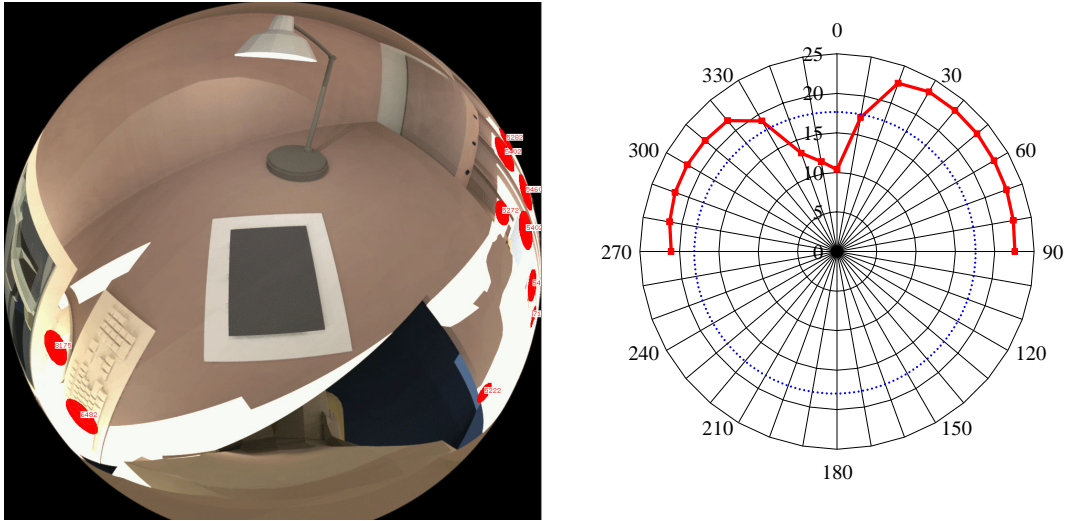


Fig. 4.27 Identification of the glare sources and DGI index for Dec 21, at 13:00

### Spectral Content

Sufficient spectral content of the lighting is necessary for achieving a desired visual effect and accurate color rendering. Moreover, recent studies have demonstrated that the spectral content of the light spectrum affects the pupil size, which significantly affects the visual acuity at typical interior light levels [88, 106-108]. The pupil becomes relatively smaller with the scotopically rich light sources, and smaller pupil size provides better visual acuity.

As discussed in Chapter II and III, it is not possible to analyze the full spectral data with the current capabilities of physically based rendering. However, as demonstrated in Chapter III, the virtual colorimeter and virtual scotopic meter provides information about the color content of the light in three channels. The CCT, CIE chromaticity, and scotopic luminance data can be analyzed in multiple levels as demonstrated throughout this chapter, i.e., total data, regional data, and per-pixel data analysis.

**Remarks**

It is important to note that the examples presented in this chapter are chosen to provide a general overview of the capabilities and procedures within the VLL. The analysis revealed that the nighttime condition of the office space provides reasonable visual comfort and performance conditions. However, the daytime conditions suffer from excessive amount of daylight, particularly sunlight. In Chapter V, the same setting is used to demonstrate the design decision-making process for an appropriate daylight admission control system.

**CHAPTER V**  
**DESIGN DECISION-MAKING PROCESS IN THE VIRTUAL LIGHTING**  
**LABORATORY**

From a design perspective, architectural lighting is a decision-making process that integrates lamps, luminaires, controls, daylight apertures, surface materials, and colors. The choices affect the resultant visual effects, comfort, and performance. Lighting designs cannot be evaluated or compared through a single quantity or performance indicator. It is not possible to have a well-defined selection method for choosing a lighting design among alternatives. Lighting design is a creative process and different projects impose different criteria and goals. Satisfying the codes, recommendations, and legislations is just one of requirements. There are analytical approaches that improve and accelerate the decision-making process. The VLL provides a rich visual and numerical environment with a large variety of information and analysis capabilities that can be custom tailored for each design project.

In Chapter IV, several analysis techniques have been used to demonstrate the capabilities of the VLL. In a design decision-making process, the designer may not need all of the demonstrated analyses, or may need other methods that have not been exemplified. In this chapter, an architectural lighting design decision process is discussed through an example that utilizes some of the data analysis techniques illustrated in Chapter IV.

## **Design Objectives**

The base office space, as discussed in Chapter IV, has a clear and unobstructed glazing that does not have any daylight admission controls. The different analysis techniques have revealed the problems associated with the excessive daylight. The occupant suffers from objectionable amounts of illuminance and luminance; and is subject to inapt spatial distributions, which causes poor visibility and glare. As a self-luminous, vertical, glossy task, the computer screen poses various other problems. The excessive light creates a reflected image of the environment on the computer screen, which may distract the occupant. The reflected image potentially triggers fatigue as the eyes are forced to accommodate at different focal distances between the computer screen and the reflected image.

Within a generic scenario, the overall design objective is set to have good quality lighting that supports the visual performance and comfort in the office space. It requires maintaining reasonable quantities of illuminance and luminance with adequate variation. One obvious solution for the existing problems is to decrease the vertical illuminance on the computer screen. Since the office activity creates a dynamic situation in which the user has to change fixation between the computer screen, keyboard, and the paper, the illumination and luminance quantities and distributions have to be balanced with respect to the task and ambient lighting requirements.

The design decision process with daylight is particularly challenging because the lighting design needs to fulfill the evaluation criteria throughout the year with various sky conditions. Evidently, different sky conditions and different times of the day/year have to be considered. Temporal dynamics in daylighting is attributed to the movement of sun throughout the day and the year, and to the sky conditions. The sun movement, solely, is responsible for three simultaneous dynamic phenomena: the position of the sun changes; the sky distribution varies with respect to the position of the sun; and the glass admission

function varies with respect of the incidence angle. However, in most cases, it is neither necessary nor feasible to simulate the scene for each time frame (such as per-hour), throughout the year, and for different sky conditions. The usual approach is to select the critical situations; prioritize and/or optimize the objectives; and assess the performance accordingly. Critical situations do not necessarily correspond to the lowest daylight availability or low sun angles. The function of the space as well as the occupancy schedules and patterns could dictate the critical conditions that have to be evaluated.

The base case is modeled throughout Dec. 21 with the CIE Clear Sky. Dec. 21 is the winter solstice, which provides the lowest sun angle ( $24^\circ$  at 12:00 for Ann Arbor) and potentially causes the most severe visibility and discomfort problems. The window orientation is south, which is susceptible to maximum direct sunlight exposure throughout the day. With the higher sun altitudes ( $48^\circ$  for the equinoxes and  $71^\circ$  for the summer solstice at 12:00), the direct solar penetration will have comparatively moderate consequences. The main objective is to achieve reasonable visual comfort and performance even with the low sun angle conditions, so conditions on Dec. 21 are appropriate to analyze. If the main objective has been to assess daylight availability and incorporate it with electrical lighting, the overcast sky could have been the critical scenario to study.

For the sake of practicality, three hours have been studied instead of an hourly analysis throughout the day: 9:00, 12:00, and 17:00. The analysis in Chapter IV has proven 12:00 to be one of the most problematic hours both for the paper and computer based tasks. 9:00 and 17:00 are chosen as the times that mark the start and end of the working hours in the office; they also refer to the outermost east and west azimuth variation of the sun within the working hours.

## Design Alternatives

The analytic approach is to control the direct sunlight radiation while permitting the skylight through the windows. The intense direct sunlight can either be shielded or redirected. The design problem could be tackled with numerous design alternatives, such as using different glazing types, retractable and adjustable louvers, fixed overhangs, fins, and lightshelves. Three alternatives are selected to exemplify the process (Figures 5.1 and 5.2):

- Clear glass is replaced with a fritted glass: The fritted glass is a composite material of a translucent glass (5% diffuse transmission) and the original clear glass. The frit is a dot pattern that has a unit space of 0.5 and a radius/spacing fraction of 0.5.
- Horizontal venetian blinds are placed inside the window. They are 1.3 cm (0.5 inch) wide.
- A double skin façade system has been utilized with two clear glass façades located 0.7m (2.3 ft) apart. The horizontal venetian blinds have been placed inside the outer skin.

## Analysis Results

The illuminance at the eye is studied when the viewer is looking at the computer screen and the paper task (Fig. 5.3). The changes are notable, especially at 12:00. In all cases, the fritted glass provides the lowest illuminance, which is expected because it is the alternative that provides the lowest total transmission. The ‘double skin façade with blinds’ has a lower total transmission value than the ‘clear glass with blinds’. Therefore, the resultant illuminance within the environment is expected to be lower, but in some instances it is higher due to the interreflection between the two glazing surfaces.

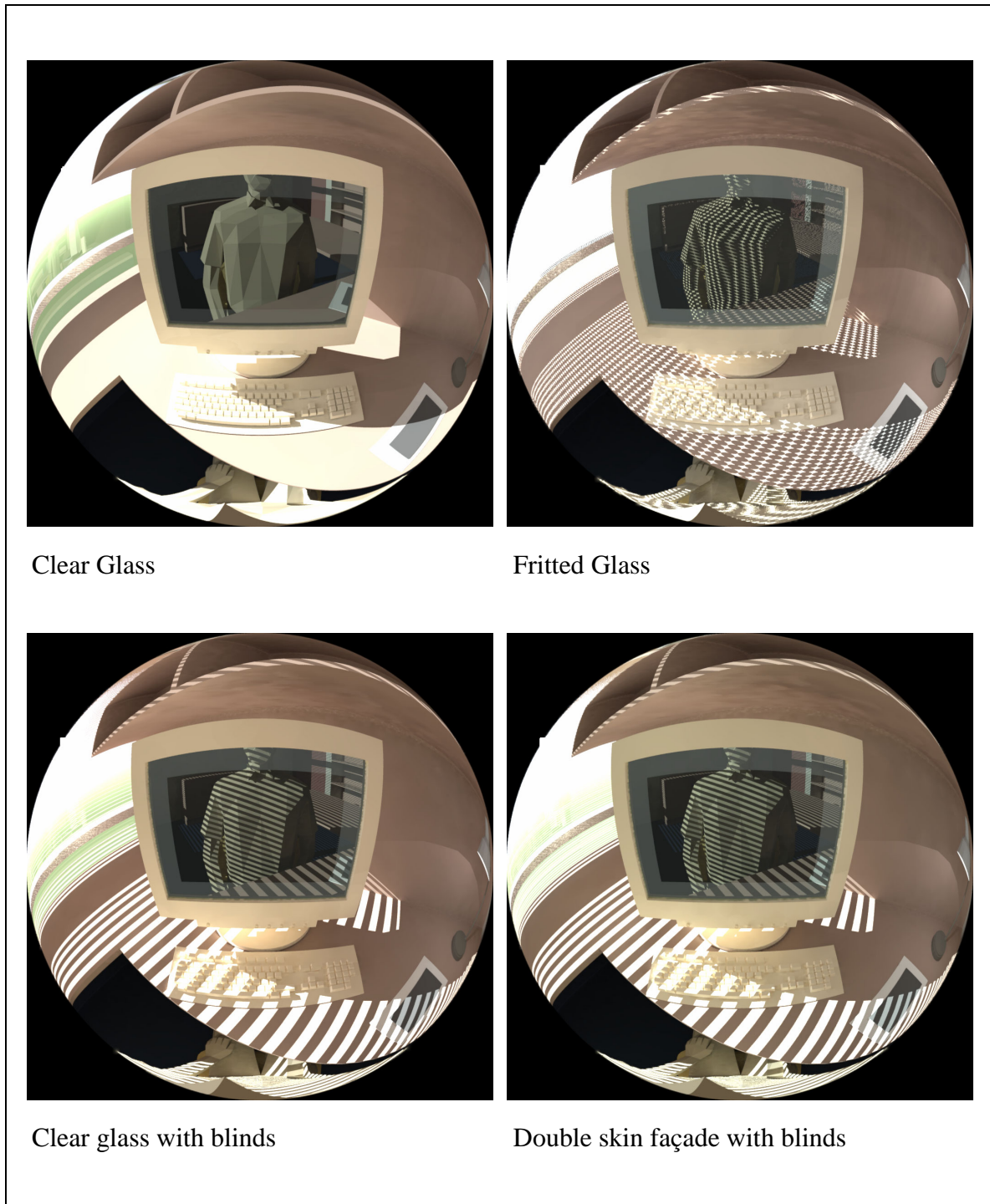


Fig. 5.1 The base case and the design alternatives analyzed in comparison to the base case, when the viewer is looking at the computer screen on Dec. 21, at 12:00

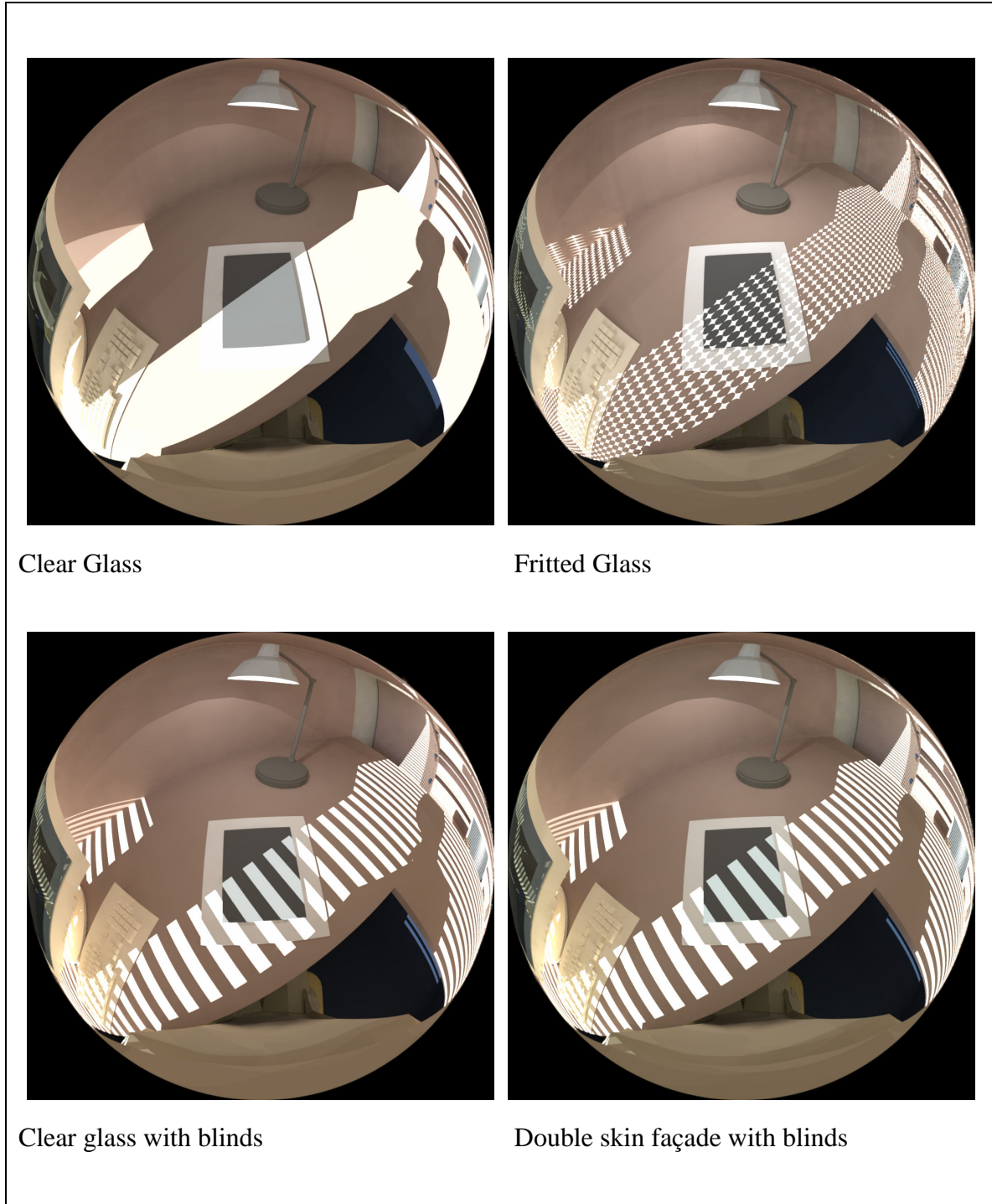


Fig. 5.2 The base case and the design alternatives analyzed in comparison to the base case, when the viewer is looking at the paper task on Dec. 21, at 12:00

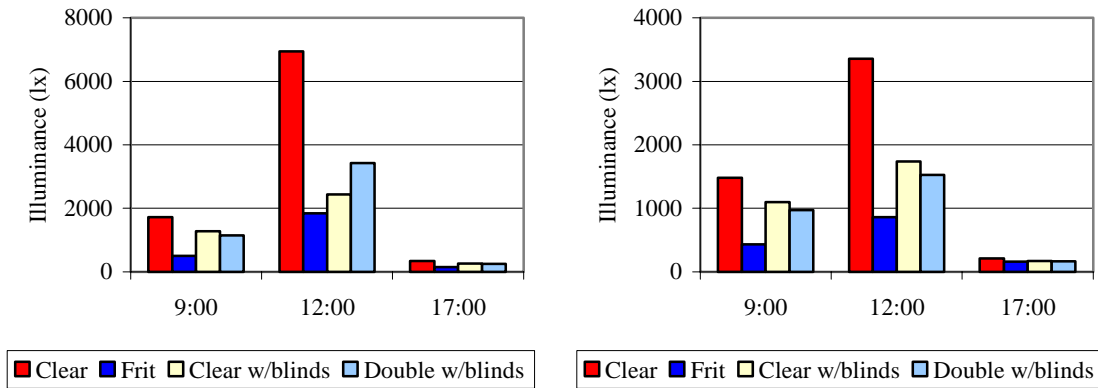


Fig. 5.3 The illuminance at the eye when the viewer is looking at the computer screen and paper on Dec. 21

Fig. 5.4 illustrates the illuminance on the tasks, i.e. the vertical illuminance on the computer screen, and horizontal illuminance on the paper. Although the illuminance values are less than the base case in all design alternatives, they are still far from the IESNA recommendations. This is again predictable, since the analysis is being done for the lowest sun angles throughout the year. Therefore, the objective should not be to achieve the precise IESNA recommendations. It is also known that people have more tolerance for light quantities and variations with daylight compared to electric lighting.

Given the amount of variability occurring with daylighting, it may be infeasible, if not impossible, to achieve satisfactory lighting conditions throughout the year. The occupant naturally adjusts his position and task position while performing the visual task to achieve comfortable task-source-eye geometry. For instance, the paper can be shifted on the table or the computer screen could be rotated and tilted. In this respect, providing flexibility and control to the occupant over the lighting conditions is very effective. Retractable and adjustable louvers and blinds provide options such as removing the shade from the window and shielding or redirecting the direct sunlight.

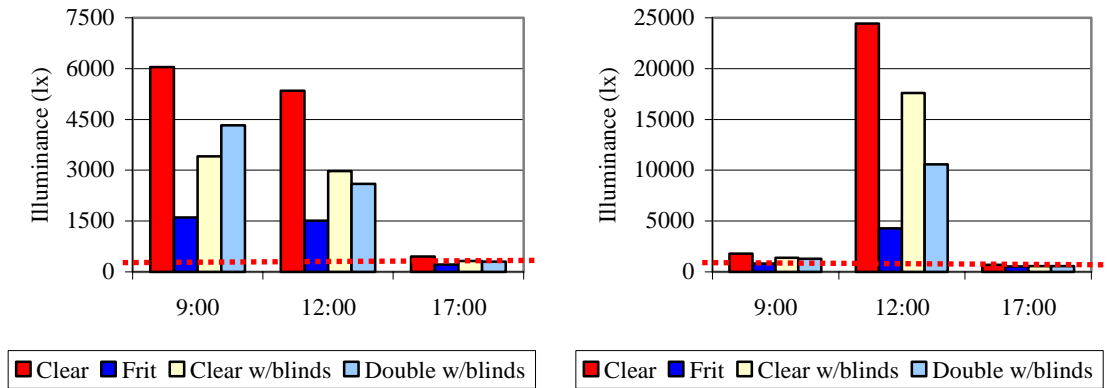


Fig. 5.4 Illuminance on the computer screen and paper on Dec. 21

The effectiveness of adjusting blinds has been demonstrated in Fig. 5.5. The ‘double skin façade with blinds’ alternative has horizontal venetian blinds. For the ‘double skin façade with tilted blinds’ alternative, the same blinds have been tilted 30°. The results clearly indicate that significant control can be achieved on the illuminance and luminance quantities by simply providing the flexibility and control of the venetian blinds to the occupant. Further reduction can be achieved by tilting the blinds towards a vertical position.

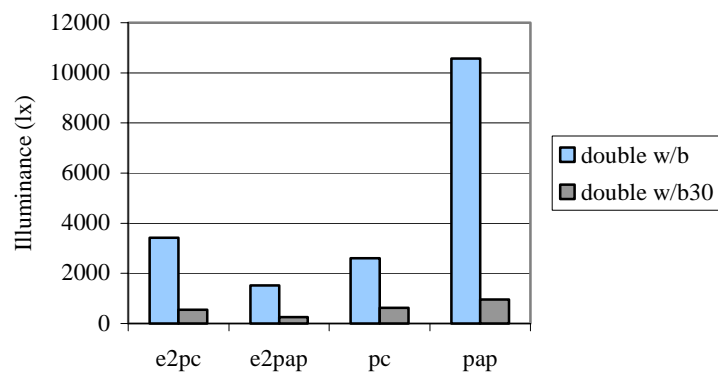


Fig. 5.5 Comparison of the illuminance values between the horizontal and 30° tilted venetian blinds for the double skin façade alternative

The contrasts on the computer screen and paper are compared in Fig. 5.6. It is important to emphasize once again that lower contrast denotes better visibility for the computer task and higher contrast denotes better visibility for the paper task. For the computer task, 12:00 still poses visibility problems. With the tilt ( $30^\circ$ ) of the venetian blinds, the contrast on the computer screen improves to 0.17 as compared to 0.70 with the horizontal blinds. Unlike the base case, all of the design alternatives produce reasonable contrast values for the paper task.

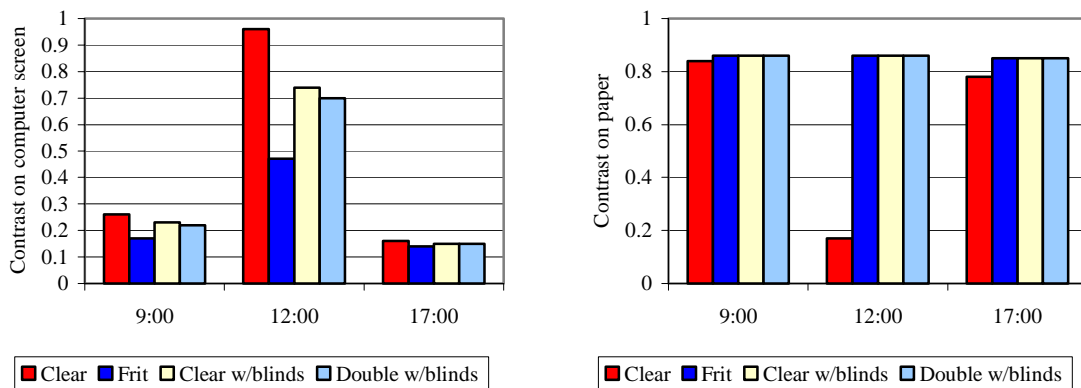


Fig. 5.6 The contrast on the computer screen and paper on Dec. 21

The luminance distribution ratios between the task and the surrounding are studied and shown in Fig. 5.7. The averages of the luminance on the paper, the computer screen, and the surfaces are calculated and compared. The first plot shows the total range of the ratios. The computer screen-to-window ratios are unsurprisingly high in all cases. Yet the 'clear window with blinds' and the 'double skin façade with rotated blinds' satisfy the criterion that the ratio of the task luminance to any surface in the field of view should not exceed 1:40 or 40:1 ratio. The second plot is a close-up view, where the ratios are shown up to 15. Although all of the design alternatives provide better ratios between the task and the surroundings compared to the base case, there is no dominant difference among the design alternatives.

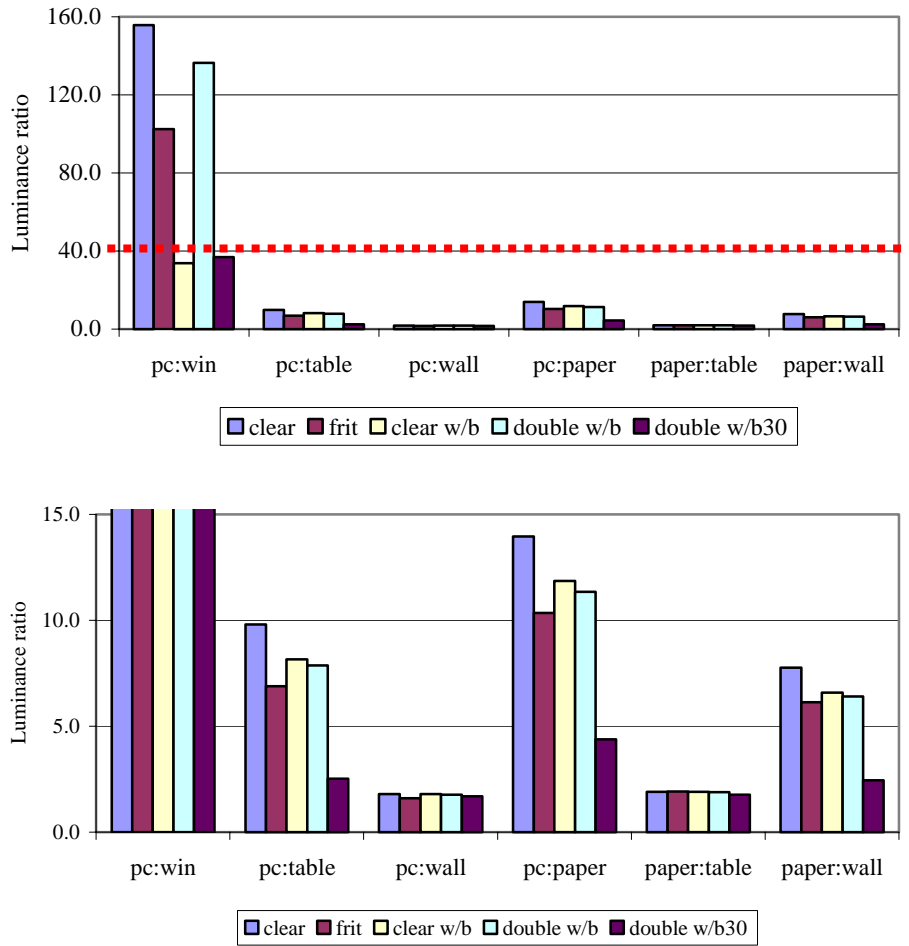


Fig. 5.7 Luminance ratios between the task and the surrounding on Dec. 21, at 12:00<sup>21</sup>.

The luminance distribution patterns in the whole scene are also studied. Table 5.1 shows the maximum, minimum, and the mean luminance values occurring when the viewer is looking at the computer screen. Although the maximum values vary considerably, almost 100% of the data in all cases are below 10,000  $\text{cd/m}^2$  (Fig. 5.8).

<sup>21</sup> The ratios plotted in Fig. 5.7 refer to the division of the higher value to the lower value. The ratios of 'pc-to-surrounding' are extracted from the scene where the occupant is looking at the computer screen; and the ratios of 'paper-to-surrounding' are extracted from the scene where the occupant is looking at the paper.

Therefore, the maximums occur in very few pixels as outliers. Actually, as seen from the figure, most of the values are below 1000  $\text{cd}/\text{m}^2$ . Histograms are generated for all studied cases for the pixel values ranging between 0 and 1000  $\text{cd}/\text{m}^2$  (Fig 5.9). The potential highlights and peak luminances have been removed; and uniformity is sought to a certain extend for the rest of the scene.

Design alternative with	Maximum	Minimum	Mean
Clear glass	261,579,980	1.5	2211
Fritted glass	21,384,572	0.2	585
Clear glass with blinds	1,152,500	0.5	777
Double skin façade with horizontal blinds	44,310,559	0.5	1088
Double skin façade with tilted blinds	5,450	0.1	176

Table 5.1 The maximum, minimum, and mean luminance values ( $\text{cd}/\text{m}^2$ ) when the viewer is looking at the computer screen

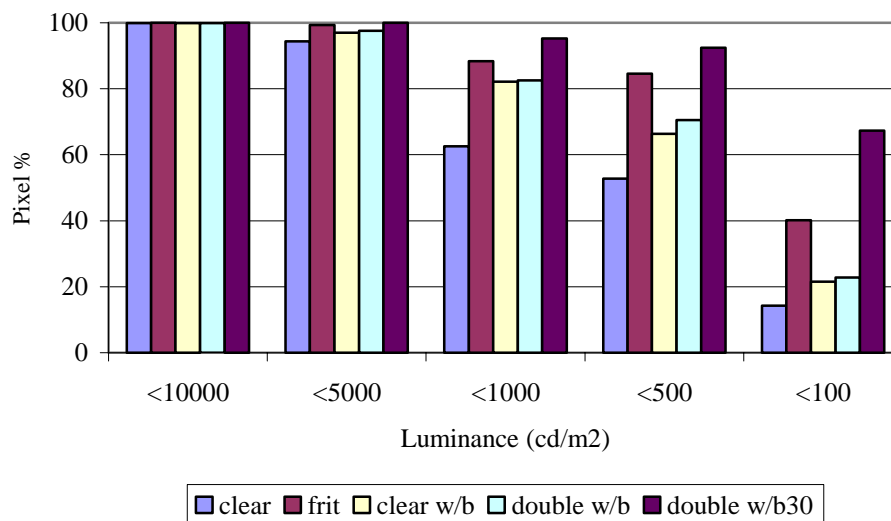


Fig. 5.8 Luminance distribution patterns between the design alternatives

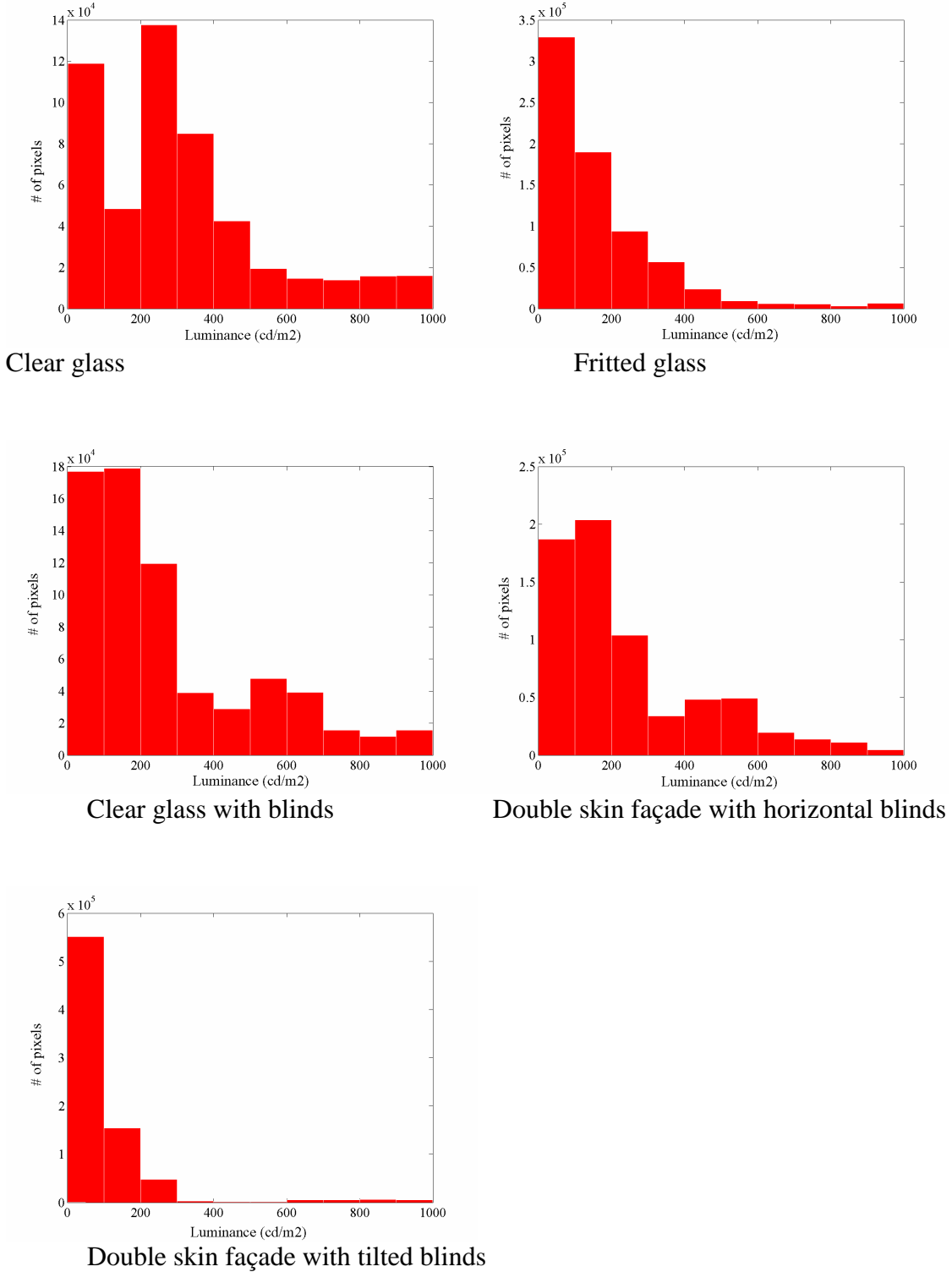


Fig. 5.9 Luminance distribution histograms of the design alternatives on Dec.21, at 12:00, when the viewer is looking at the computer screen

The histogram for the base case ('clear glass') in Fig. 5.9 points to a wide spread of the data, which indicates high luminance ratios that causes poor visibility and discomfort. The histograms for the 'fritted glass', 'clear glass with blinds', and 'double skin façade with horizontal blinds' are all unimodal and skewed to left, though the latter two alternatives display a wider spread. The last histogram reveals that 'double skin façade with tilted blinds' has a unimodal data, skewed to left with little spread. That is, most of the pixels are in close range, which points to reasonable luminance ratios between the pixels.

The resultant visual effects can be studied through the images. Figures 5.1 and 5.2 have revealed the distinct light and shade patterns caused by the alternatives on Dec. 21 at 12:00. It is known that light and shade patterns from sunlight are well tolerated by humans and mostly found to be warm and cheerful. However, they can also be distracting. For instance, the circular fritted pattern is somewhat interfering with the rest of the scene. The alternatives with the blinds option provide the flexibility to adjust the tilt angle to minimize the disturbing light and shade pattern. Fig. 5.10 illustrates the office for the same date and time for the double skin façade option with tilted blinds (30°).

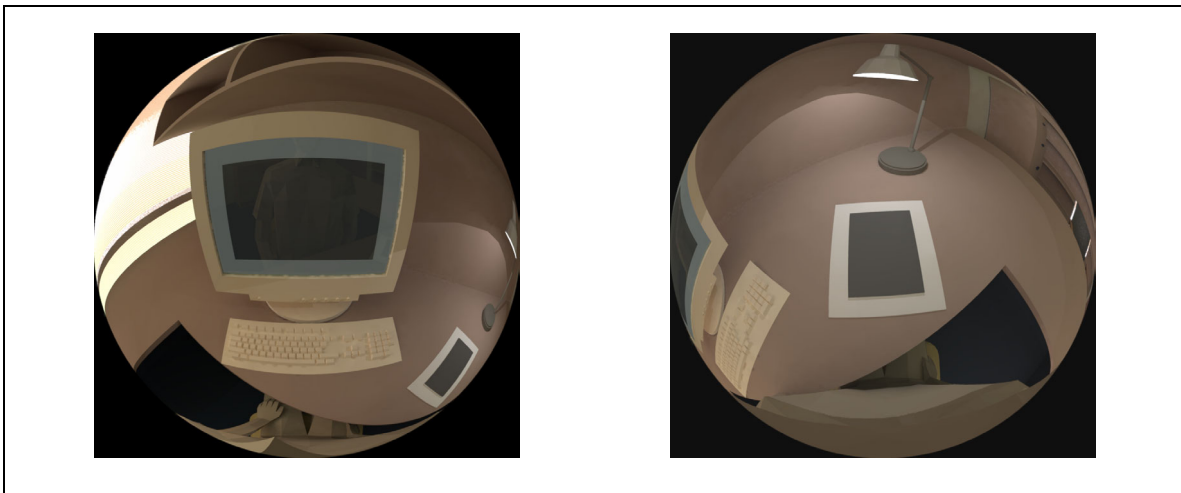


Fig. 5.10 Viewer's sight of the computer screen and paper for the 'double skin façade with tilted blinds (30°)' alternative on Dec. 21, at 12:00

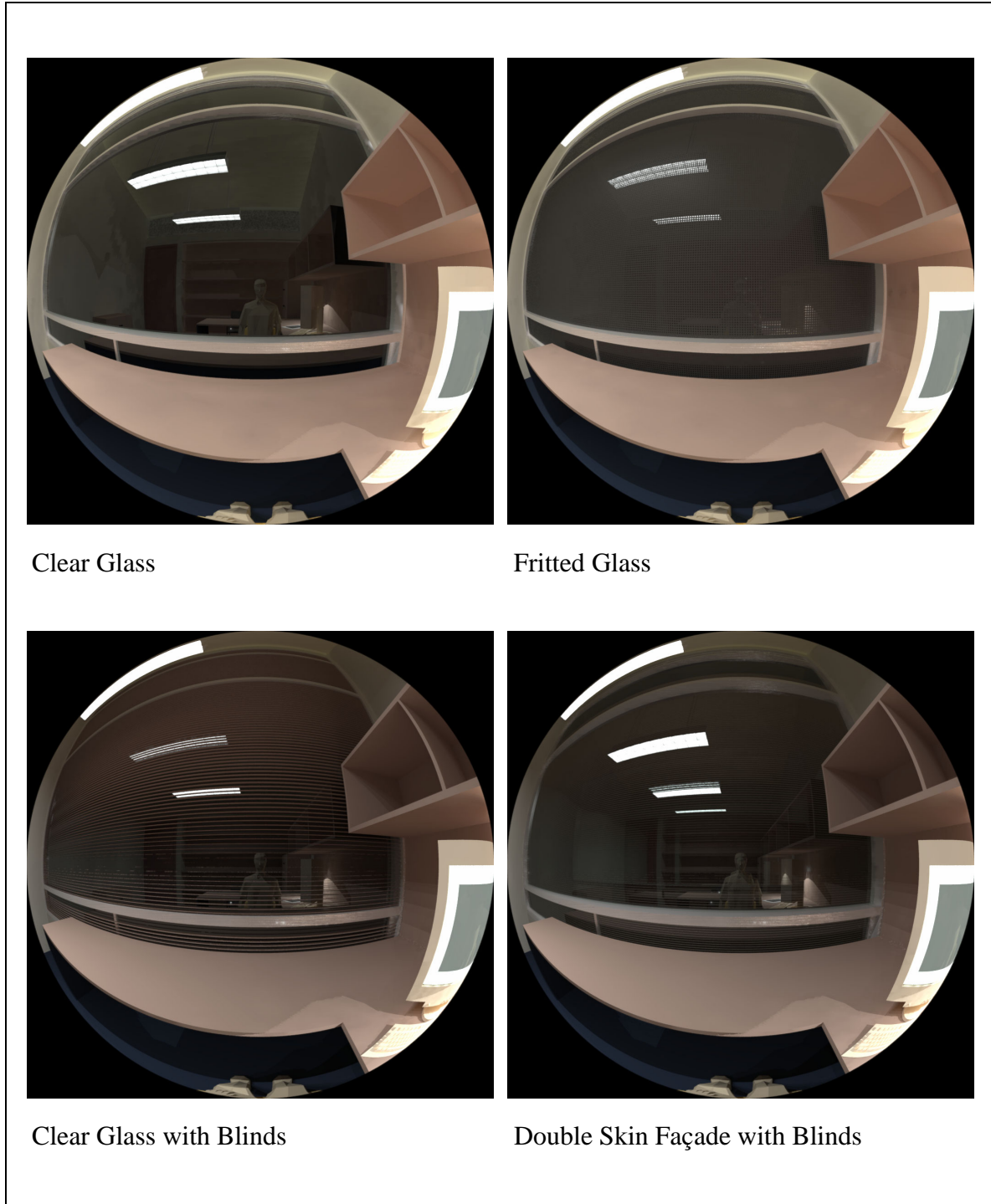


Fig. 5.11 The base case and the design alternatives at night

It is also necessary to look at the night conditions and study the reflections of the environment from the glass (Fig. 5.11). The reflections of light sources from the glass surfaces are quite unavoidable at night. The double skin façade poses further problems with its double glazing which causes multiple reflections. Fig. 5.12 shows the illuminance variation at the eye when the viewer is looking at the window at night. Although the quantities are in close range, the achieved appearance is somewhat different.

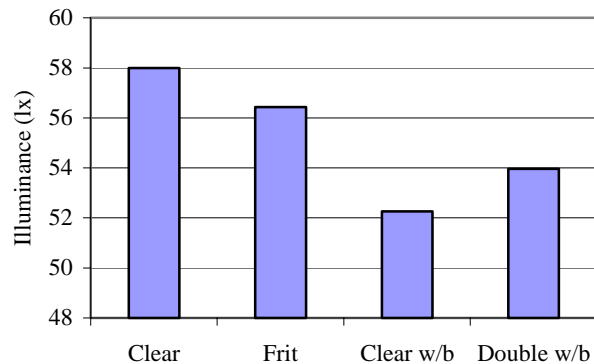


Fig. 5.12 Comparison of the illuminance at the eye when the viewer is looking through the window at night

One factor that has deliberately not been introduced so far is the outside conditions. It has been kept simple. In actual applications and decision-making process, the outside obstructions, the surrounding surfaces, and material properties have a significant impact on the interior luminous environment. Therefore, it should be modeled meticulously. Fig. 5.13 illustrates the double skin façade with and without outside obstructions. The outside obstructions are two nearby buildings that have reflective glass surfaces. The images are generated for Dec. 21 at 9:00. The reflective surfaces change not only the view from the window, but affect the interior light levels, distribution, and appearance. For instance, interior light levels can decrease (in the studied case, the

illuminance at the viewer's eye decreased from 9038 to 8521 lx as the result of the obstruction) or increase when the obstruction reflects light towards the interior space.

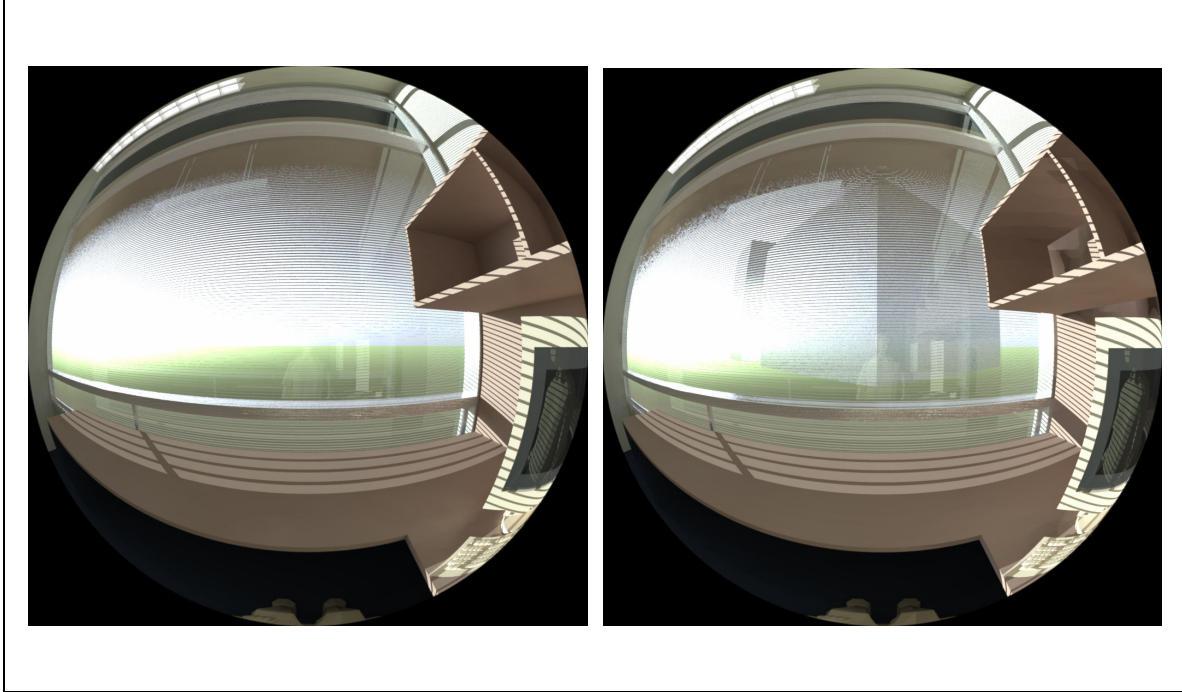


Fig. 5.13 The window view with and without outside obstructions

### Remarks

Lighting is one of the many components in an architectural design process. The decisions are made in relation to other components. The design decision-making process exemplified in this chapter is limited to the data and information presented here. 'Fritted glass' alternative performs well in terms of the quantities and the ratios, but the resultant visual appearance is somewhat cluttered and confusing. 'Clear window with blinds' and 'double skin faced with horizontal blinds' have revealed similar performances. Alternative with the tilted blinds provides the best performance. To summarize, providing flexibility of the venetian blinds to the occupant is very effective in controlling the excessive daylight and light distribution in the office, which in return provides adequate visual comfort, performance, and visual effects.

## **CHAPTER VI**

### **CONCLUSIONS**

#### **Dissertation Summary**

This dissertation has presented a framework for a computer generated environment that can be used for architectural lighting design, research, and education. Gathering knowledge from Architecture, Illuminating Engineering, and Computer Graphics, the VLL offers major transformations in the utilization of digital visualization in lighting analysis. It is unique because it provides full autonomy over the lighting data, acknowledging the idiosyncratic nature of each design and research project that might require flexible evaluation techniques, procedures, and experimentation.

In Chapter II, lighting algorithms of physically based rendering tools are discussed. The discussions address the comparative definition and modeling of the light, light transport, and light reflection/refraction/transmission in the physical and virtual worlds. Physically based HDR images can be used for qualitative and quantitative lighting analyses. However, the lighting information extracted from the digital images is as accurate as the input data that it is based upon; and the rendering algorithms that it is generated with. It is also important to recognize that there are limits on what can be measured and what can be simulated with the current measuring devices and algorithms. It is necessary for the researchers and designers to understand the underlying theories, assumptions, simplifications, and limitations of the physically based rendering tools so that it would be possible to interpret the numerical and visual data achieved from the digital images.

The VLL is introduced in Chapter III at a conceptual level. The development of the virtual meters is explained in reference to their physical counterparts. The virtual lighting meters and photometer systems (virtual luminance meter, illuminance meter, contrast meter,

integrating sphere, colorimeter, and scotopic meter) are the basic equipments in the VLL; and they provide the lighting data (i.e. the photopic and scotopic luminances, illuminance, CCT, CIE chromaticity coordinates) in the form of matrices that are equivalent to the image resolution. The metrics are based on the theoretical definitions of light and are developed by filtering the radiance values by the CIE Standard Observer and CIE Colorimetric Observer functions.

It is possible to consider the physically based HDR images as laboratory-like controlled environments that are adequately equipped with meters to perform lighting experimentation, observation, and practice. The data analysis techniques developed in Chapter IV are the syntheses of the current practices in lighting design and the novel practices that can be done with the unique capabilities of the virtual photometry. The total, regional, and per-pixel data analysis techniques provide a comprehensive approach to study the quantity, distribution, directionality, glare, and spectral properties of light. It is possible to divide the luminous environment into layers, and perform analysis in any required detail.

Finally, Chapter V demonstrates an example, in which the VLL improves and accelerates the decision making in lighting design with an analytical approach.

### **Contributions**

The VLL provides a design and research framework and innovative capabilities that suggest transformations in the architectural lighting domain, both on theoretical and practical levels. The VLL provides three distinct benefits: First it creates a medium where various analysis methods can come together to support and complement each other. Second, it offers unique analysis options that are pertinent to a computer-based approach. Third, it creates a circle of knowledge acquisition between theory and practice.

On the practical level, virtual meters and data analysis techniques make it possible to perform all current physical analysis in a virtual environment, with additional advantages. Obviously, this work is not suggested to replace the physical lighting laboratories. There are measurements and analyses that cannot be done in the VLL. For instance, as explained in Chapter III, goniometric and spectrometric measurements are excluded. In fact, most of the

information in the virtual laboratory originates from physical measurements, either as the input data or the theoretical foundation of the image generation algorithms. On the other hand, some of the analysis techniques used in the VLL cannot be performed in physical environments. Major contributions of the dissertation on a practical level are summarized as follows:

- Virtual meters offer many advantages over physical ones in terms of availability, cost and labor efficiency, and theoretical rationale.
- Current analysis techniques can be easily determined within the VLL with detail (due to the ability to attain high resolution per-pixel lighting data), flexibility (due to the ability to develop new meters and metrics as required, instead of limiting the user to predetermined ones), and rigor (due to the ability to systematically manipulate and analyze the data) that may be infeasible or impossible to achieve in the physical environments with traditional lighting analysis approaches.
- New lighting analysis techniques are suggested in the VLL:
  - The scenes can be studied in terms of the luminance variations in different parts of the field of view. This kind of analysis is useful for providing a better understanding of lighting in relation to the performance of human vision; and for studying the luminance transition occurring when the occupant switches between different visual targets.
  - The Virtual Criterion Rating uses the per-pixel data to define the probability that a specific criterion is met.
  - The different lighting components can be studied independently in the VLL, which simplifies the description and understanding of the complex phenomena. The image subtraction method is suggested to isolate the effects of one parameter from the rest of the lighting data. For instance:
    - It is possible to divide the lighting data into layers, such as the directional and diffuse lighting components. The directionality can be evaluated through a directional-to-diffuse luminance ratio.

- It is possible to isolate the effects of the sun, by simulating the non-overcast skies with and without sun. The effect of the direct solar radiation can then be evaluated.
- Current lighting analysis techniques mostly utilize instantaneous, single lighting values (such as luminance, illuminance, CCT), which do not inform about the quantity and quality of light throughout a particular environment. It is appropriate to study the temporal and spatial variability as a dynamic phenomena instead of a mere amount of quantity at a certain time. Per-pixel analysis is suggested specifically to study lighting distribution patterns. The rate of change in lighting quantities throughout time can also be studied with the image subtraction approach.
- On the whole, the VLL supports the integration of lighting analysis into the architectural design process through a computational tool. The design decision making process is supported for the quantitative and qualitative lighting issues, at all design levels, for various configurations of form, function, material, and light source selection. Therefore, the luminous environment could be better understood during the design process. The degree to which the VLL is useful to the architect, lighting designer, and consultant depends on the person's ability to relate the analyses results with the design. However, the VLL provides many numerical and visual means to endorse the practicability of advanced lighting analysis throughout the design decision process.

On the theoretical level, the VLL proposes substantial restructuring in architectural lighting analysis by providing high resolution measuring capabilities and novel data analysis techniques which can lead to the generation of new indices and the transformation of psychophysical experiments from laboratory environments to real world environments. They have been discussed in Chapter IV, and are referred here briefly:

Visual comfort and visual performance indices are the mathematical models resulting from psychophysical experiments which involve the responses of a group of human subjects to a particular lighting setting. Scientists have conducted most of these lighting experiments in simplified laboratory settings because it was not possible to measure or simulate the complex

environments, and it is difficult to establish a cause and effect relationship or correlation in complex environments. These studies pose validity and generalizability problems because it is not possible to calibrate the response of the observer in relation to the deviations of the real world setting from the experimental setting. Although, some of these studies incorporate multiple experiments where the formulae have been revised over the years for achieving improved models, the gaps between laboratory settings and the complex real world environments have remained.

New approaches to the psychophysical research are needed to make further advances in lighting indicators and analysis. By using the features of the VLL, lighting researchers will be able to document the complex visual and numerical features of real world environments where psychophysical experiments can take place. In this respect, this dissertation is the beginning of research that can be done in this area since there are many potential applications. It will be possible to develop a better understanding of the complex processes underlying lighting and vision which will further improve the theoretical foundation, usability and efficiency of architectural lighting analysis.

### **Future Work**

Although many different virtual meters and data analysis techniques have been developed and presented in the dissertation, there are possibilities for future improvements:

- The current implementation of the VLL is not provided through a Graphic User Interface (GUI). A flexible and comprehensive GUI would be required for wide-ranging usage.
- A “virtual lighting application/demonstration environment” will be developed as an educational tool. This will be an environment, where students can experiment with various architectural lighting features, design decisions, lighting configurations, and viewing directions through the comparison of visual and numerical data.
- A useful addition is to incorporate HDR photography into the VLL. HDR photography, as discussed in Chapter II, captures scenes with pixel values that are proportional to the real radiance values. Therefore, it should be possible to calibrate the captured pixel values with the absolute radiance/luminance values through a few physical measurements taken at the

scene. HDR photography would be useful for collecting quick (in comparison to physically based rendering) and accurate high resolution lighting data from existing architectural spaces. Then, these images can be analyzed in the VLL.

- As explained in the previous section and in Chapter IV, the VLL opens up many applications in architectural lighting research with many prospective benefits toward psychophysical research. The following items are worthy of further investigation: calculation of adaptation luminance; calculation of the transient adaptation factor; calculation of new glare indices that account for luminance variations in field of view; investigation of psychological effects of lighting, perception, aesthetics correlated with the quantified features of the luminous environments. Another agenda for future work is to incorporate the tone mapping algorithms and HDR display devices (discussed in Chapter II) into the psychophysical experiment procedure. These studies would require multi-disciplinary approach and collaboration with researchers from Architectural Lighting, Illuminating Engineering, Vision Science, Computer Graphics, and Ergonomics; which in return could provide benefits to all of these fields.

## **BIBLIOGRAPHY**

## BIBLIOGRAPHY

- [1] Brainard, G.C. "The Biological Potency of Light in Humans: Significance to Health and Behavior", *Proceedings of the CIE 2003 Conference*, San Diego, June 26-28, 2003.
- [2] IESNA, Rea, M., (Ed.), *Lighting Handbook Reference & Application*, Illuminating Engineering Society of North America, 1999.
- [3] Inanici, M.N. "Transformation of High Dynamic Images into Virtual Lighting Laboratories", *Proceedings of the Eight IBPSA Conference*, Eindhoven, Netherlands, August 11-14, 2003.
- [4] Inanici, M.N. "Utilization of Image Technology in Virtual Lighting Laboratory", *Proceedings of the CIE 2003 Conference*, San Diego, June 26-28, 2003.
- [5] Inanici, M.N. "Post-processing of Radiance Images: Virtual Lighting Laboratory", *First International Workshop on Radiance*, University of Applied Sciences of Western Switzerland, September 30 - October 1, 2002.
- [6] Inanici, M.N. "Application of the state-of-the-art Computer Simulation and Visualization in Architectural Lighting Research", *Proceedings of the Seventh IBPSA Conference*, Rio de Janeiro, Brazil, August 13-15, 2001.
- [7] Greenberg, D.P., Torrance, K.E., Shirley, P., Arvo, J., Ferwerda, J.A., Pattanaik, S., Lafortune, E., Walter, B., Foo, S.C., and Trumbore, B. "A Framework for Realistic Image Synthesis", *ACM SIGGRAPH Proceedings of the 24th Annual Conference on Computer Graphics and Interactive Techniques*, 1997, 477-494.
- [8] IESNA, "Lighting Design Survey 2002", *Lighting Design + Application*, 32(7), July 2002, 35-43.
- [9] Walsh, J.W. *Photometry*, London: Constable, 1958.
- [10] Wyszecki, G. and Stiles, W.S. *Color Science: Concepts and Methods, Quantitative Data and Formulae*, New York: John Wiley and Sons, 2000.
- [11] Berns, R.S. *Billmeyer and Saltzman Principles of Color Technology*, New York: John Wiley and Sons, 2000.
- [12] Hall, R. *Illumination and Color in Computer Generated Imagery*, New York: Springer-Verlag, 1989.

- [13] Hall, R. “Comparing Spectral Color Computation Methods”, *IEEE Computer Graphics and Applications*, 19(4), July/August 1999, 36-45.
- [14] Ward, G. and Eydelberg-Vileshin, E. “Picture Perfect RGB Rendering Using Spectral Prefiltering and Sharp Color Primaries”, *Thirteenth Eurographics Workshop on Rendering*, Pisa, Italy, June 26-28, 2002.
- [15] Garret, M.J. and Fairchild, M.D. “Full-Spectral Color Calculations in Realistic Image Synthesis”, *IEEE Computer Graphics and Applications*, 19(4), July/August 1999, 47-53.
- [16] Akenine-Moller, T. and Haines, E. *Real Time Rendering*, Natick, Massachusetts: AK Peters, 2002.
- [17] Glassner, A.S., *Principles of Digital Image Synthesis*, California: Morgan Kaufman Publishers, 1995.
- [18] Beall, J., Doppelt, A., and Hughes, J. Brown University and National Science Foundation Graphics and Visualization Center,  
<http://www.cs.brown.edu/exploratories/freeSoftware/catalogs/repository.html>.
- [19] Boyce, P. *Human Factors in Lighting*, London: Taylor and Francis, 2003.
- [20] Carroll, W. (Ed.) *Daylighting Simulation: Methods, Algorithms, and Resources*, International Energy Agency, Solar Heating and Cooling Program -Task 21 and ECBCS-Annex 29, LBNL Report 44296,  
<http://eande.lbl.gov/Task21/dlgorithms.htm>
- [21] Mardaljevic, J. “Daylight Simulation”, In *Rendering with Radiance* (Ward, G. and Shakespeare, R.), San Francisco: Morgan Kaufmann Publishers, 1997.
- [22] Mardaljevic, J., *Daylight Simulation: Validation, Sky Models, and Daylight Coefficients, Dissertation*, DeMontfort University, 2000,  
<http://www.iesd.dmu.ac.uk/~jm/thesis/>.
- [23] CIE, *Spatial Distribution of Daylight – CIE Standard General Sky* (Draft), CIE DS 011.2/E, 2002.
- [24] Roy, G.G., Ruck, N.C., Reid, G., Winkelmann, F.C., Julian, W. “The Development of Modeling Strategies for Whole Sky Spectrums under Real Conditions for International Use”, *ARC Project A89131897 Report*, The University of Sydney and Murdoch University, September 1995.
- [25] Darula, S. and Kittler, R. “CIE General Sky Standard Defining Luminance Distributions”, *Proceedings of E-Sim 2002*, IBPSA-Canada, Montreal, Quebec Canada, September 11-13, 2002.

- [26] CIE, *International Recommendations for the Calculation of Natural Daylight*, CIE no. 16, Paris: Bureau de la CIE, 1970.
- [27] Moon, P., and Spencer, D.E. "Illumination from a Non-uniform Sky", *Illuminating Engineering*, 37(12), 1942, 707-726.
- [28] CIE, *Standardization of Luminance Distribution of Clear Skies*, CIE no.22, Paris: Bureau de la CIE, 1973.
- [29] Kittler, R. *Standardization of Outdoor Conditions for Daylight Factors for Clear Skies*, CIE no. 22, Paris: Bureau de la CIE, 1967.
- [30] Navvab, M., Karayel, M., Ne'eman, E., and Selkowitz, S. "Analysis of atmospheric Turbidity for Daylight Calculations", *Energy and Buildings*, 6(3), 1983, 293-303.
- [31] Navvab, M., "Validation Algorithms for Daylight Outdoors and Indoors", *Proceedings of the CIE 2003 Conference*, San Diego, June 26-28, 2003.
- [32] Nakamura, H., Oki, M., and Hayashi, Y. "Luminance Distribution of Intermediate Sky", *Journal of Light and Visual Environment*, 9(1), 1985, 6-13.
- [33] Perez, R., Searl, R., and Michalsky, J. "An All-Weather Model for Sky Luminance Distribution", *Solar Energy*, 6(23), 1991, 293-303.
- [34] *SDFClient*, Java Applet, Murdoch University, School of Engineering, Computer Science, Perth, WA, Australia, <http://eng-sun3.murdoch.edu.au/~geoff/webpages/SDFclient.html>.
- [35] Chain, C., Dumortier, D., and Fontoynt, M. "Consideration of Daylight's Color", *Energy and Buildings*, 33(3), 2001, 193-198.
- [36] Preetham, A.J., Shirley, P., Smits, B. "A Practical Analytic Model for Daylight", *ACM SIGGRAPH Proceedings of the 26th Annual Conference on Computer Graphics and Interactive Techniques*, 1999, 91-100.
- [37] Nishita, T., Dobashi, Y., Kaneda, K., and Yamashita, H. "Display Method of the Sky Color taking into account Multiple Scattering", *Pacific Graphics*, 1996, 117-132.
- [38] IESNA, *ANSI Approved Standard File Format for Electronic Transfer of Photometric Data and Related Information*, Publication no. LM-63-02, 2002.
- [39] CIE, *Recommended File Format for Electronic Transfer of Luminaire Photometric Data*, CIE no. 102, 1993.
- [40] *ELUMDAT Photometric Data File Format Specification*, <http://www.Helios32.com>.
- [41] Ehrlich, C. "Lighting Analysis", In *Rendering with Radiance* (Ward, G. and Shakespeare, R.), San Francisco: Morgan Kaufmann Publishers, 1997.

- [42] Mistrick, R. *Desktop Radiance Overview*, 2000, <http://radsite.lbl.gov/deskrad/drad-overview.pdf>.
- [43] Hunter, R.S. and Harold, R.W. *The Measurement of Appearance*, New York: John Wiley and Sons, 1987.
- [44] Cook, R.L. "Shade Trees", *Computer Graphics (Proceedings of SIGGRAPH 1984)*, 18(4), July 1984, 223-231.
- [45] He, X.D., Torrance, K.E., Sillion, F.X., Greenberg, D.P. "A Comprehensive Physical Model for Light Reflection", *Computer Graphics (Proceedings of SIGGRAPH 1991)*, 25(4), July 1991, 175-186.
- [46] Kajiya, J.T. "The Rendering equation", *Computer Graphics (Proceedings of SIGGRAPH 1986)*, 20(4), Aug. 1986, 143-150.
- [47] Goral, C.M., Torrance, K.E., Greenberg, D.P., and Bennett, B. "Modeling the Interaction of Light between Diffuse Surfaces", *Computer Graphics (Proceedings of SIGGRAPH 1984)*, 18(3), July 1984, 212-222.
- [48] Whitted, T. "An Improved Illumination Model for Shaded Display", *Communications of ACM*, 23(6), June 1980, 343-349.
- [49] Jensen, H.W. *Realistic Image Synthesis Using photon Mapping*, Natick, Massachusetts: AK Peters, 2001.
- [50] Ferwerda, J.A. "Elements of Early Vision for Computer Graphics", *IEEE Computer Graphics and Applications*, 21(5), Sep/Oct. 2001, 22-33.
- [51] Debevec, P.E. and Malik, J. "Recovering high dynamic range radiance maps from photographs", *ACM SIGGRAPH Proceedings of the 24th Annual Conference on Computer Graphics and Interactive Techniques*, 1997, 369-378.
- [52] Ward, G., Rushmeier, H., and Piatko, C. "A Visibility Matching Tone Reproduction Operator for High Dynamic Range Images", *IEEE Transactions on visualization and Computer Graphics*, 3(4), Oct/Dec. 1997, 291-305.
- [53] Ferwerda, J.A., S.N. Pattanik, P. Shirley, and D.P. Greenberg, "A Model of Visual Adaptation for Realistic Image Synthesis", *Proceedings ACM SIGGRAPH Proceedings of the 23th Annual Conference on Computer Graphics and Interactive Techniques*, 1996, 249-258.
- [54] Pattanaik, S.N., Ferwerda, J.A., Fairchild, M.D., and Greenberg, D.P. "A multiscale Model of Adaptation and Spatial Vision for Realistic Image Display", *ACM SIGGRAPH Proceedings of the 25th Annual Conference on Computer Graphics and Interactive Techniques*, 1998, 287-298.

- [55] Seetzen, H., Stuerzlinger, W., Vorozcovs, A., Wilson, H.R., Ashdown, I., Ward, W., and Whitehead, L. "High Dynamic Range Display System", SIGGRAPH 2003, Emerging Technologies Program, <http://www.siggraph.org/s2003/conference/etech/hdr.html>
- [56] Ward, G. "A Wide Field, High Dynamic Range, Stereographic Viewer", *Proceedings of PICS 2002*, April 2002.
- [57] Ward, G. "Real pixels". In *Graphics Gems II*, (Arvo, J. (ed)). Boston: Academic Press, Inc., 1991.
- [58] Ward, G. *High dynamic range images*, 1997, <http://www.anywhere.com/gward/pixformat/index.html>
- [59] Industrial Light and Magic (ILM), *OpenEXR*, <http://www.openexr.com/>.
- [60] Ward, G. and Shakespeare, R. *Rendering with Radiance*, California: Morgan Kaufman Publishers, 1997.
- [61] Rogers, D.F. *Procedural Elements for Computer Graphics*, Boston: WBC McGraw-Hill, 1997.
- [62] Ward, G. *Radiance Visual Comfort Calculation*, 1992, <http://radsite.lbl.gov/radiance/refer/Notes/glare.htm>.
- [63] Ashdown, I. "Virtual Photometry", *Lighting Design and Application*, 23(12), Dec. 1993, 33-39.
- [64] Feng, O., Nguyen, Q., Glaser, D. Canny, J., Do, E.Y.L. "Scythe and Sew: A Tool for Creating and Analyzing Meaningful Patterns of Lighting Simulation Data", *Proceedings of the Eight IBPSA Conference*, Eindhoven, Netherlands, August 11-14, 2003.
- [65] Kalawsky, R.S. *The Science of Virtual Reality and Virtual Environments: A Technical, Scientific and Engineering Reference on Virtual Environments*, Reading, Massachusetts: Addison-Wesley, 1993.
- [66] *Merriam-Webster Online Dictionary*, The Language Center, Merriam-Webster Inc., <http://m-w.com/home.htm>.
- [67] Matlab, <http://www.mathworks.com/>.
- [68] Foley, J.D., van Dam, A., Fisher, S.K., and Hughes, J.F. *Computer Graphics Principles and Practice*, Reading: Addison-Wesley, 1997.
- [69] Patterson, D.A. and Hennessy, J.L. *Computer Architecture: A Quantitative Approach*, San Francisco: Morgan Kaufmann Publishers, 1996.

- [70] *Radiance Lighting Simulation and Rendering System*, <http://radsite.lbl.gov>.
- [71] Ward, G. "The Radiance Lighting Simulation and Rendering System", *ACM SIGGRAPH Proceedings of the 21th Annual Conference on Computer Graphics and Interactive Techniques*, 1994, 459-472.
- [72] Ashdown, I. "Thinking Photometrically Part II", *Lightfair International*, Las Vegas, May 29, 2001.
- [73] CIE, *Methods of Characterizing Illuminance Meters and Luminance Meters: Performance, Characteristics, and Specification*, CIE no. 69, Vienna: Central Bureau de la CIE, 1987.
- [74] Grynberg, A., "Validation of Radiance", *LBID 1575*, LBL Technical Information Department, Lawrence Berkeley National Laboratory, Berkeley, California, July 1989.
- [75] Mardaljevic, J., "Validation of a lighting simulation program under real sky conditions", *Lighting research and Technology*, 27(4), 1995, 181-188.
- [76] Khodulev, A. and E. Kopylov, "Physically accurate lighting simulation in computer graphics software", *6. International conference on Computer Graphics and Visualization*, St. Petersburg, Russia, July 1-5, 1996.  
<http://rmp.kiam1.rssi.ru/articles/pals/index.htm>
- [77] Houser, K.W., D.K. Tiller, and I.C. Pasini, "Toward the accuracy of lighting simulations in physically based computer graphics software", *Journal of the Illuminating Engineering Society*, 28(1), Winter 1999, 117-129.
- [78] Ubbelohde, M.S. and Humann, C. "Comparative evaluation of four daylighting software programs", *1998 ACEEE Summer Study on Energy Efficiency in Buildings Proceedings*, American Council for an Energy-Efficient Economy, 1998.
- [79] Bourke, P. "Computer generated angular fisheye projections",  
<http://astronomy.swin.edu.au/~pbourke/projection/fisheye>.
- [80] B&K Technical Review, *Methods of Calculation Contrast*, 1984.
- [81] Sorensen, K., Nielsen, O., and Agesen, L. "Methods for the calculation of contrast", *Journal of the Illuminating Engineering Society*, 13(2), Jan. 1984, 277-285.
- [82] CIE, *Guide on Interior Lighting*, 2. Ed., CIE no. 29.2, Vienna: Central Bureau de la CIE, 1986.
- [83] *Guide to Integrating Sphere Theory and Applications*, Labsphere Technical Publications,  
[http://www.labsphere.com/tech\\_info/docs/IS\\_Theory\\_Application.pdf](http://www.labsphere.com/tech_info/docs/IS_Theory_Application.pdf).

- [84] National Institute of Standards and Technology (NIST), Physics Laboratory, Optical Technology Division,  
<http://www.physics.nist.gov/Divisions/Div844/facilities/photo/photo.html>.
- [85] Kessler, J. and Selkowitz, S. “Integrating Sphere Measurements of Directional-Hemispherical Transmittance of Window Systems”, *Journal of the Illuminating Engineering Society*, 13(2), Oct. 1984, 136-150.
- [86] McCamy, C.S. “Correlated Color Temperature as an Explicit Function of Chromatic Coordinates”, *Color Research and Application*, 17(2), 1992, 142-144.
- [87] Committee on Colorimetry, Optical Society of America, *The Science of Color*, Washington D.C.: Optical Society of America, 1963.
- [88] Berman, S.M. “Energy efficiency consequences of scotopic sensitivity”, *Journal of the Illuminating Engineering Society*, Winter 1992, 21(1), 3-13.
- [89] Siminovitch, M., Navvab, M., and Kowalewski, H. “Contrast potential, an assessment technique using large solid angle illuminance measurements”, *Conference Proceedings of 1992 IEEE Industrial Applications Society Annual Meeting*, Vol. 2, 1992, 1818-1824.
- [90] Siminovitch, M. *Experimental Development of Efficacious Task Source Relationships for Interior Lighting Applications*, Ph.D. Thesis, University of Michigan, College of Architecture and Urban Planning, 1993.
- [91] IEA, *Daylighting in Buildings: A Sourcebook on Daylighting Systems and Components*, A Report of the IEA SHC ((International Energy Agency Solar Heating and Cooling), Task 21, July 2000.
- [92] Matlab, *Image Processing Toolbox for Use with MATLAB*, User’s Guide, Version 2, 1997.
- [93] *Advanced Lighting Guidelines*, New Buildings Inc., 2001.
- [94] Ishida, T. and Iriyama, K. “Estimating Light Adaptation Levels for Visual Environments with Complicated Luminance Distribution”, *Proceedings of the CIE 2003 Conference*, San Diego, June 26-28, 2003.
- [95] Hopkinson, R.G. *Architectural Physics: Lighting*, London: Her Majesty’s Stationary Office, 1963.
- [96] Cuttle, C. *Lighting by Design*, Oxford: Architectural Press, 3003.
- [97] Worthey, J.A. “Light Source Area, Shading, and Glare”, *Journal of the Illuminating Engineering Society*, 20(2), Summer 1991, 29-36.

- [98] Worthey, J.A. "Geometry and Amplitude of Veiling Reflections", *Journal of the Illuminating Engineering Society*, 18(1), Winter 1989, 49-62.
- [99] Love, J.A. and Navvab, M. "The Vertical to Horizontal Illuminance ratio: A New Indicator of Daylighting Performance". *Journal of the Illuminating Engineering Society*, 23(2), Summer 1994, 50-61.
- [100] Lynes, J.A., Burt, W., Jackson, G.K., and Cuttle, C. "The Flow of Light into Buildings", *Transactions of IESGB*, 31(3), 1996, 65-91.
- [101] Cuttle, C. "An Integrated System of Photometry, Predictive Calculation and Visualization of the Shading Patterns Generated by Three-Dimensional Objects in a Light Field", *Proceedings of the CIE 2003 Conference*, San Diego, June 26-28, 2003.
- [102] Ashdown, I. "The Virtual Photometer: Modeling the Flow of Light", Ledalite Architectural Products Inc, White Paper, 1998.
- [103] CIE, *Discomfort Glare in Interior Lighting*, CIE no. 117, 1995.
- [104] Chauvel, P., Collins, J.B., Dogniaux, R., and Longmore, J. "Glare from Windows: Current Views of the Problem", *Lighting Research and Technology*, 14(1), 1982, 31-46.
- [105] Fontoynt, M. (Ed.) *Daylighting Performance of Buildings*, James & James Science Publishers for the European Commission Directorate General XII for Science, Research and Development, 1999.
- [106] Berman, S.M., Fein, G., Jewett, D.L., Saika, G., Ashford, F. "Spectral Determinants of Steady-State Pupil Size with Full Field of View", *Journal of the Illuminating Engineering Society*, 21(2), Summer 1992, 3-13.
- [107] Navvab, M. "A Comparison of Visual Performance Under High and Low Color Temperature Fluorescent Lamps", *Journal of the Illuminating Engineering Society*, 30(2), Summer 2001, 170-175.
- [108] Navvab, M. "Visual Acuity Depends on the Color Temperature of the Surround Lighting", *Journal of the Illuminating Engineering Society*, 31(1), Winter 2002, 70-84.